1969

High-energy Electron Dosimetry

Krishnan Namboordiri Kartha

NATIONAL LIBRARY OF CANADA

CANADIAN THESES

ON MICROFILM

BIBLIOTHÈQUE NATIONALE DU CANADA

THÈSES CANADIENNES

SUR MICROFILM

NL-101(1/66)

HIGH ENERGY ELECTRON DOSIMETRY

by

K. N. Mukund Kartha

Department of Physics

Submitted in partial fulfillment

of the requirements for the degree of

Doctor of Philosophy

Faculty of Graduate Studies

The University of Western Ontario

London, Canada.

September 1968

ABSTRACT

Radiation dosimetry is concerned with the determination of the energy absorbed in a medium during irradiation by ionizing radiations. The use of high energy electrons in cancer treatment has created a need for sensitive and accurate dosimetric systems which are applicable in electron dose measurements. In this work, the ferrous sulphate, LiF and ionization chamber dosemeters were studied, with a view to extending their use to clinical electron dosimetry.

The ferrous sulphate dosimetric technique developed here allows measurements of doses of 500 rads in volumes of 0.5 cm^3 or less, with a standard deviation of 3%. The LiF dosemeter can now be used to measure, routinely, doses at separations of less than 0.5 mm using "monocrystalline" layers and a specially-designed automated reader. This technique has been used to study the rapidly changing dose distributions in the region of interfaces in a heterogeneous absorber.

To date no experimental evaluation of the polarization correction has been reported for high energy electrons. In the work reported here, this has been found to range from 6.2% at 4.7 MeV to

20.1% at 28 MeV. The measured values of the C_F factors which may be used to convert the ionization readings of a commercial dosemeter to absorbed dose, are in good agreement with the values calculated on the basis of the Bragg-Gray relation.

ACKNOWLEDGMENTS

The author wishes to express his gratitude to Dr. J. C. F. MacDonald of the Ontario Cancer Treatment and Research Foundation, London Clinic, and the departments of Physics and Therapeutic Radiology, under whose supervision this work was performed, to Dr. E. Brannen, Dr. T. W. W. Stewart and Dr. B. Y. Tong, of the Physics department and Dr. D. J. Dawson of the London Clinic for the help and suggestions. Thanks are due to my wife, Sethulakshmi, for the continued inspiration and understanding during the course of this work. The financial support received from the Ontario Cancer Treatment and Research Foundation, and the research facilities provided at its London Clinic are acknowledged with thanks.

The technical assistance of Messrs. D. Jones, A. Vaart, M. Taylor, and A. Edney are greatly appreciated. Mrs. M. Alderson is deserving of thanks for the careful typewriting of this thesis.

TABLE OF CONTENTS

LIST OF TABLES

LIST OF FIGURES

Preceding page

CHAPTER I.

INTRODUCTION

CHAPTER I

INTRODUCTION

The interaction of high energy electrons with living cells brings about physical and chemical changes within the cells. These radiation-induced changes result in an inability of the cells to divide and multiply, or in cell death. Thus a mass of malignant cells in the human body can be eradicated by controlled electron bombardment; this is the principle of cancer treatment using electrons.

It is obvious that the extent of the effects of the electron beam within the patient must be made to coincide with that of the mass of malignant cells. In addition, the amount of radiant energy absorbed by the tumour from the beam must be controlled to within relatively narrow limits. The effect on the tumour depends not only upon the total energy absorbed, but also upon the magnitude and spacing of the fractions by which it is administered. These latter parameters will not be considered in this thesis — here we are concerned only with the total energy absorbed, and with the instantaneous rate of delivery.

A. ABSORBED DOSE

Even though the ability to produce ionization in air is not a direct specification of radiation intensity, it has long been employed as a significant and measurable characteristic of radiation. It has been given the designation EXPOSURE, the unit of which is the "roentgen" - R (58). Exposure, however, is defined only for x- and γ-radiations within a limited range of energies; the concept is not applicable to particulate radiations. The most relevant quantity in clinical radiation dosimetry is the amount of energy actually absorbed by a material from the beam. This quantity is a function of the type and energy of the radiation, and of the atomic composition and density of the absorber. The energy retained at the point of interest and made locally available in the surrounding medium is termed the ABSORBED DOSE or DOSE (57). The unit of absorbed dose is the RAD, and is defined as 100 ergs per gram (58).

B. HISTORICAL REVIEW

Radiation dosimetry has evolved primarily to satisfy the needs of medical radiology. Many different physical effects were employed in the early measurement of radiation (39). Of these, the one involving ionization of air gained general popularity because of its convenience, high sensitivity, stability and reproducibility. Following the recommendations of the International Commission on Radiological

Units and Measurements - ICRU (57, 58) on the necessity for international dose standards, radiation standardization laboratories have been organized in most of the countries where radiation therapy is practiced. Medical radiation users employ, in their routine measurements, sub-standard thimble ionization chambers (28, 31, 40), which are calibrated at the national standardization laboratory.

Upon the adoption of the absorbed dose concept, the necessity arose for calibrating these standard instruments to allow the determination of dose in rads. The Bragg-Gray relation (18, 43) facilitated this conversion subject to certain conditions. This relation, between the energy E_m absorbed per unit mass of the medium and the number J_m of ions formed per unit mass of gas in a cavity embedded in it, in which the ionization is produced, is

$$E_m = W \rho_s J_m, \qquad (i)$$

where W is the average energy expended in the production of an ion pair and ρ_s is the ratio of the mass stopping power of the absorbing medium to that of the gas.

The absorbed dose at a point within an irradiated medium can be determined indirectly by means of a roentgen-calibrated ionization chamber placed at the point. Having measured the exposure X in roentgens, which would exist at that point in the medium in the absence of the chamber, the absorbed dose D_m, in rads is obtained

from the relation

$$D_m = f\ X \qquad \text{(ii)}$$

This is a consequence of the Bragg-Gray relation, and f is the roentgen-to-rad conversion factor. Values of f for monoenergetic x-rays up to 10 MeV energy, and for x-ray spectra up to 400 keV are available (59).

C. ELECTRON DOSIMETRY

The theory of the interaction of electrons with matter in "good geometry" is quite complete (see Appendix I), but its application is limited under the conditions obtaining in therapy. The requirement of broad therapeutic beams necessitates the introduction of scatterers which produce varying degrees of energy degradation. Collimation of the electron beam to match the dimensions of the tumour introduces further scattering; this adds further low energy electrons to the spectrum incident upon the patient or absorber. Thus any approach to the problems of electron dosimetry for medical applications must be primarily experimental.

National standardization laboratories in most countries (including Canada) offer as a service the calibration of ionization chamber dosemeters for use with x- and γ-rays of energies up to 3 MeV. As yet a comparable service is nowhere available for high

energy electron dose-measuring systems. Consequently, most centers employing electron therapy develop their own dosimetric measurement methods.

This thesis describes the intercomparison of a number of these dosimetric systems, with a view to determining their relative merit for the solution of various problems that arise in electron dosimetry. In the course of this work, certain problems peripheral to this basic purpose have been studied, and the results are reported in the text.

Of the many dosimetric systems that are available, the ones which are most nearly "tissue-equivalent" are to be preferred in clinical dosimetric applications. The introduction of the material of the dosemeter into a tissue-equivalent phantom must cause a minimum perturbation in the pattern of energy absorption and in the spectrum of the radiation. This thesis describes the techniques and results of electron dosimetry investigations using an aqueous chemical system, a solid-state system based on thermoluminescence, and a cavity ionization system.

1. Chemical Dosimetry System

In order to determine the electron dose in rads an absolute dosimetric system is required. Calorimeters designed for radiation

dose measurement have the principal merit that they measure directly the amount of energy deposited around the point of measurement. Thus calorimetric measurement of absorbed dose is the most direct method, but one that requires considerable complex equipment and a clear understanding of its limitations. As an alternative to calorimetry various chemical reactions have been employed for the determination of absorbed dose in radiation dosimetry (2, 32). These chemical dosimetric systems are based upon the observation that certain oxidation or reduction reactions are initiated by irradiation, and that these changes are directly proportional to the dose. In clinical dosimetry aqueous systems are usually employed because of their near tissue-equivalence.

The ferrous sulphate chemical dosemeter has been widely used (59, 100) because of its reliability and reproducibility. The theory of this dosimetric system is given in Appendix II. The density of the dosimetric solution is only 1.5% higher than that of water, and its chemical composition makes it very nearly tissue-equivalent (33, 34). For these reasons the ferrous sulphate dosemeter has been recommended for use as a dosimetric standard (94).

The use of the ferrous sulphate dosemeter in a water phantom involves the risk of contaminating the dosemeter solution. Since doses measured under identical conditions in polystyrene and

water have been shown to agree to within 3% (68), a polystyrene phantom was used for most of the measurements reported in this work. The containers for the solution, in various sizes and shapes, were also of polystyrene and fitted snugly into the phantom. Thus the presence of the dosemeter in the phantom introduced a minimal perturbation in the electron field (68).

2. Solid State System

Any solid material that exhibits at least one measurable parameter, which is a function of the absorbed dose in the material, can serve as the basis for a solid state dosimetry system. A complete review of the solid state dosemeters studied to date is given elsewhere (30).

Thermoluminescent (TL) dosimetry has been investigated in this work, to study its possible role in electron dosimetry. Practically all crystalline materials exhibit TL; a brief review of the theory of radiation-induced TL is given in Appendix III. Many TL crystals have been studied by various workers, with a view to their usefulness as TL dosemeters. Doped LiF, produced by Harshaw Chemical Company, and known as "TLD-100" has been shown to have the following advantages over other TL systems for dosimetry.

1. The measured TL is linear with dose up to 10^5 rads (60).

2. The TL is dose-rate independent up to 2×10^8 rads per second (60).

3. The TL output is 2 to 3 times greater than that of CaF_2 : Mn, and 10 times greater than that of lithium borate - i. e. $Li_2B_4O_7$: Mn (89).

4. A properly-annealed sample has only one glow peak. The integrated light in the peak fades by less than 5% over a storage period of one year after irradiation (20).

5. The emitted light is blue (of the order of 400 nm) and hence thermal radiations may be filtered out without introducing any significant errors (8).

6. The crystals are inert and insoluble, and are relatively free from triboluminescence.

7. TLD-100 LiF exhibits less energy dependence upon electron energy than other TLD systems (22, 82, 101).

8. Because of the low atomic number of both Li and F, LiF has a stopping power close to that of water. It has been shown that, even though the stopping power of LiF and H_2O vary with electron energy, their ratio remains constant at energies between 0.2 and 50 MeV (101). This ratio is the same as that for Co-60 γ-rays.

Considering these advantages TLD-100 LiF has been chosen for use in this work. The TLD has the special advantage over

all other dosimetric systems that it can be employed conveniently for in vivo measurements.

3. Ionization Chamber

It has been suggested (4, 93) that measurements with thimble ionization chambers could be used for the determination of absorbed dose produced by high energy electrons, using the Bragg-Gray relation. The values measured with the ionization chamber instrument are multiplied by the Co-60 γ-ray calibration factor, supplied by the National Standardization Laboratory. The value R_o so obtained is equated to the dose D_m in rads, by

$$D_m = C_F R_o \qquad \text{(iii)}$$

The conversion factor C_F is a strong function of energy of radiation and the depth of measurement (93).

These C_F factors can be evaluated theoretically or experimentally. The few experimental values of C_F that are available are not in good agreement with those derived theoretically. Further, the experimental results reported to date form an inadequate basis for clinical electron dosimetry. A detailed experimental study of the application of the ionization chamber in electron dosimetry has been carried out, and the results are reported in this thesis.

4. Photographic Film

The oldest of the dosimetric systems is based upon the blackening of a photographic emulsion. Although the accuracy of this system is of the order of 10%, it is still used extensively for the mapping of high energy radiation fields employed in therapeutic radiology. The response of a photographic emulsion to radiation depends upon the environment and processing, and also upon the quality and dose-rate of the radiation used. Photographic film was employed in this work only for the study of relative dose distribution.

D. THE RADIATION SOURCE

The Asklepitron 35, which was the source of the high energy electrons, was designed primarily for radiation therapy. The practical energy range for this purpose is 10 to 35 MeV; this was the range of interest in this work.

The electrons accelerated in the donut, after penetrating the donut wall emerge in a very narrow beam. To suit the medical application, this is converted into a broad beam by thin laminated copper scatterers. The electrons in this broad beam must then pass through a transmission ionization chamber, which serves as an electron beam monitor. The presence of the scatterer and monitor chamber produces a degradation in the effective energy of the electron beam.

The effective energy of the electron beam, after it has penetrated the donut wall, the scatterer, and the monitor chamber, was measured by the threshold techniques recommended by SCRAD (94) and by range-energy measurements in water (68). In determining the energy of the incident electrons, the same threshold reactions were obtained by the introduction of a 2 mm thick lead sheet over the irradiated sample. The bremsstrahlung produced by the interaction of the electrons with the lead initiated the photonuclear interactions.

The electron beam emitted by the betatron is not sharply delineated at the periphery, as required for cancer therapy. The initial limitation of the beam is achieved by the master collimator shown in Fig. 1. The electron field size is finally defined by means of an extended diaphragm of lucite (Fig. 2), or a continuously variable collimator (Fig. 1). A plastic applicator provides a beam size fixed in cross section, where as the four-sided variable collimator can be set to give any beam size between 4 x 4 cm and 14 x 12 cm.

As mentioned previously, the electron beam is monitored with a parallel-plate transmission ionization chamber placed in the beam. The ionization charge collected by this chamber is fed into an integrating circuit, the output of which drives an electro-mechanical counter. The amount of charge collected by the chamber which is required to actuate the counter is referred to as a CLICK in this thesis.

Figure 1.

Electron beam collimator assembly.

A - Master collimator; B - Electron monitor chamber;

C - Variable electron collimator; D - Beam defining diaphragm.

Figure 1

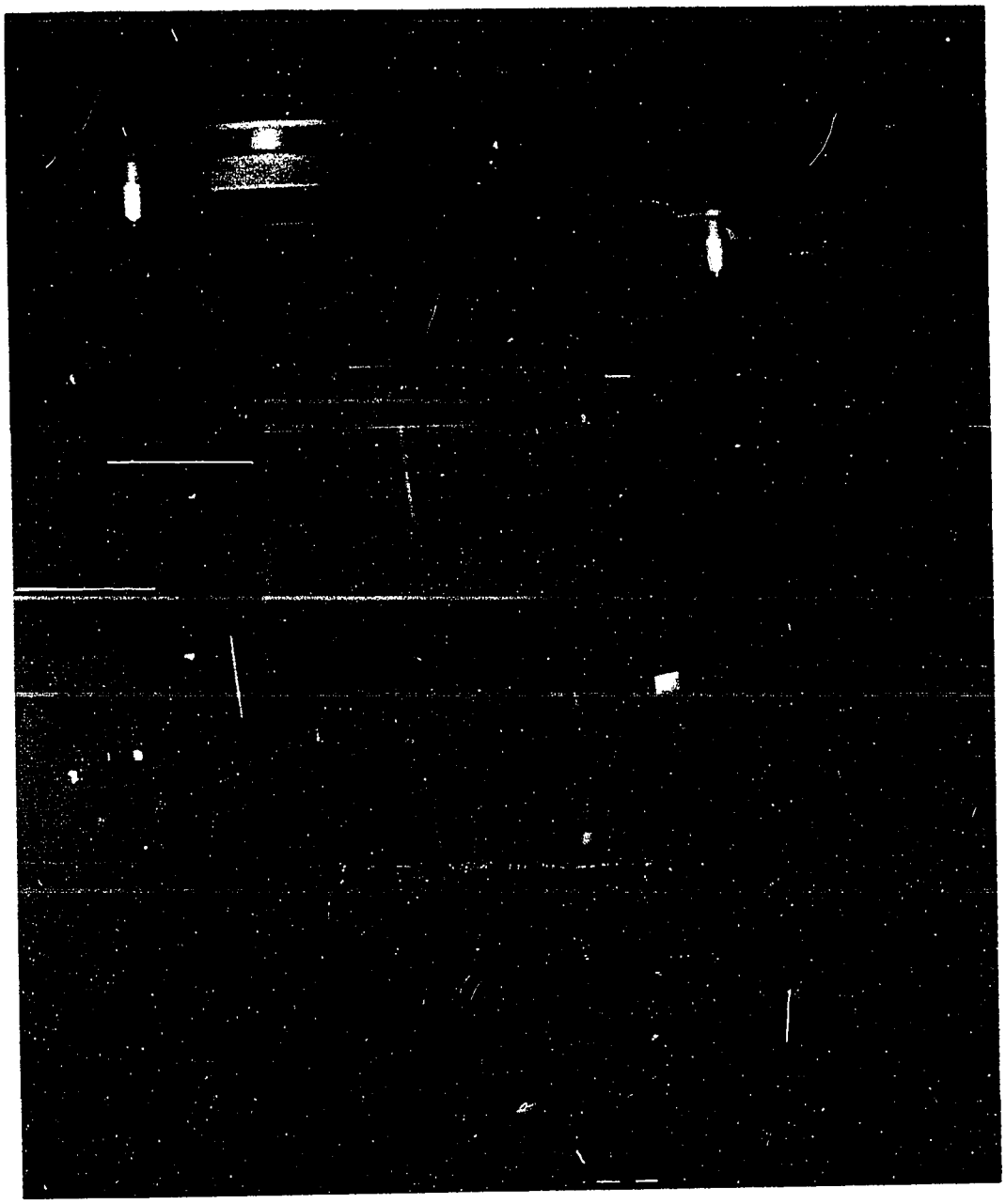

A

Figure 2.

Plastic electron applicators.

Figure 2.

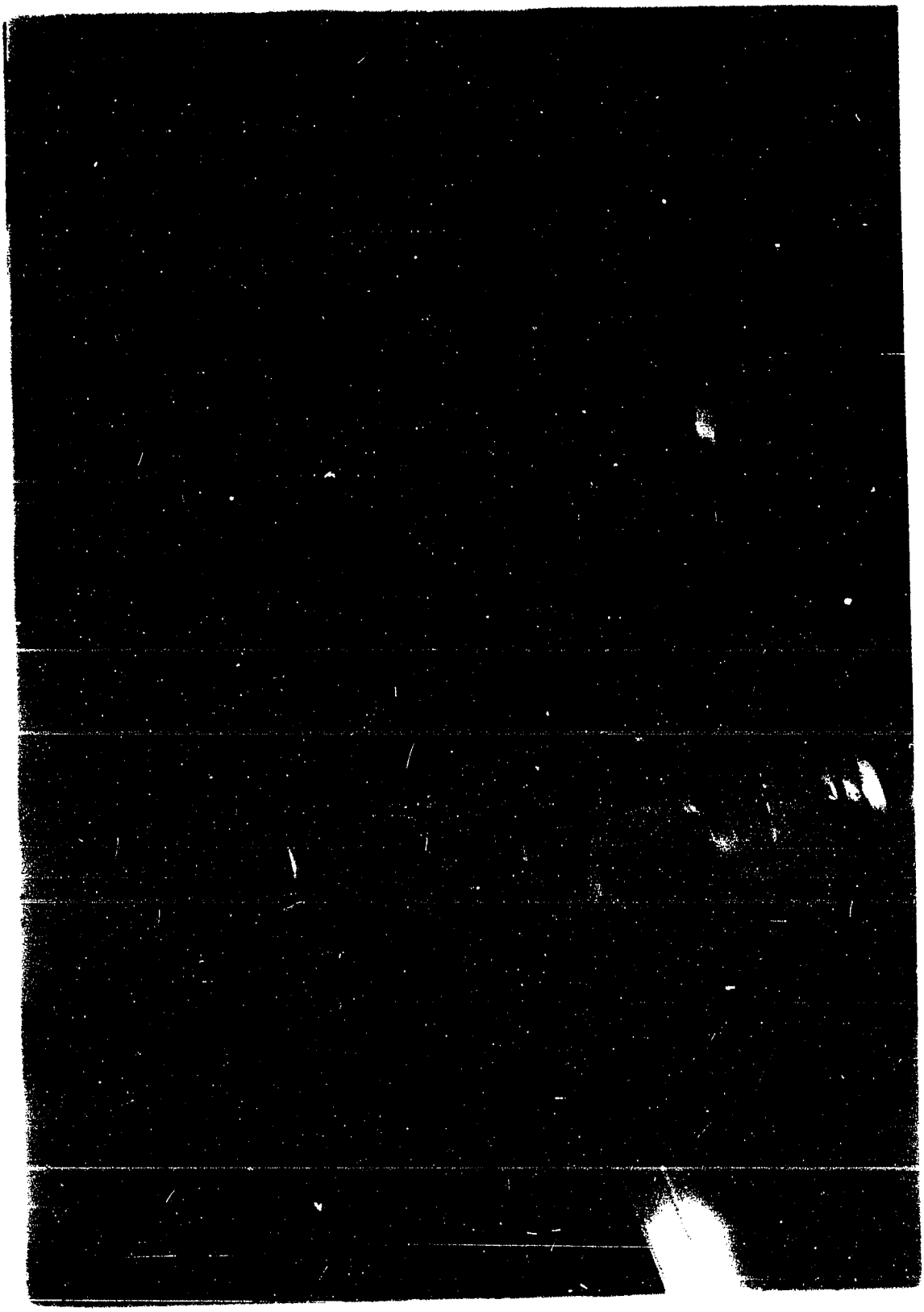

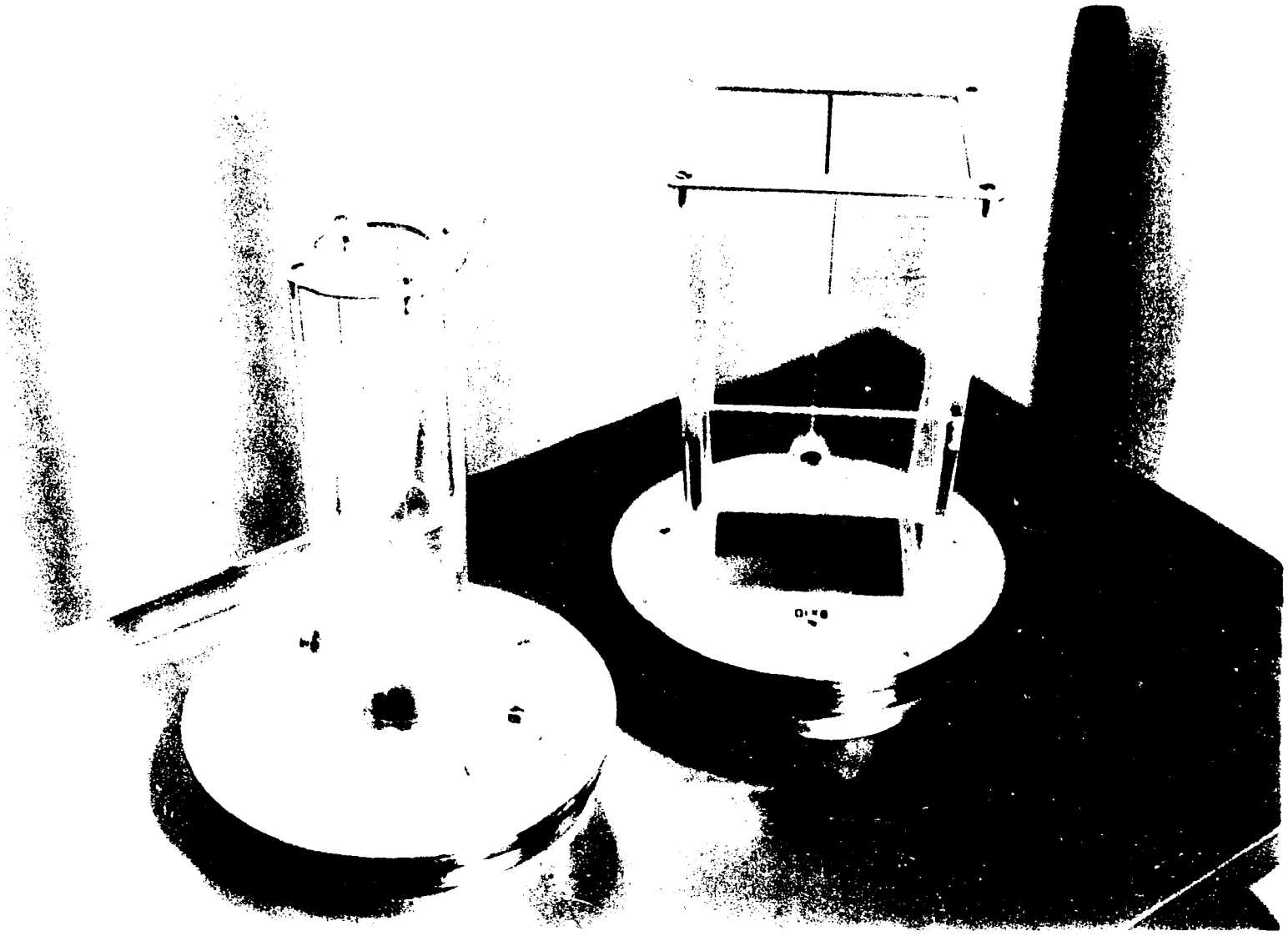

The electron output varied from 60 clicks per min. at 10 MeV to 600 clicks per min. at 35 MeV. The click is taken as the reference for dosimetric determinations.

In the following chapter the experimental methods used are described in detail. The development of new techniques and the improvement of standard methods for application in electron dosimetry are described. Chapter III is a discussion of the experimental findings. A summary of the work is presented in Chapter IV, together with the conclusions derived therefrom.

CHAPTER II.

EXPERIMENTAL METHODS

CHAPTER II

EXPERIMENTAL METHODS

In this chapter the specific dosimetric methods and techniques employed in this investigation are described. The background information and basic principles of the methods, as reported by others, are outlined in the Appendices. The techniques described here have been developed with the requirements of clinical dosimetry in mind. Specifically, doses in the range 100 to 500 rads should be measurable by the use of sensitive volumes of 0.5 cm^3 or less, if these requirements are to be met.

A. FERROUS SULPHATE DOSIMETRY

1. Irradiation Procedures

Since ferrous sulphate dosemeter was the only absolute dosimetric system employed in this work, it was used in calibrating the dose-rate meter on the betatron control console. In addition it was employed in measuring point dose, dose distribution and

calibration of other dosimetric systems used in this work. All measurements were taken in a polystyrene phantom, whose cross-sectional area was 25 x 25 cm and the depth was chosen to suit each measurement. The irradiation cells used were specially constructed of polystyrene, and were of different sizes and shapes (Fig. 3).

The clean irradiation cells were pre-irradiated to doses of 10^6 rads or more of ionizing radiation in distilled water. In this way H_2O_2 is produced in the aerated water by radiolysis and it destroys the organic matter on the surface and that buried in submicroscopic fissures, which is not removed by hot water and detergents (3). After irradiation the cells were rinsed and kept immersed in purified water, until they were used.

At the time of irradiation, these pre-irradiated cells were rinsed with distilled water and unirradiated dosimetric solution. Then they were filled with the dosimetric solution, placed in the phantom and irradiated. Fig. 5 illustrates an experimental set up. In each experiment two aliquots were irradiated to a known dose with Co-60 γ-rays in order to check the dosimetric response of the solution.

For calibrating the output meter of the betatron, the 1.5 cm deep polystyrene irradiation cells were used. These cells, after filling with the dosimetric solution, were placed in the phantom at the depth of the peak of the build-up (determined by the TLD - as described in section III B - 3). For measurement of central-axis depth dose, the

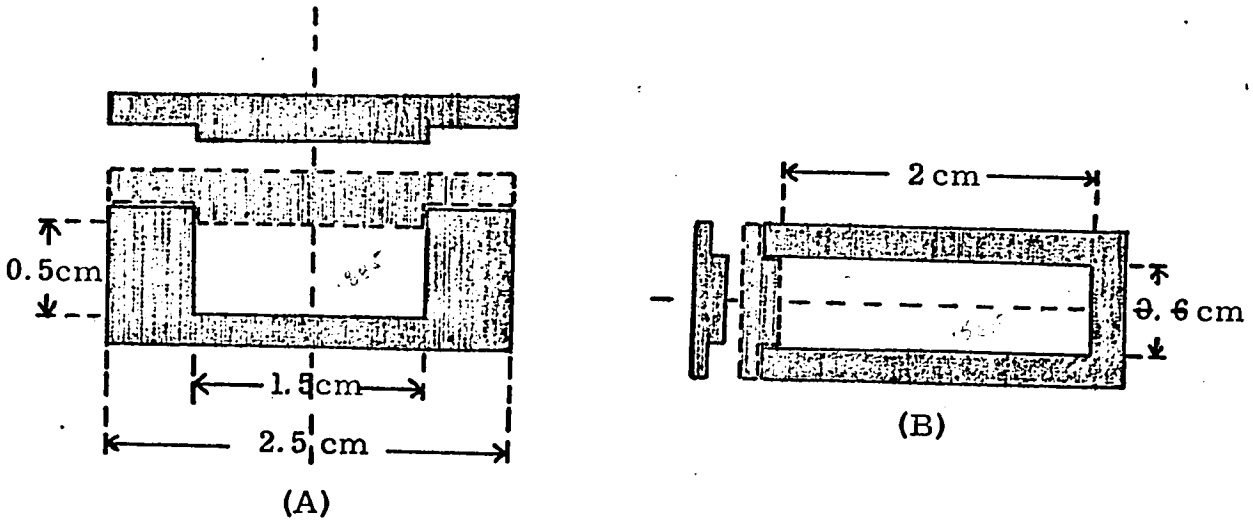

Fig. 3 : Cross-sections of the polystyrene irradiation cells for ferrous sulphate dosimetry. (A) that of pillbox shaped cell, and (B) that of cylindrical cell which is comparable to the ionization cavity of the Baldwin-Farmer instrument.

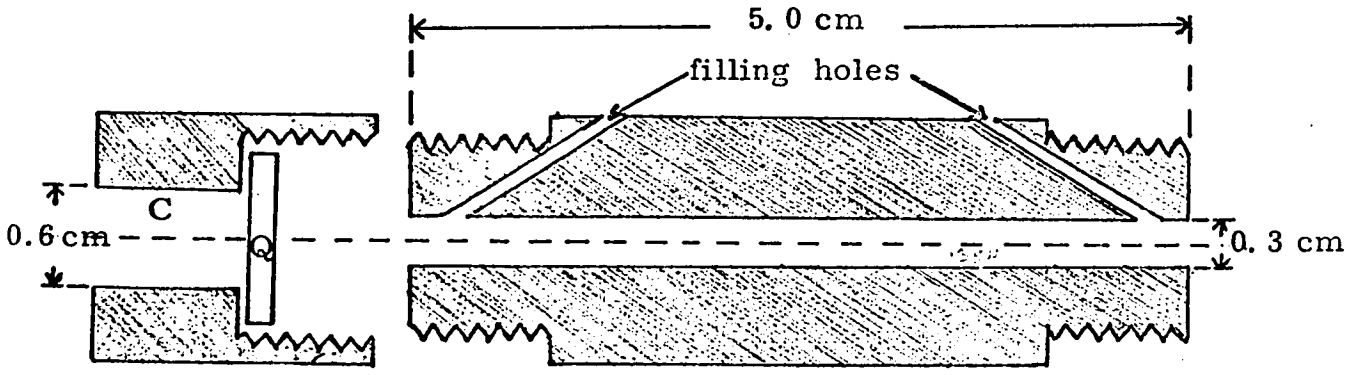

Fig. 4 : Cross-section of the teflon microcell, for measuring the absorbance of ferrous sulphate solution. Q is the quartz window, and C is the cap. The window and cap on the other end are not shown.

Figure 5

Experimental set-up for electron dose measurements in a polystyrene phantom. The dark circular spot at the top of the phantom, at the center of the plastic applicator, shows the hole in which the dosemeters were placed at chosen depths, using polystyrene plugs.

A - master collimator; E - plastic electron applicator;

P - polystyrene phantom.

Figure 5.

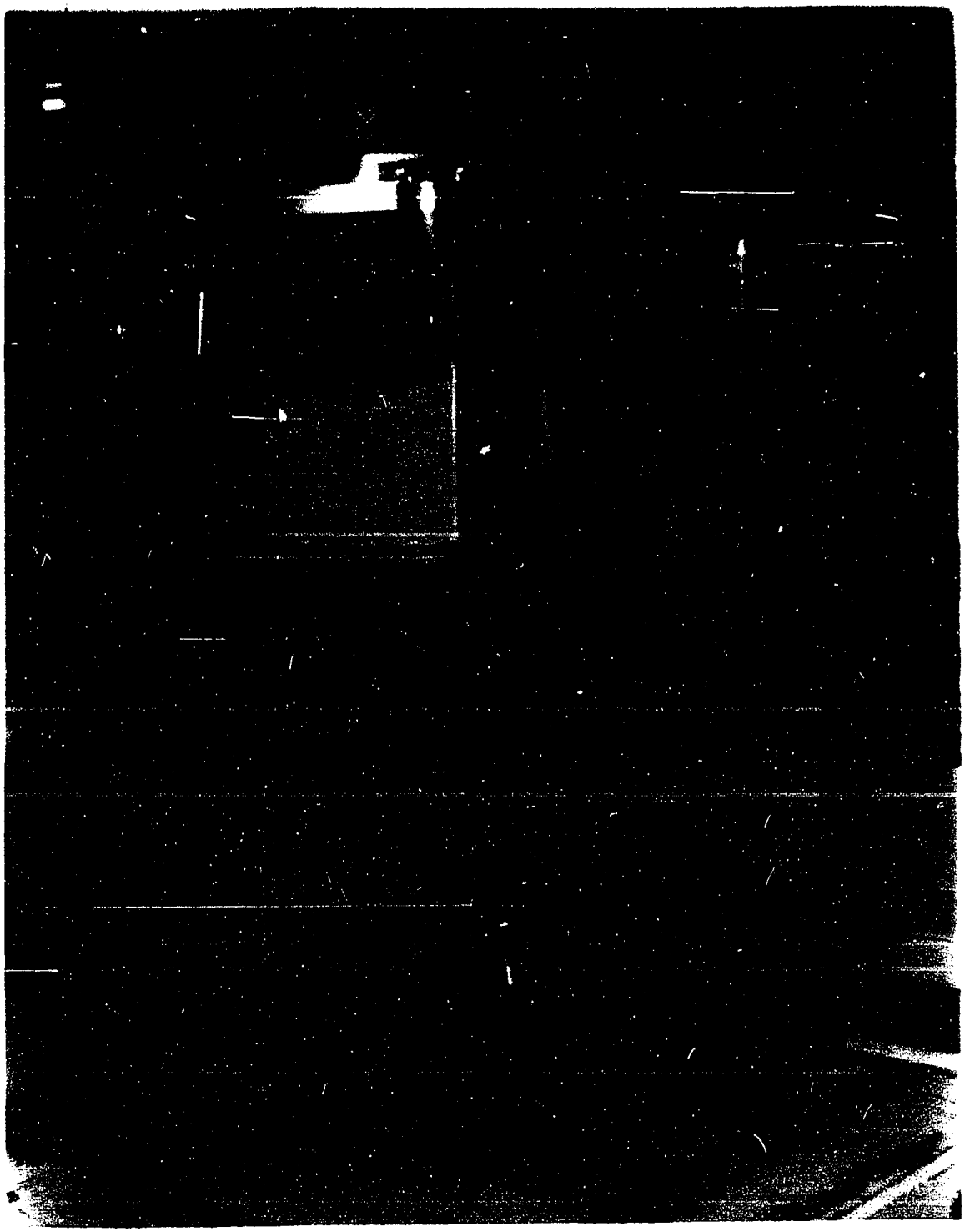

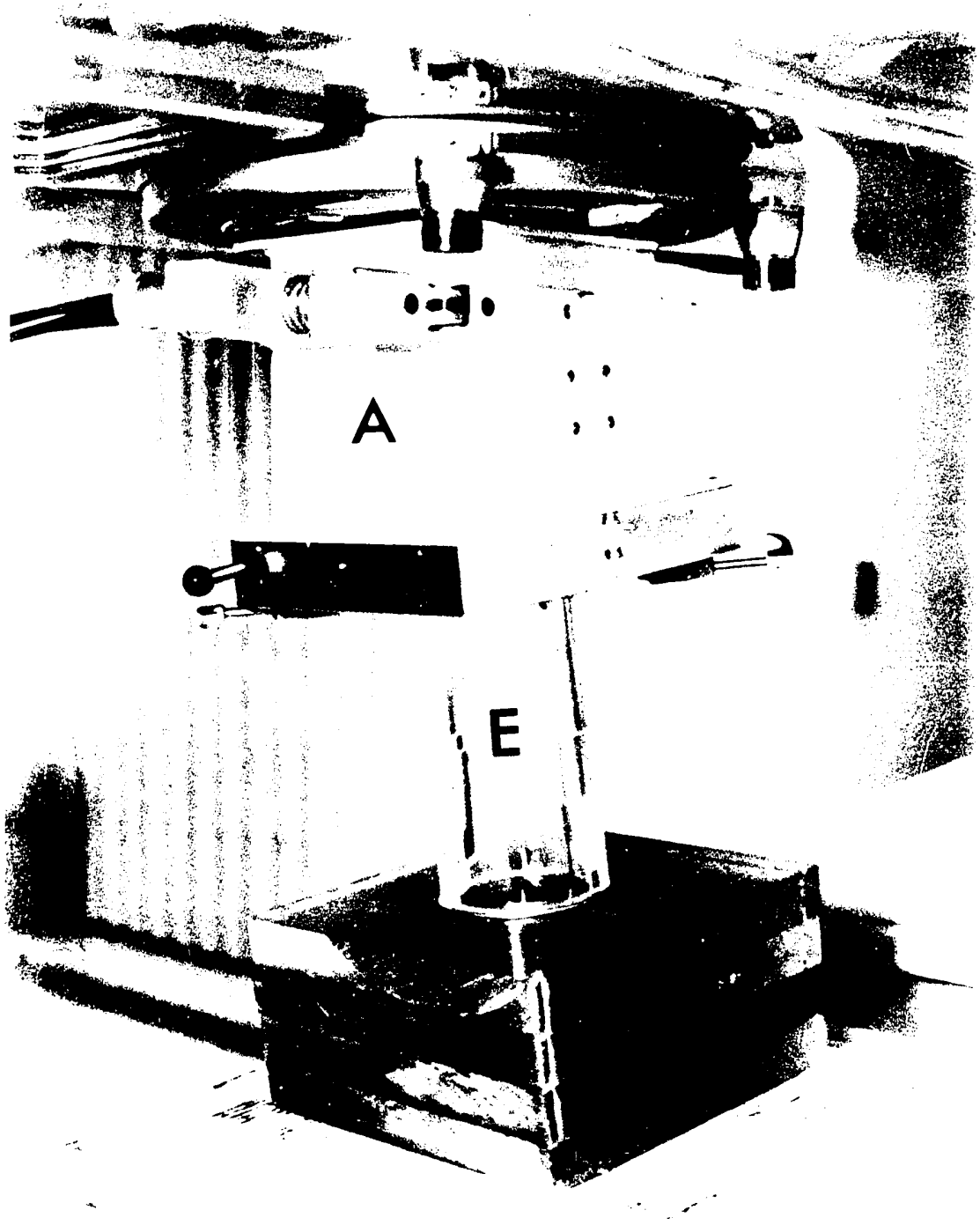
A
E

irradiation cells with the solution were stacked one over the other, and irradiated together in the polystyrene phantom. The doses used in the output calibrations were of the order of 1000 clicks. In the central-axis depth dose measurements, the doses involved were of the order of 10,000 to 15,000 clicks in order that the dose at the 5 to 10% points would be enough to produce a measurable absorbance.

The electron irradiations were monitored by the ionization chamber discussed in section I D. This chamber is not sealed and the air density and hence the ionization current, in the collecting volume depends upon the ambient temperature and pressure. Since the number of clicks registered on the integrator depends upon the time integral of the current, this must be corrected for air density. To conform with the clinical dosimetric practice, this correction is referred to 760 mm Hg and 22^{o}C.

2. Measurement Methods

The change in absorbance resulting from the production of ferric ions in the irradiated solution was measured by comparison with an identically-treated, but unirradiated, sample. The absorbance measurements were made using a Hitachi-Perkin-Elmer Model 139 UV-Vis Spectrophotometer. In this instrument the spectral source is a hydrogen lamp and the detector is a phototube. The absorbance reading accuracy is $\pm$ 1% in the range 0.3 to 0.7. The cells used for

absorbance measurement were the standard 1 cm silica cells, and specially-built 5 cm "microcells" of 0.5 cm^3 volume. The 1 cm cells are matched and the difference in absorbance is negligible. The capacity of these cells is 4 cm^3 (Fig. 6). For this work the size of the limiting diaphragm in the 1 cm cell holder was reduced to a 1 cm circle, which permitted absorption measurements with a useful volume of 1.2 cm^3 of solution.

The lower limit of dose which can be measured with the 1 cm path length cells at a wavelength of 304 nm and allowing for 1% uncertainty in the absorbance measurement, is reported to be 4,000 rads (96). As the doses of interest in radiation therapy range from 100 to 1000 rads, it was felt that a dosimetric technique for measuring such doses would be more useful in clinical dosimetry. In addition, although the concept of dose at a point is hypothetical, a dosemeter closely approximating a point is desirable. By using the 224 nm absorption peak, instead of that at 304 nm (section III A - 5), the minimum dose-limit can be lowered to 2,000 rads. The absorption band at 224 nm is broad enough so that measurements taken at this peak are insensitive to small changes in wavelength setting.

As stated in equation 6 of Appendix II, the absorbance is proportional to the optical path length L of the dosimetric solution. By increasing L to 5 cm in the specially designed microcells, the

Figure 6

Ferrous sulphate dosimetric accessories: - c - 0.6 cm dia. x 2 cm cylindrical polystyrene irradiation cell; h - 1 cm cell holder; m - 5 cm teflon microcells; p - 1.5 cm dia. x 0.5 cm pillbox-shaped polystyrene irradiation cell; q - quartz window; and s - 1 cm silica cell.

Figure 6.

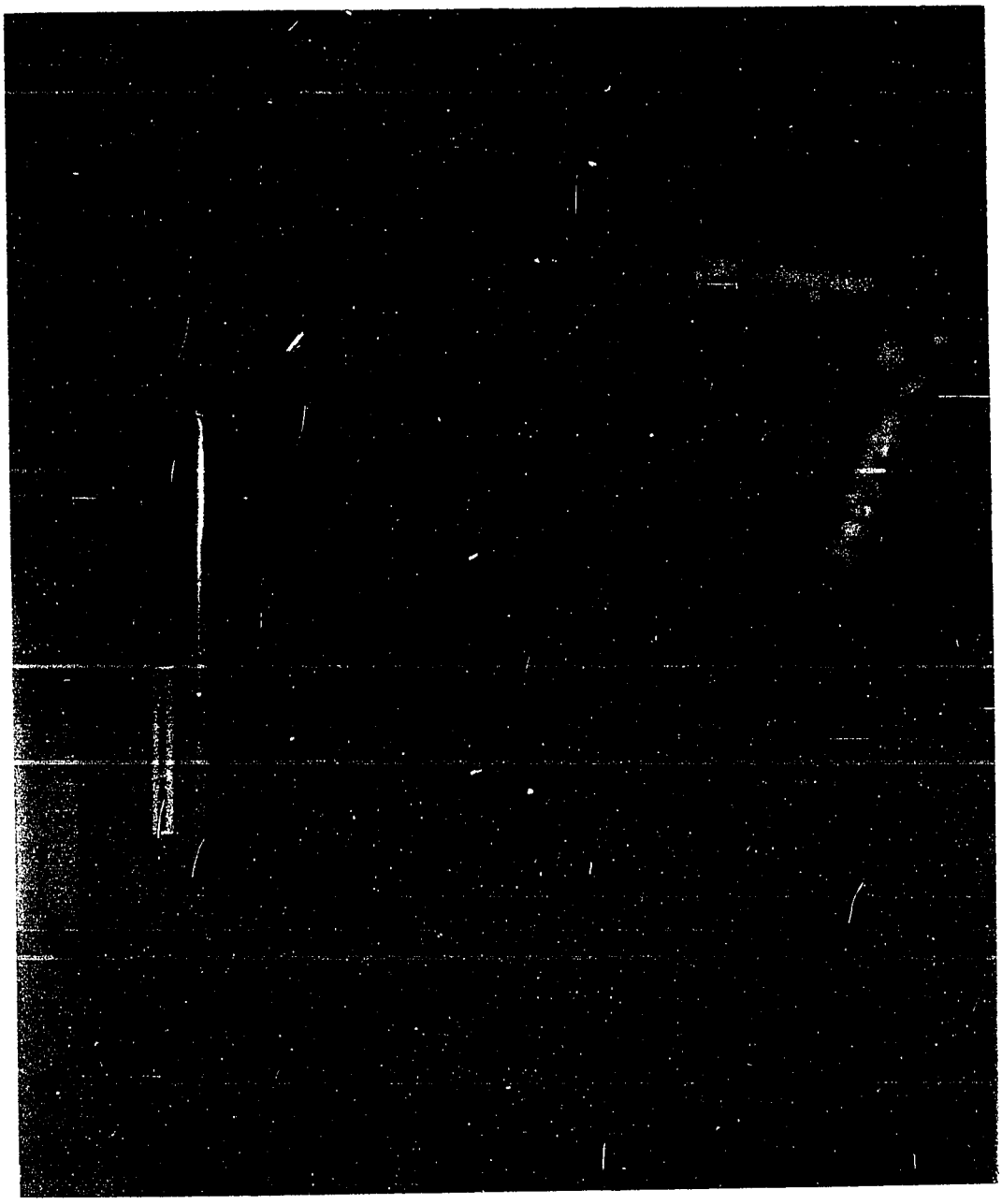

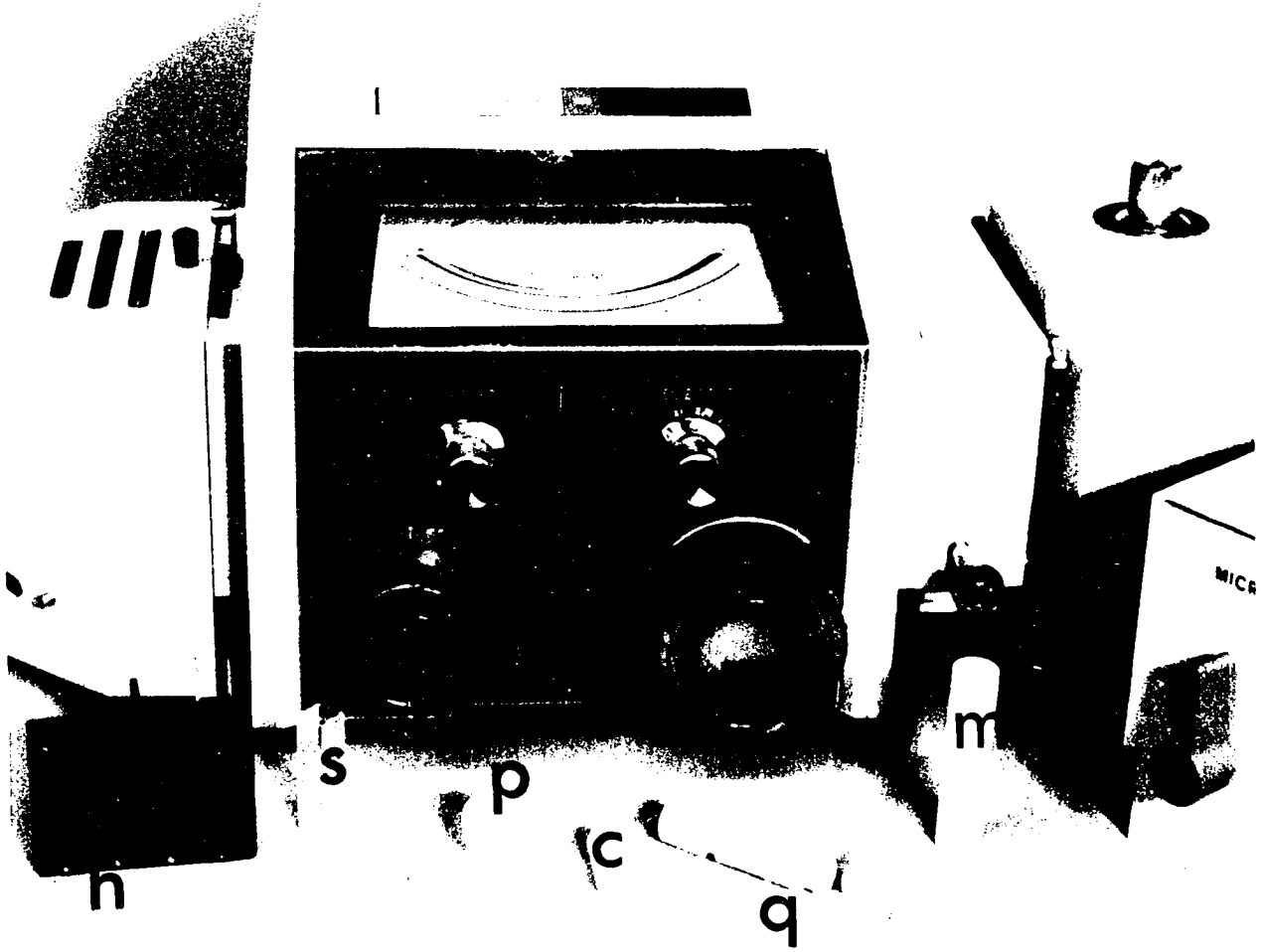
m
s
p
c
q
h

minimum measurable dose using the 224 nm peak is 500 rads. When the irradiation is done in glass containers, the reproducibility of the measurements is 1%. These cells are made of teflon with quartz windows, and are cylindrical in shape (Fig. 4). Their use is an innovation in dose-measuring techniques, which is of special use in clinical dosimetry.

These microcells could not be matched and showed a maximum variation of 10% absorbance between cells. To determine the change in absorbance, one of the cells was filled with purified water and its absorbance was used as a reference. The absorbance of the unirradiated control samples and the irradiated samples were measured using a second cell. The difference in absorbance between the irradiated and unirradiated samples gives the change in absorbance A (discussed in Appendix II). Although the absorption measurements were generally made at 224 nm, some comparison measurements were made at 304 nm.

Since the temperature in the irradiation and measuring areas did not vary significantly (within $\pm$ 1C^{o}), no temperature control of the cell compartments was necessary. The temperature at the time of measurement was noted and corrections as stated in equations 7 and 8 of Appendix II were applied.

3. Limitations and Accuracy

The doses involved in the standard technique (using 1 cm cell at 304 nm) were 4 kilorads and above, and allow reproducibility of 1% when glass irradiation cells are used. When the irradiation cells were made of polystyrene the inaccuracy increased to 3%, as the results in section III A - 5 show. This technique required long irradiation times (15 to 90 minutes on the Asklepitron 35). Use of the micro-dosimetric technique reduces the time involved in ferrous sulphate dosimetry and produces results of the same accuracy.

The uncertainty in the reported G-values and the lack of sufficient data for electron energies above 20 MeV are the principal limitations of this dosimetric system. Assuming a constant G-value at all electron energies employed in this work, the spread in G-values as determined by the calorimetric method is $\pm$ 2% (Appendix II).

As reported by others, influence of impurities in the H_2SO_4, which cannot be eliminated by adding NaCl, is found to vary between dose equivalents of approximately 50 rads (79) and 1000 rads (24). The error due to impurities in ferrous ammonium sulphate is even greater. In addition, these errors seem to depend on the individual handling the dosimeter, even when chemical samples from the same stock are used (24).

The enhanced absorbance produced by the use of polystyrene irradiation cells, as shown in section III A - 3, is a

result of electronic nonequilibrium at the interface (called boundary effects). The 100 to 150 rads dose-equivalent background resulting from this effect is negligible when large doses are measured. In microdosimetry, however, this would be very significant.

B. THERMOLUMINESCENT DOSIMETRY

1. Form of Dosemeters and Dispensing

TLD-100, in the loose powder form, has been used in this work in quantities of 35 to 100 mg. For irradiation the powder is contained in the plastic capsules shown in Fig. 7. These capsules are made of nylon and have water-tight caps, so that they can be used for intracavitary measurements in patient treatment as well as for measuring doses in water phantoms. Since the electron density of nylon is higher than that of polystyrene, a comparison was made, at various photon and electron energies, between the nylon and polystyrene capsules of identical dimensions. The results of this test is given in Table I, which demonstrated that the 1 mm nylon wall does not significantly affect the TL response, and hence produces negligible inhomogeneity in the medium.

To facilitate the measurement of dose at the surface and in the build-up region of an irradiated absorber, monocrystalline layers of TLD-100 were spread uniformly in a slight recess (1.5 cm in diameter) in polystyrene discs (Fig. 7) which were designed and

Figure 7

Thermoluminescent dosimetric accessories: -

a - monocrystalline layer TLD; d - manual dispenser;

h - heating planchet on drawer; n - TLD capsules; and

v - automated dispenser.

Figure 7.

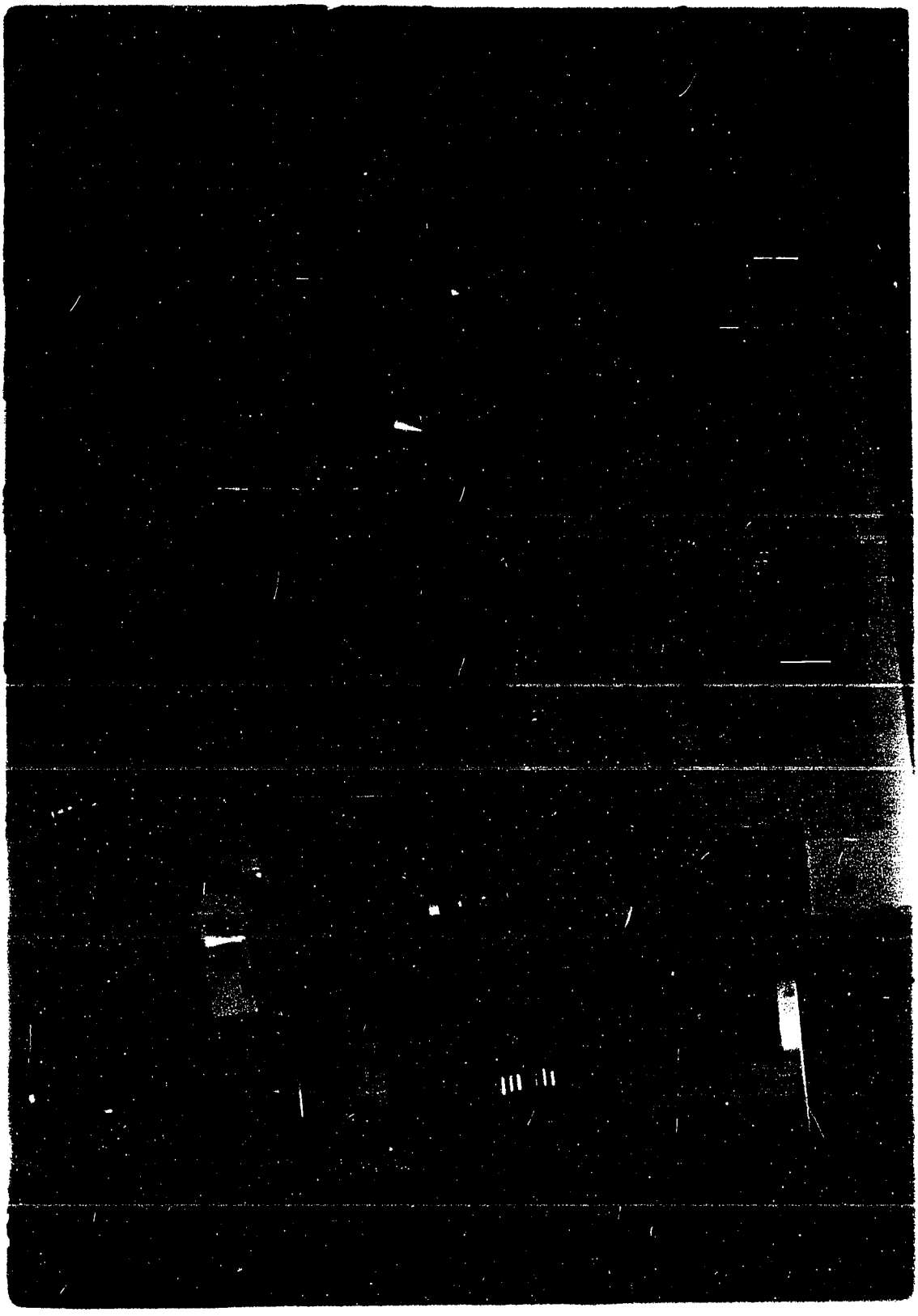

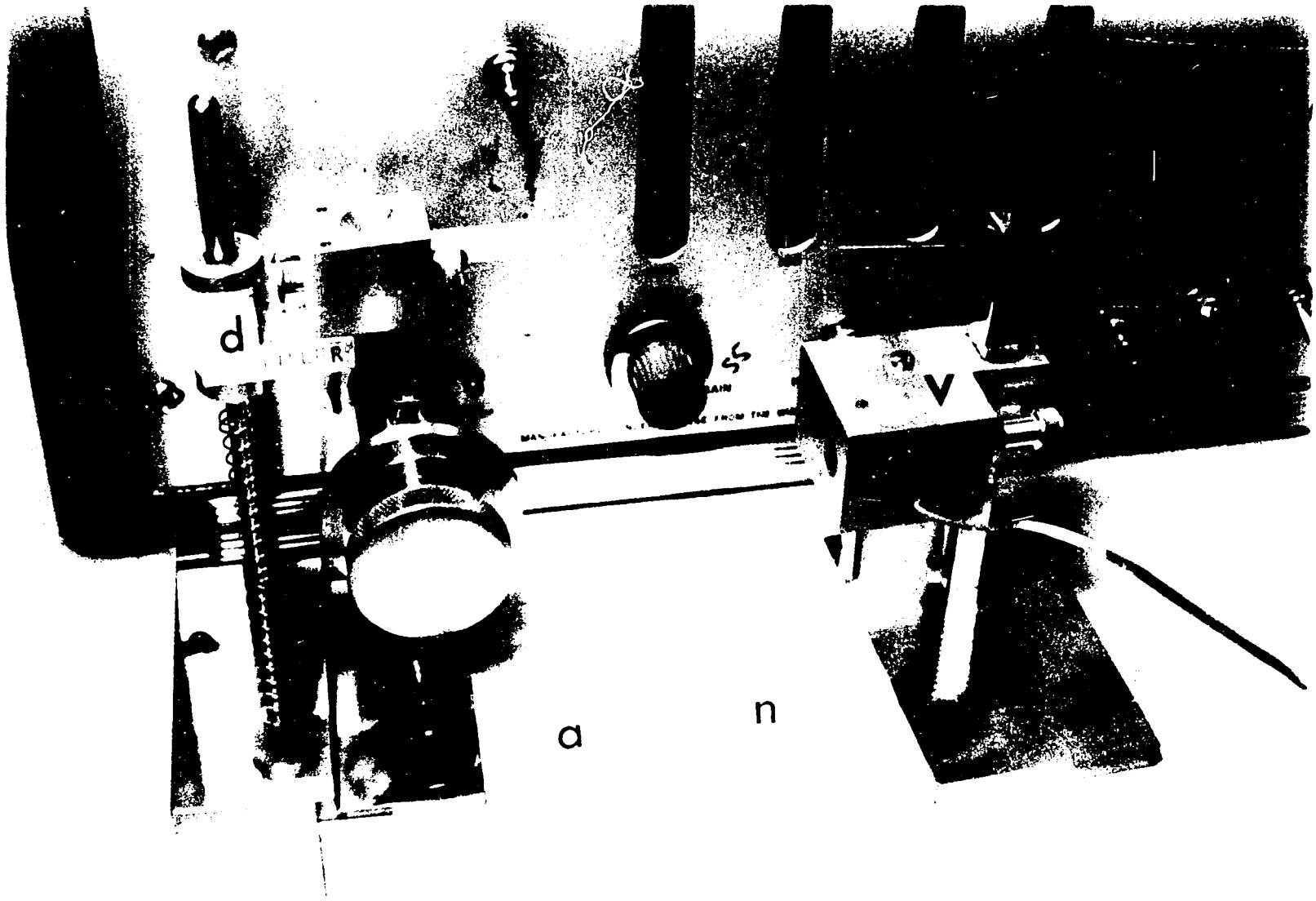
d
a
n

TABLE I

Results of Comparison of Nylon and Polystyrene TL Capsules

Type of radiation	TL response measured with capsules of nylon	polystyrene
90 kV x-rays	1.00 ± 0.01	1.01 ± 0.01
250 kVp x-rays	1.00 ± 0.01	1.00 ± 0.01
Co-60 γ-rays	1.00 ± 0.01	1.00 ± 0.01
32 MV x-rays	1.00 ± 0.01	0.99 ± 0.01
10 MeV electrons	1.00 ± 0.01	0.99 ± 0.01
35 MeV electrons	1.00 ± 0.01	1.01 ± 0.01

built as a part of this work. These discs vary in thickness from 1 mm to 5 mm, so that doses in the build-up region can be measured at 1 mm separations. They can be filled and stacked one over the other, and irradiated en masse to determine a depth dose distribution.

The fixed quantity of TLD-100 for irradiation or measurement, is measured out in a specially constructed dispenser (Fig. 7). The dispenser measures a fixed volume of the powder, which fills a hole in the sliding rod. When this rod is in the filling position the MANUAL DISPENSER must be tapped gently and consistently to ensure proper filling. In the AUTOMATED DISPENSER this effect is achieved by an electrical vibrator. After filling, the rod is slid into the dispensing position, to dispense the powder into the capsule, polystyrene disc, heating planchet, or other receiver. The integrated thermoluminescent output, for a given dose, depends on the weight of the powder used; thus the amount of irradiated powder used for each TL reading must be measured with the dispenser. The accuracy, as determined by dispensing and weighing more than 100 batches, was 0.7% with the manual dispenser, and 1% for the vibrator dispenser. When this test was repeated by another person, not so skilled, the manual dispenser gave a standard deviation of 2%, while the vibrator standard deviation was unchanged.

2. Irradiation Techniques

For relative measurements of doses in the range 50 to 1000 rads, TLD-100 is very useful because of its reproducibility of 1%. It has the additional advantage that it can be read at any convenient time after irradiation. However, since thermoluminescent dosimetry is not absolute, it must be calibrated with reference to an absolute system. In the electron dosimetry reported here, the calibration was done by comparison with the ferrous sulphate dosemeter. During the calibration exposures the ferrous sulphate and TL dosemeters were placed side by side in the polystyrene phantom (Fig. 8), in an equi-dose region, and irradiated to the desired dose. The exposure was controlled by the monitor chamber, and registered in clicks.

In relative measurements of depth dose and field distributions, TLDs alone were used. When measuring relative dose distributions in a plane, the TLD capsules were inserted into a matrix provided in a block of polystyrene (Fig. 8). This block was then placed in the polystyrene phantom so that the capsules were centered at the desired depth.

Build-up and depth dose measurements were performed using the monocrystalline layers of TLD-100. In Fig. 9, three build-up curves, measured in this way, illustrate build-up of dose due to irradiation with 250 kVp filtered x-rays, Co-60 γ-rays and 32 MV

Figure 8

Polystyrene irradiation phantoms: - R - for simultaneous irradiation and dosimetric comparison; S - for depth dose and point dose measurements; and T - for distribution studies.

Figure 8.

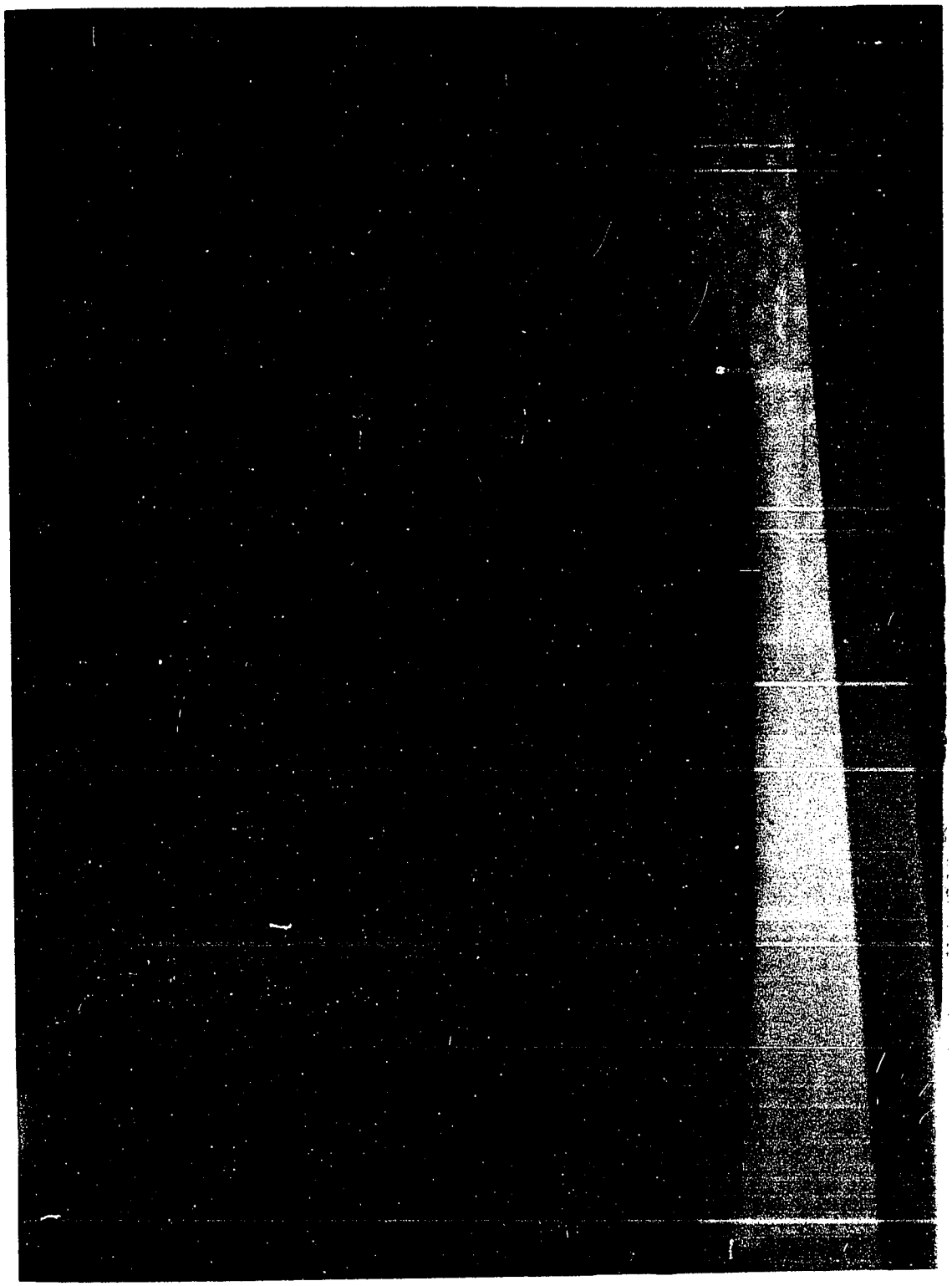

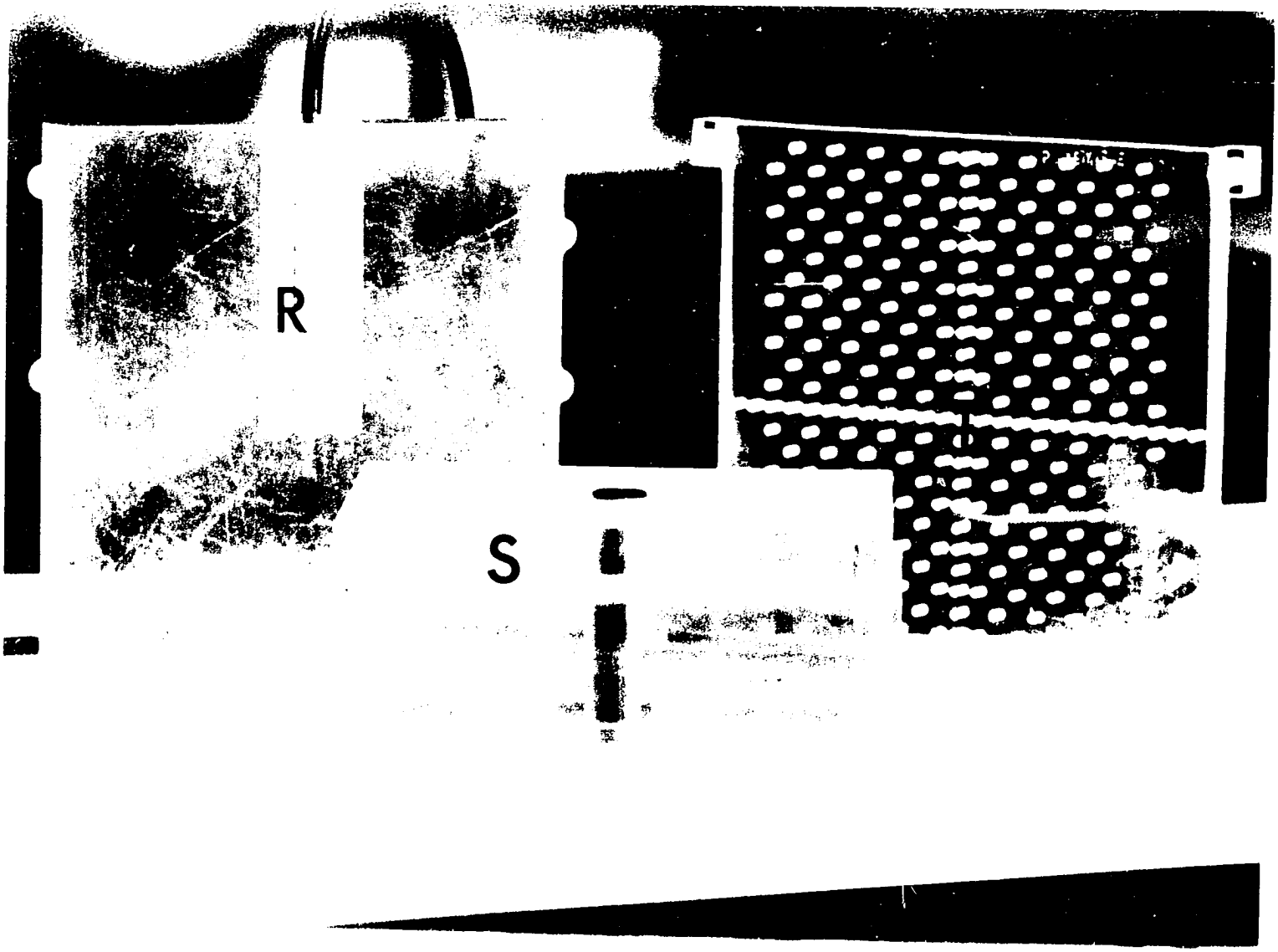
R
S

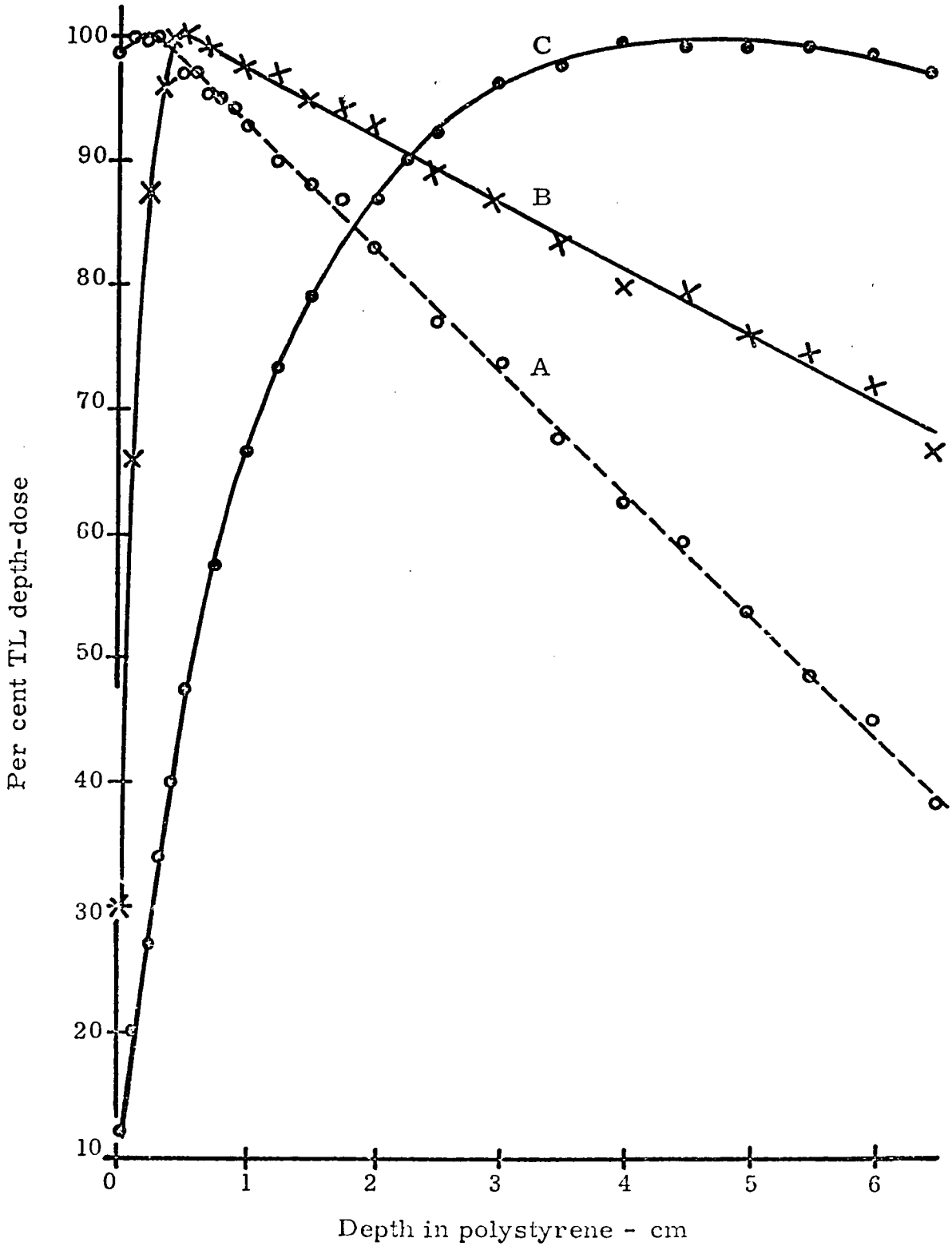

Fig. 9 : Build-up curves measured by the monocrystalline TLD-100 discs. A - 250 kVp (filtered) x-rays; B - Cobalt-60 gamma rays; and C - 32 MV x-rays. The surface doses are 98, 30, and 12 per cent of peak dose, respectively. The field size for all measurements were 4 x 4 cm.

x-rays. When measuring these curves, a stack of discs containing monocrystalline layers of TLD-100 was inserted into the polystyrene phantom, as shown in Fig. 8. The phantom was then placed in the radiation beam, with its surface perpendicular to the central-axis of the beam, and the stack of dosemeters were made to coincide with the central-axis. In all such comparative studies using electrons, the exposure was in the range 100 to 250 clicks.

To examine the possibility of error introduced by stack irradiation, a comparison was made of the results of a single irradiation of stacked dosemeters, multiple irradiations of single monocrystalline dosemeters, and a single irradiation of nylon capsule dosemeters. The results are shown in Fig. 10, and the agreement is within experimental limits.

3. Measurement Methods

The TL output was measured using a Madison Research Model S-2 Thermoluminescent Radiation Exposure meter. This is equipped with a planchet, 1 cm in diameter and 3 mm deep, into which the TLD-100 is dispensed for TL measurements. The planchet and the powder are heated from a high current transformer, at 80 to 150 amps. A powerstat is provided in the primary circuit to control the maximum heating temperature. In addition, a timer in the operating circuit can be set to limit the heating time up to a maximum of 60 seconds. The

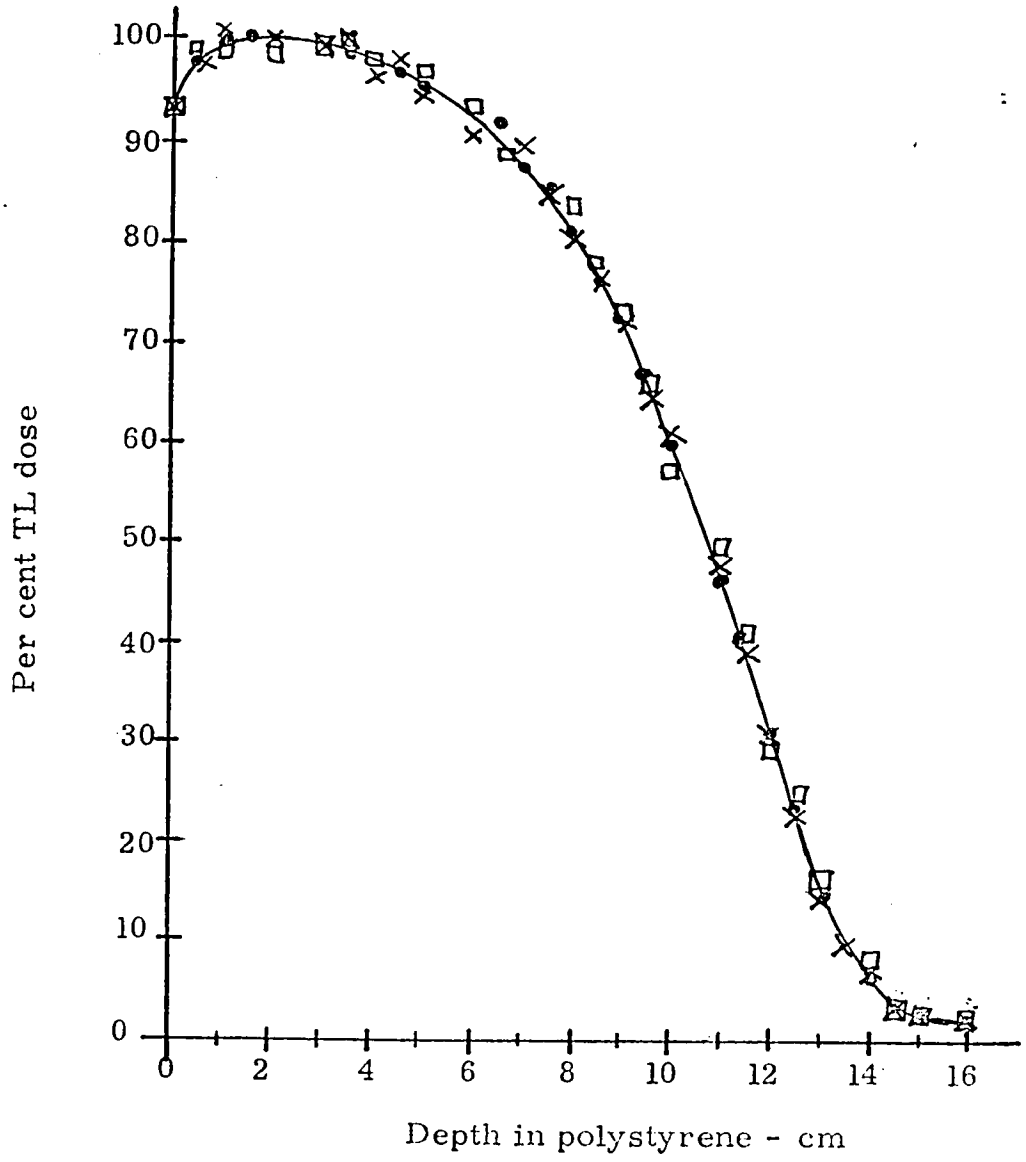

Fig. 10 : Central-axis depth-dose curve for 30 MeV electrons; 8 cm diameter beam. ○ - measured in stack irradiation of the microcrystalline layers; □ - measured in multiple irradiation of one monocrystalline layer TLD-100 at a time; × - measured with TLD-100 capsules. The standard deviation of measurement is 1%.

heating rate, as shown in Fig. 11, is non-linear for any setting on the powerstat. The nearly-linear heating curve is the result of a modification made in the course of this work. The heating current is continuously varied by changing the powerstat setting through 80% of its range in 60 seconds, by means of a reversible motor. At the end of the heating-reading cycle the motor is reversed to drive the powerstat back to its starting position.

A precisely measured weight, usually 30 to 35 mg, of irradiated powder is placed in the planchet, which is attached to the drawer shown in Fig. 7. When this drawer is pushed in, the planchet is positioned under the photomultiplier tube, and the heating cycle is started automatically. The temperature of the TLD sample reaches $300^{o}C$ by the end of the heating cycle.

The emitted light, after passing through a blue filter, is detected by a photomultiplier tube whose output is fed into an analog-to-digital converter. The digital readout is proportional to the integrated light output of the samples. With careful dispensing technique these TL readings can be reproduced with a standard deviation of 1%.

The instantaneous photomultiplier current can be plotted, after amplification, to obtain a "glow curve" of the emitted light, as discussed in the following section. The light output may be plotted against heating time or against powder temperature with the aid of a

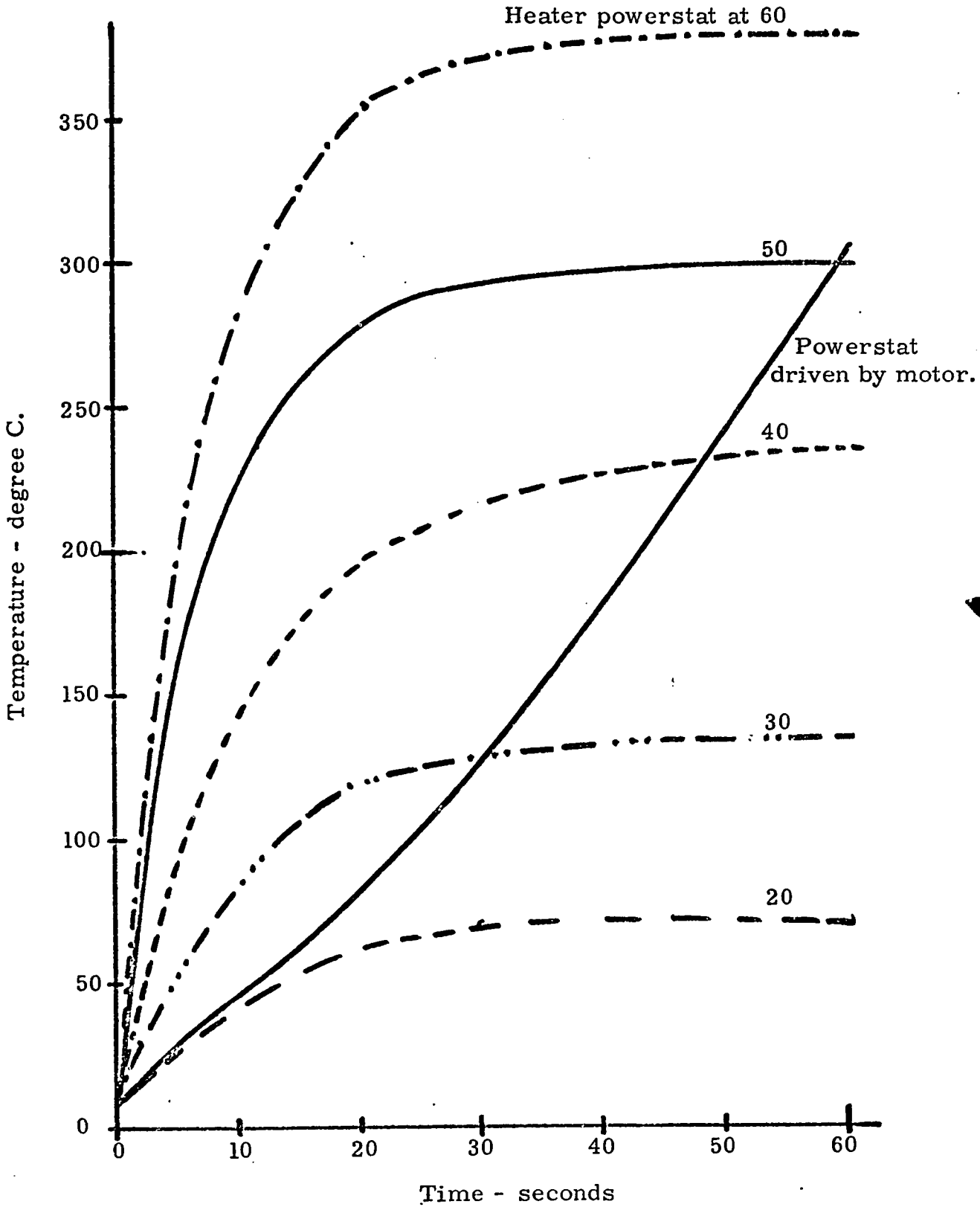

Fig. 11 : The heating rate of the TLD reader planchet at different voltage setting on the powerstat in the primary circuit of the heater transformer. The heating rate which is almost linear is obtained after modification.

thermocouple attached to the planchet.

4. Glow Curves - Temperature Peaks

A curve of thermoluminescent emission as the temperature of the phosphor is raised is referred to as a GLOW CURVE; it gives a qualitative indication of the performance of the phosphor as a dosemeter. The shape of the glow curve of a phosphor depends upon the "trap depth" and the number of filled traps (84). The binding energy of the trapped electron is called the trap depth. Each set of trap depths results in a glow peak at a characteristic temperature; the TL intensity of the peak is proportional to the number of filled traps at the corresponding depth.

According to Randall and Wilkins (84), the TL intensity and temperature of the peak depend on the rate of heating. The glow curves of Fig. 12 illustrate this dependence, Curve A is the glow curve of a sample of used TLD-100 annealed at 400°C for one hour, irradiated to 100 rads, and then heated at the uniform rate of the modified TL reader. There are three glow peaks, at approximately 110°, 160°, and 215°C. The glow curve of an identical sample heated at the non-uniform rate of the unmodified reader, is given alongside (Fig. 12, curve B). In this the separate glow peaks are not apparent and the shape of the curve is distorted. In both cases the principal glow peak corresponds to a trap depth of 1.25 eV (60).

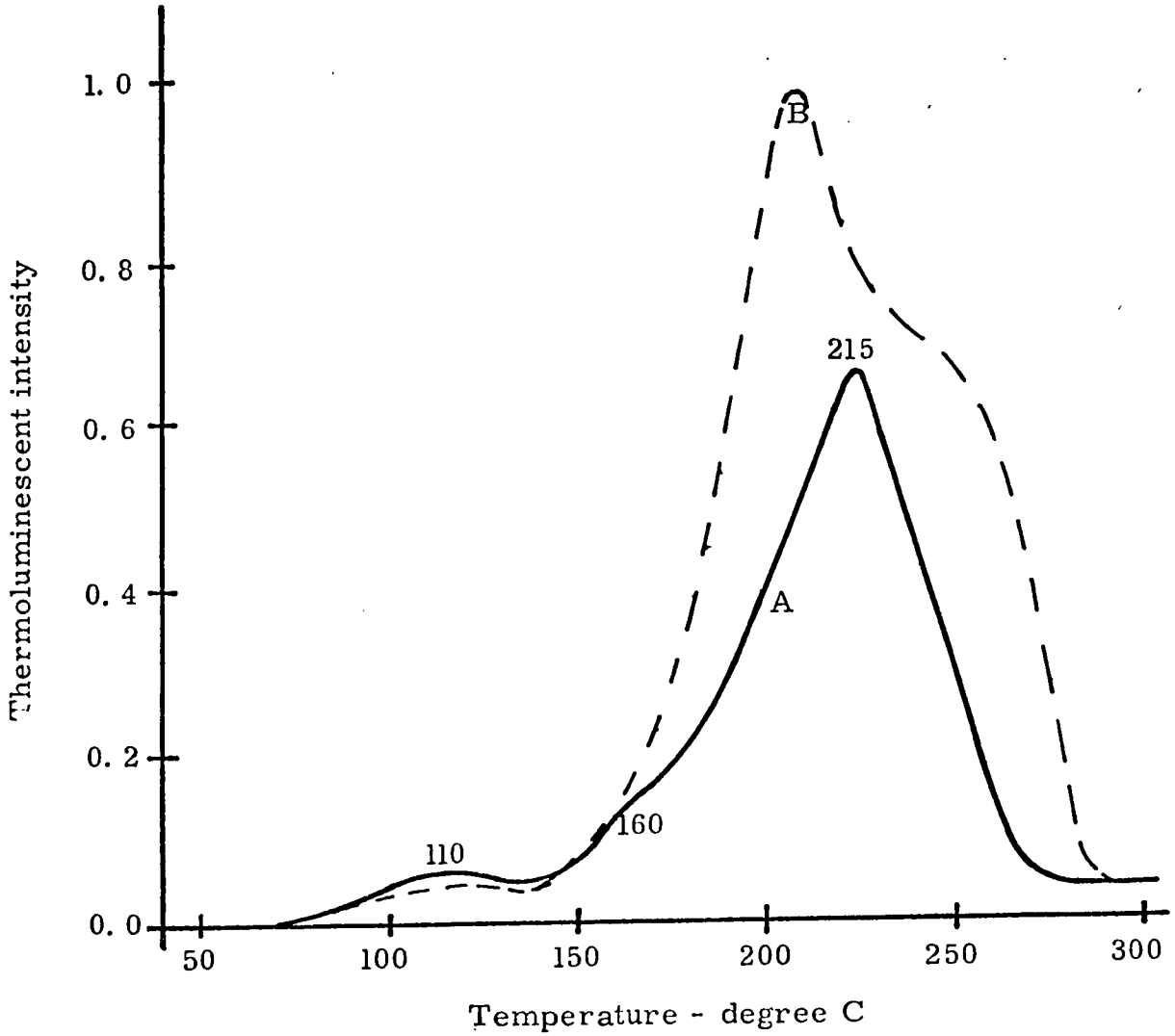

Fig. 12: Glow curve of TLD-100 annealed at 400°C for 1 hour and irradiated to 100 rads at 30 MeV electron energy. The solid curve is taken with the linear heating rate shown in Fig. 11 and the dashed line curve is taken at the non-linear heating rate.

5. Automation of Measurements

Successive reading of a number of TLD samples is tedious and time-consuming. Loading the planchet, heating, recording the result, unloading, and cooling requires two minutes of undivided attention per measurement. To date no commercial manufacturer of TL readout equipment has produced an automated device, so one was designed and constructed in order to minimize the measurement time in TL dosimetry (Fig. 13).

The electrical circuit of this device is shown in Fig. 14. The operating cycle is as follows: after the table is rotated by motor M_1 to place the next planchet into position under the readout photomultiplier tube, the floating terminals XY are brought into contact with planchet at AB by solenoid P_2. Cam 3 of the timer* then causes P_4 to close, to provide heating current through XY to the planchet. The TL dosemeter is then heated on the planchet to 300°C at a rate of 20C° per second. Relay P_3, operating with P_4, starts the counter which registers the TL "counts". These are stored in the memory of a 512 channel analyzer and the data printed out by a typewriter at the end of the operation.

Table II gives the TL counts measured using the automated readout device, of 23 samples of a batch of TLD-100 irradiated with electrons to a dose of 200 rads. The standard deviation of these

* Metrix Super MSC miniature camshaft timer.

Figure 13

Automated Thermoluminescent dosimetry reader: - H - turn-table with heating planchets; P - photo-multiplier tube detector assembly.

Figure 13.

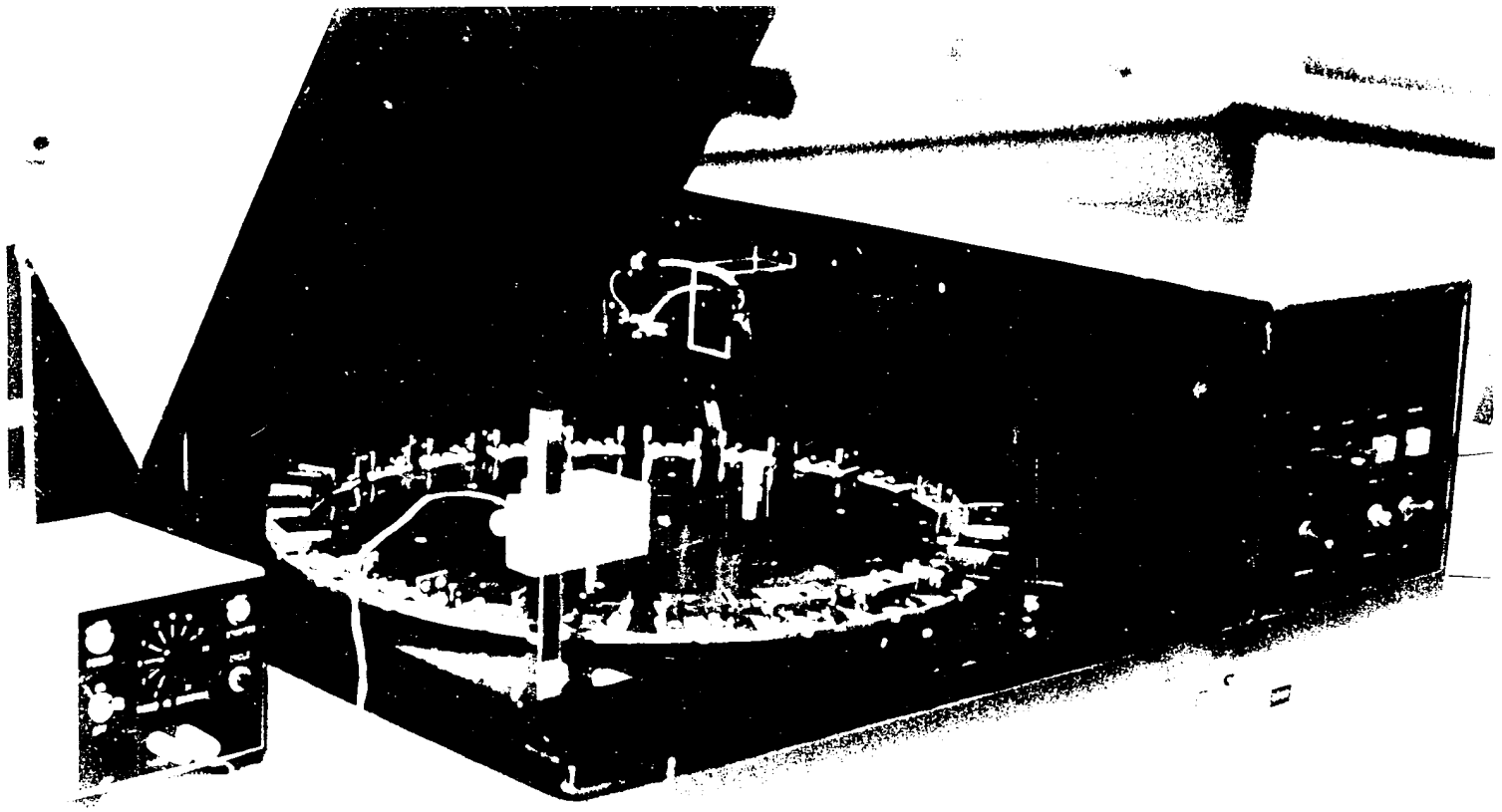

Figure 14

Wiring diagram for the Auto-TLD Reader.

Microswitch: K_1 - start, K_2 - stop, K_3 - light source safety, K_4 - turn-table positioning.

Relay: P_1 - hold and put power into the cycling circuit, P_2 - pulls down heater terminals, P_3 - zeros and starts the counting (ADC), P_4 - puts power in the heating circuit.

Switch: S_1 - power on, S_2 - momentary operate.

Transformer: T_1 - power transformer, T_2 - powerstat.

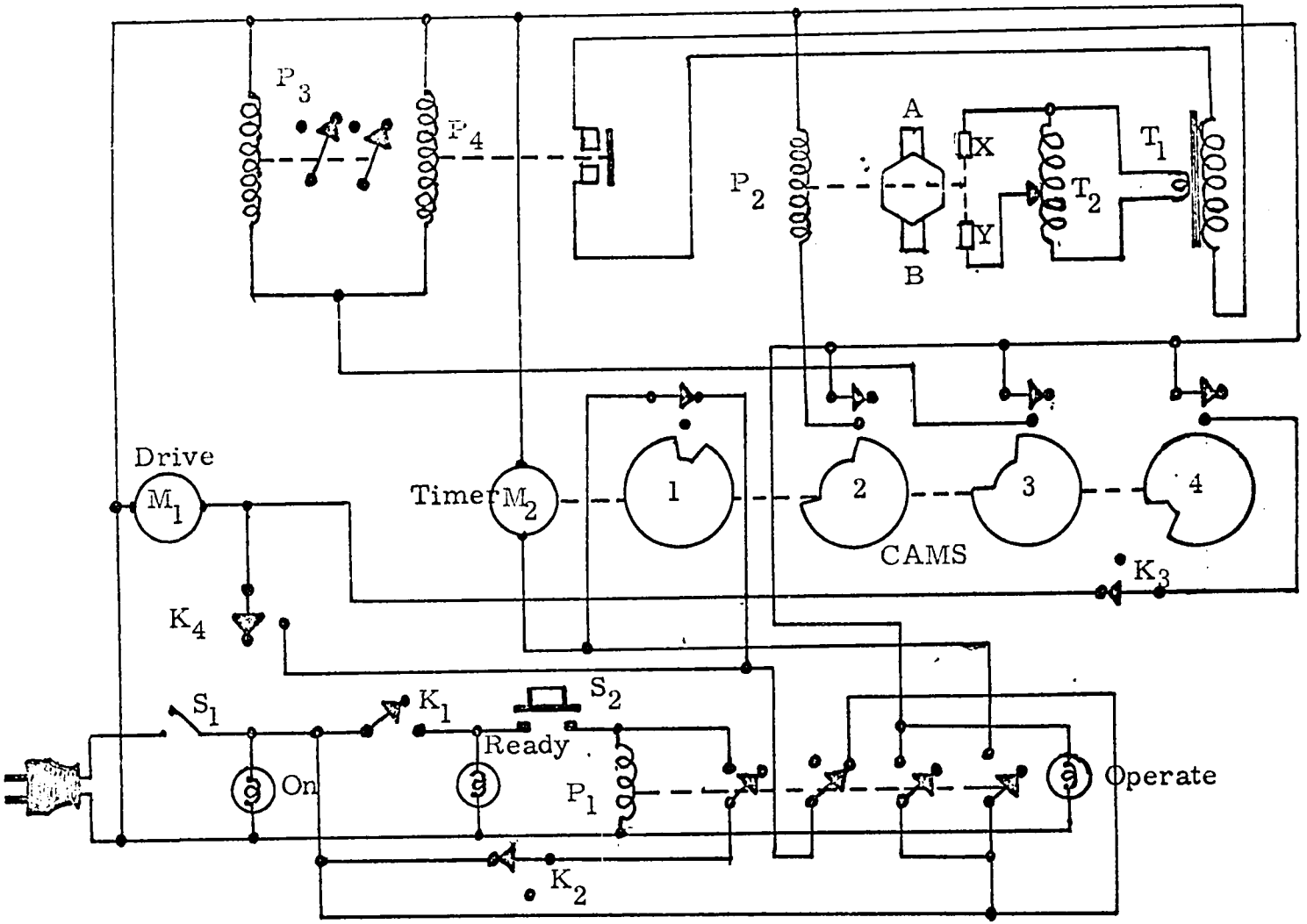

Fig. 14: Wiring diagram for the Auto-TLD Reader.

TABLE II

TL counts of TLD-100 samples irradiated to 200 rads (35 MeV electrons) and measured with the automated TL reader. The data have been stored in the 512 channel analyser and printed out at the end of measurements. The background values obtained on remeasuring these TLD samples have been subtracted from the measured counts to obtain net TL counts.

Planchet number	Net TL counts at photomultiplier voltage of 1300	1500
1	..	..
2	1552	5003
3	1556	4901
4	1430	4781
5	1436	4879
6	1569	4879
7	1462	4739
8	1458	4728
9	1464	4636
10	1497	4920
11	1581	5008
12	1504	4977
13	1500	4881
14	1516	5031
15	1547	4983
16	1480	4732
17	1524	5051
18	1478	4870
19	1503	4870
20	1466	4978
21	1487	4889
22	1515	5034
23	1539	4996
24	1492	4897
average	1502	4898
standard deviation	42	113
% s. d.	2. 8	2. 3

measurements is 2.6%, compared with 1% when read on the manually-operated Madison Research reader. The increase of 1.6% is purely instrumental, and is caused by the variation in heating by the floating contacts and the difference in resistance between planchets. Another source of error is the non-uniform spread of the TLD powder in the planchets of the automated reading device. Considering the advantages of automating the measurements, this 1.6% increase in the standard deviation is acceptable in clinical dosimetry.

C. IONIZATION CHAMBER DOSIMETRY

1. Principles of Measurements

Ionization chamber measurements depend on the separation and collection of the positive and negative ions produced in a gas by ionizing radiations. To avoid recombination of these ions, an electrostatic field must be maintained in the volume containing the gas. In order to have a maximum collection efficiency, the voltage applied to the electrodes must be great enough to produce a saturation current.

Air ionization measurements of energy dissipated in a medium necessitate the introduction of a volume of air into the medium. This constitutes a discontinuity, referred to as a CAVITY. The first rigorous statement of a relationship between energy absorbed in a medium and the ionization produced in a cavity in the medium is contained in the Bragg-Gray principle, given in equation (i).

The cavity theory was originally derived for x- and γ-rays. The use of a gas-filled cavity to determine the absorbed dose in a medium irradiated with electrons does not present any essentially new problem. In both cases the absorbed dose at a point in a medium depends upon the particle fluence and spectrum at the point. When high energy electron beam enters an absorbing medium, the particle fluence and electron spectrum change rapidly along the beam direction. Under these conditions it is difficult to determine the energy spectrum of electrons crossing the cavity. Consequently, the determination of the mass stopping power ratio of the medium relative to air, becomes difficult. The increase of polarization correction with electron energies above 2 to 3 MeV (Appendix I) causes this mass stopping power ratio to vary significantly. Mass stopping power ratios and polarization corrections must be averaged over the electron spectrum at the point of measurement.

2. Measurements with Air-filled Cavity Chambers

Two cylindrical cavity ionization chambers (called thimble chambers) were employed in this work; one was a commercial "Baldwin-Farmer" type while the other, of pure polystyrene, was designed and constructed (shown in Fig. 15) for the reasons mentioned below. In most of the measurements the charge collection method was used (35).

Figure 15

Ionization chamber dosemeters -

A - Baldwin-Farmer chamber;

E - all polystyrene parallel-electrode chamber; and

T - all polystyrene thimble chamber.

Figure 15.

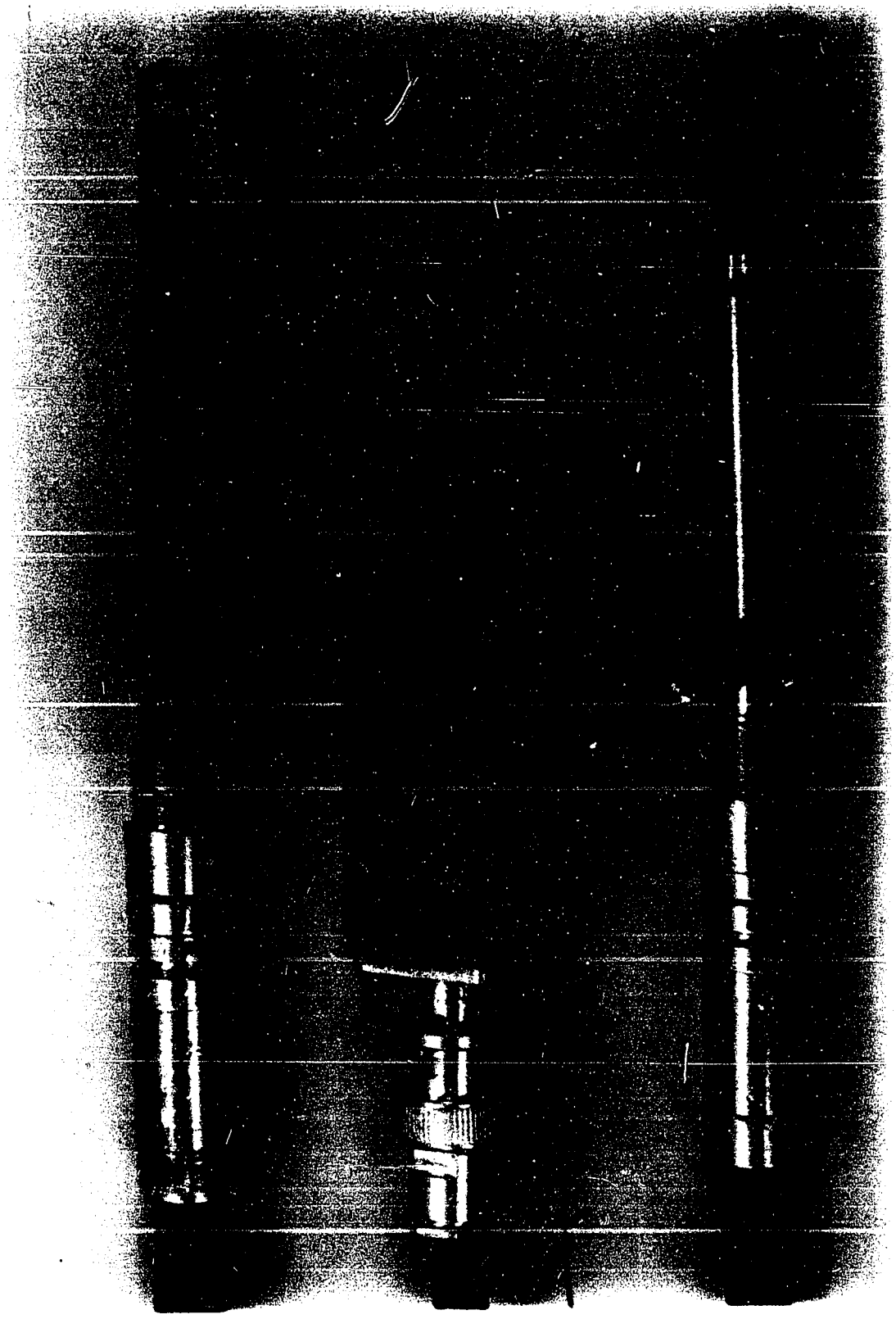

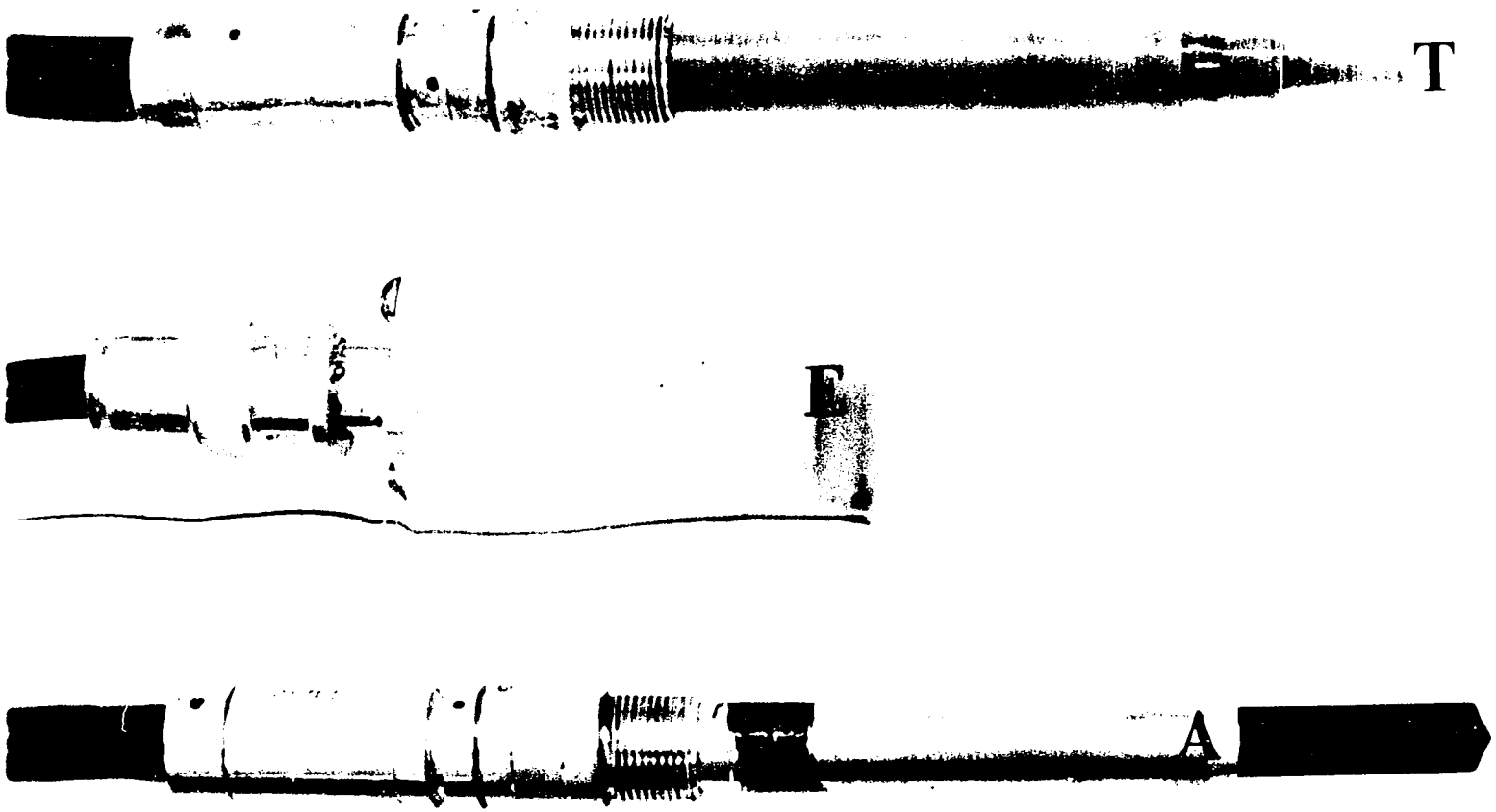
T
F
A

The Baldwin-Farmer chamber is constructed of tufnol (a mixture of phenol resin and cloth) and aluminum. Since the stopping powers of these materials differ from that of polystyrene (the phantom material), the electron spectrum might be disturbed by the introduction of this chamber into the phantom. To examine this effect, an all polystyrene chamber was built (Fig. 16). The wall and the 0.5 mm diameter central electrode of this chamber are made of polystyrene and coated with aquadag ($\sim$ 0.02 mm thick). The outside dimensions of this polystyrene chamber are the same as that of the Baldwin-Farmer (BF) chamber. Inserted into a polystyrene phantom, it should produce a better approximation to a Bragg-Gray cavity than that afforded by the Baldwin-Farmer chamber.

Both these thimble chambers, like the TL and ferrous sulphate dosemeters, were irradiated in a polystyrene phantom (Fig 8). As an example, when the BF chamber was used to measure electron beam output, it was irradiated side-by-side with the ferrous sulphate dosemeter in the polystyrene phantom. The dosemeters were centered at the preselected depth. Since the calibration of the ionization chamber instrument must yield a conversion factor in terms of Baldwin-Farmer "R" per rad, the air-density corrected Baldwin-Farmer reading was divided by the number of rads as determined by the ferrous sulphate method. The result of this procedure may then

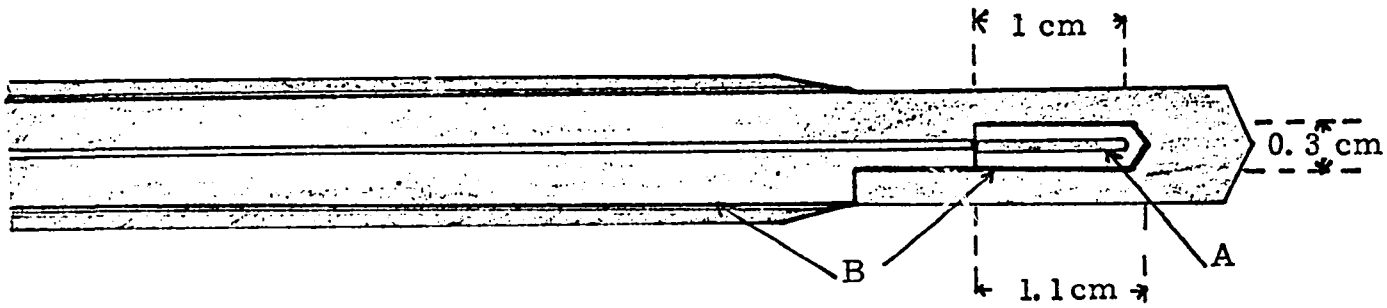

A - Collecting electrode, 0.5 mm diameter polystyrene wire coated with aquadag.

B - Outer electrode, aquadag coated on polystyrene wall.

Cavity dimensions: 0.03 cm diameter cylinder, 1.1 cm long.

Fig. 16 : All polystyrene thimble ionization chamber.

be applied to the determination of absorbed dose in rads by the use of the commercial Baldwin-Farmer Instrument.

It will be recalled that, incorporated into the betatron is a monitor chamber which is connected to a charge integrator that registers one click when a specific amount of charge has been collected (section I). The response of the Baldwin-Farmer chamber under standard irradiation conditions can be related to the magnitude of the click by simultaneous measurement. In this case, since neither chamber is sealed, no correction for air density is required.

Thimble chambers are widely employed for electron dose determinations. A factor C_F has been suggested to convert the results of ionization measurements into absorbed dose in rads (4, 93). It is defined by the relation

$$D_m = R \cdot N \cdot C_F , \qquad \text{(iv)}$$

where R is the ionization chamber instrument reading corrected to $22^{\circ}C$ and 760 mm Hg, and N is the Co-60 γ-ray calibration factor of the ionization chamber, as provided by the National Laboratory. From equation (iv) and the Bragg-Gray relation given in equation (i),

$$C_F = K \cdot \rho_s \cdot W , \qquad \text{(v)}$$

where K is a constant, ρ_s is the ratio of the mass stopping powers of the medium and air, and W is the average energy dissipated in air

per ion pair formed (33.7 eV). Theoretical values of C_F have been calculated from this relation (5), and experimental values have been obtained from measured values of D_m and R. The absorbed dose D_m is usually measured with radiation calorimeters or with ferrous sulphate dosemeters. The ionization value R is measured with thimble ionization chambers and associated electrometer circuitry.

3. Variable Volume Parallel-electrode Chamber

For measuring polarization corrections, an all-polystyrene parallel-plate ionization chamber was built. A cross-section of this pillbox-shaped chamber is shown in Fig. 17. The electrode separation of this chamber could be changed in order to vary the volume between 0.25 and 1.25 cm^3. The top and bottom surfaces of the cavity were made electrically conducting with aquadag and connected to an electrometer. Measurements at known exposures of Co-60 γ-rays were used to calibrate the response of this chamber and its associated electrometer in terms of e s u per cm^3. At the maximum separation of the electrodes, the cavity dimensions are identical to those of the pillbox shaped ferrous sulphate irradiation cells, shown in Fig. 3.

D. POLARIZATION PHENOMENON

1. Effects of Polarization

The polarization of atoms in the absorber by the field of

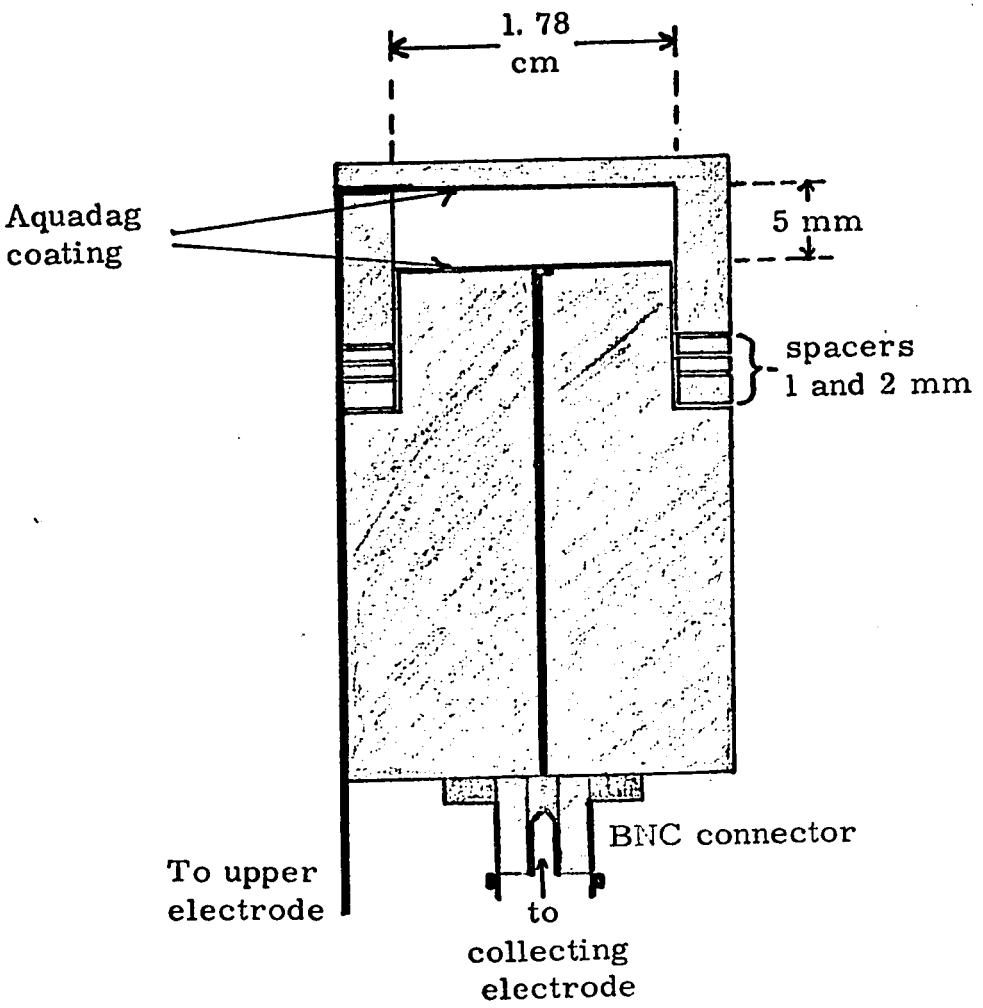

Fig. 17 : Cross-section of the pillbox-shaped parallel-plate ionization chamber.

the passing electrons shields more distant atoms and tends to reduce the effective field intensity at a distance from the electron's path. Consequently the amount of energy loss is reduced, especially that associated with distant collisions. This density effect becomes more pronounced in denser materials and hence the stopping power of a gas is greater than that of a solid or liquid. Accordingly, ionization measurements in electron beams will give indications of higher absorbed doses than those actually occuring in the surrounding material. This is one of the principal correction factors that must be evaluated if electron absorbed doses are to be derived from air ionization measurements.

The mass stopping power of any medium — gaseous, liquid, or solid — tends to increase with electron energy (Fig. 18); as does the polarization correction (Fig. 19). Absorbed dose measured in polystyrene has been shown to be 3% higher than that in water (68). Since ferrous sulphate solution has a mass stopping power which is only 0.3% greater than that of water (79), ferrous sulphate dosimetry is used as the basis for the experimental determination of the polarization correction in electron dosimetry.

2. Method of Measurement

The mass stopping power of a dense medium is reduced as a result of the polarization of the medium by the charge of the passing electron. In a tenuous medium this reduction is insignificant.

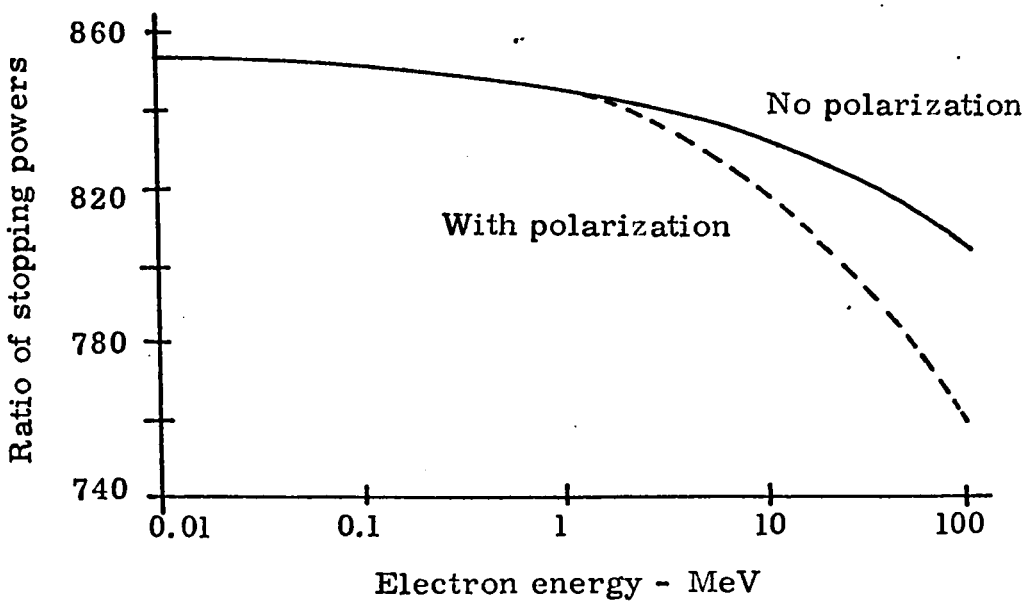

Fig. 18: Variation of the ratio of mass stopping power of water relative to air, as a function of electron energy (64).

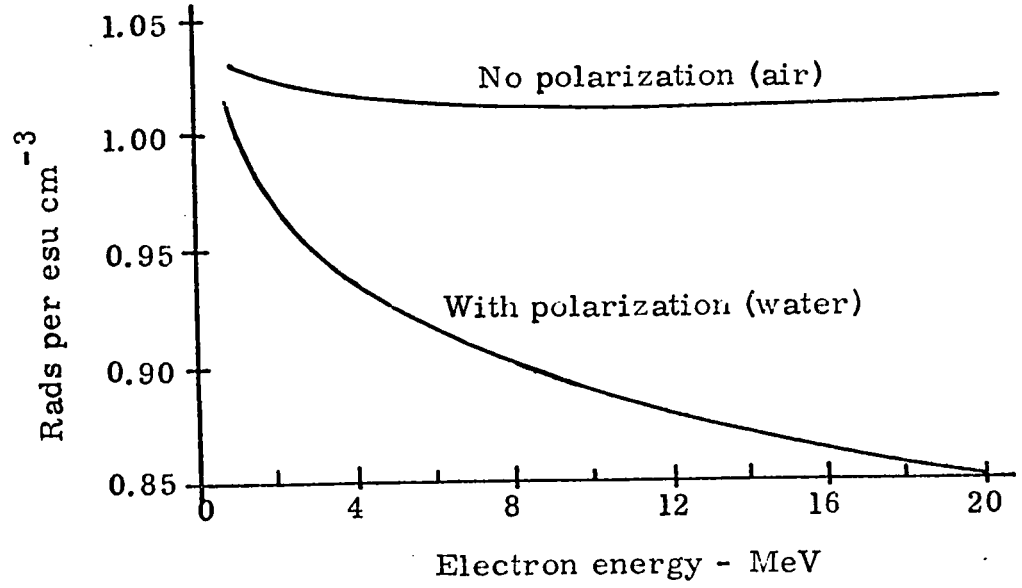

Fig. 19: Effect of polarization on absorbed energy in water and in air (adapted from 64).

Consequently, one would expect the true absorbed dose in a medium such as tissue, water or polystyrene to be less than that determined from air ionization measurements in the medium.

According to theory (64) this polarization effect is negligible in these tissue equivalent media at electron energies below 3 MeV; e. g. under conditions of Co-60 γ-ray irradiation. It has also been shown theoretically (64, 102) that the mass stopping power of water (or polystyrene) relative to air is a constant independent of energy, if the polarization effect is ignored.

As discussed previously, if an air-filled cavity embedded in the dense medium fulfills the requirements of a Bragg-Gray cavity, the ionization J_m produced within it is related to the energy E_m absorbed in the medium as shown in equation (i). So the mass stopping power ratio ρ_s at any electron energy T may be evaluated from simultaneous (or equivalent) determinations of E_m and J_m at that energy. If then the mass stopping power ratio is found experimentally for Co-60 radiation (NO POLARIZATION) and at electron energy T (WITH POLARIZATION), the difference between these two ratios is a measure of the polarization effect.

In this work, the ferrous sulphate solution was irradiated in polystyrene containers of the pillbox type (Fig. 3), centered at 2 cm depth in a polystyrene phantom of 25 x 25 cm cross section, under open field conditions. These measurements resulted in electron dose

values in rads per click, for accelerated electron energies in the range 10 to 35 MeV. The irradiations were repeated with the parallel-electrode ionization chamber discussed in section II C - 3. Its top electrode was set at a depth of 2 cm in the polystyrene phantom. Since the electrometer instrument connected to the parallel-electrode ionization chamber was calibrated to read in esu cm^{-3}, measurements in electron beams with it gave values in esu cm^{-3} per click. A ratio R_T of this dose in rads per click, to the ionization in esu cm^{-3} per click, would be proportional to the mass stopping power ratio of water relative to air.

Measurements were taken with the ferrous sulphate and the parallel-electrode ionization chamber dosemeters, using Co-60 γ-ray beam. The resultant ratio R_o in rads per esu cm^{-3} provided a quantity proportional to the ratio of mass stopping powers of water and air, with no polarization correction included. Any difference between R_o and R_T would be purely due to the polarization effect. Hence the ratio R_T/R_o would yield the polarization correction at the electron energies involved.

CHAPTER III.

DISCUSSION OF EXPERIMENTAL RESULTS

CHAPTER III

DISCUSSION OF EXPERIMENTAL RESULTS

The experimental results reported in this chapter provide a solid base for the measurement of high-energy electron doses in the treatment of cancer.

The sensitivity of the ferrous sulphate dosemeter has been extended to allow the routine measurement of doses smaller by a factor of 10 than those reported in the literature (section III A - 6). The volume of solution necessary for these measurements has been reduced by at least a factor of five to 0.5 cm^3, which approaches conditions of point dosimetry. In addition, some of the variables which affect the accuracy of ferrous sulphate dosimetry have been examined in more detail than previously.

In thermoluminescent dosimetry using LiF powder a reported and observed increase in both the weight of the dispensed volume and in the TL response upon annealing is explained (section III B - 2). The demonstrated dependence of the glow-curve (and hence of the total TL) upon annealing emphasizes the necessity of

care in the annealing of TLD-100 for reuse (section III B - 1). A dependence of the shape of the glow curve on heating rate has also been found, in conformation of the theory of Randall and Wilkins (84). Thermoluminescent dosemeters made up of monocrystalline layers of TLD-100 have been developed (section II B - 2), and their usefulness in the measurement of dose in regions of high dose gradient has been demonstrated. Finally, an automated TL reader has been built which greatly facilitates routine TL measurements (section II B - 5).

Comparative measurements using two ionization thimble chambers of quite different design have demonstrated that no significant perturbation of the electron fluence in the absorber results from the introduction of these chambers into it (section III C - 1). The results of measurements with a pillbox-shaped parallel-electrode ionization chamber provide a verification of the theory of charge deposition in a dielectric absorber irradiated by an electron beam (section III C - 2).

An intercomparison of the results of dose measurements using the three systems favours a constant ferrous sulphate G-value for 10 to 35 MeV electrons (section III D - 1). The magnitude of the polarization corrections determined in this work are in agreement with the published theoretical values (102), and have provided experimental data for incident electron energies up to 28 MeV (section III D - 4).

A. FERROUS SULPHATE DOSIMETRY

1. Preparation of Dosimetric Solution

A major disadvantage in ferrous sulphate dosimetry is its high sensitivity to organic impurities, which results in added ferric ion yields. In reactions involving radiolysis of H_2O, unusually high standards of water purity must be maintained. For ferrous sulphate dosimetry, water purity is obtained in three stages of distillation using pyrex stills. The demineralized water was distilled from acid dichromate, then redistilled it from alkaline permanganate. The final stage of distillation was done in a closed still with no added reagent (47). Even after careful distillations the water may contain impurities that affect such reactions as the formation of H_2O_2 in aerated water. Dewhurst (25) has shown that addition of chloride ion could largely inhibit the action of the impurities and insure correct yield values.

The dosimetric solution was prepared with analytical-reagent grade chemicals. In order to check the purity of the water used in preparing the ferrous sulphate solution, its response was checked with and without the addition of NaCl (25). The results of this test is shown in Table III. Since the variation is within experimental limits, it has been concluded that there is no organic impurity in the dosimetric solution. This experiment was performed with 35 MeV electrons and Co-60 γ-rays, and the doses involved were

TABLE III

Results of Water Purity Test with 35 MeV Electrons and Cobalt 60 γ-rays

Radiation employed	Dose (in rads) measured with the ferrous sulphate solution	
	With NaCl	Without NaCl
35 MeV electrons	1193 $\pm$ 30	1208 $\pm$ 30
Co-60 γ-rays	1024 $\pm$ 30	1019 $\pm$ 30

1000 clicks of 35 MeV electrons and 1000 rads of Co-60 γ-rays.

Even the most careful water purification is of no avail unless the vessels are cleaned with equal care. Glassware and other containers when exposed to atmospheric air pick-up a film of organic matter, such as grease. Much of this remains on the surface, and can be washed off with hot water and detergent, followed by rinsing several times with purified water. Extreme care has been exercised to avoid contamination of the solution during preparation, storage and handling. All precleaned vessels and containers were rinsed off with purified water before use.

2. Effects of Storage and Concentration

It is a general practice to store a stock solution of 10 millimolar ferrous sulphate, and to dilute it just prior to use. The rate of spontaneous oxidation of the solution on storage is found to be proportional to the first power of the oxygen concentration and inversely proportional to the square of the ferrous ion concentration (56). Consequently the spontaneous oxidation is slow in these stock solutions.

To study the effects of spontaneous oxidation on the 1 millimolar solution used in dosimetry, a storage test was conducted. Identical samples were stored in containers of clear pyrex glass, amber coloured glass and polypropylene. A comparative study of the effects

of storage in pyrex and amber coloured glass provided information as to whether the visible light induced the spontaneous oxidation. Storage test in polypropylene containers was to study whether plastic containers influence the spontaneous oxidation more than the glass containers. The dosimetric response of these stored solutions were studied for storage periods up to 65 days. Each aliquot of the solution was irradiated to 2000 rads of Co-60 γ- rays and the change in absorbance was measured with the microcell (section II A - 2). The resulting absorbance measurements at 304 nm for polypropylene and 304 and 224 nm for the two glasses are given in Figs. 20, 21 and 22. Each point plotted is an average of 15 separate measurements.

The solution stored in polypropylene containers showed an increased absorbance with time, and the sensitivity of the solution has dropped by 12%. This is in agreement with the findings of Pettersson and Hettinger (79). The standard procedure for eliminating the effect due to the spontaneous oxidation is to measure the change in absorbance using unirradiated, but identically treated solution as photometric reference. Such measurements will not eliminate the decreased dosimetric response of the solution stored in plastic containers. On the other hand, the solution stored in pyrex and amber coloured glass containers did not change its absorbance and dosimetric response with time. The measured change in absorbance reproduced with a standard deviation of 2.6% throughout the storage time. This showed that the

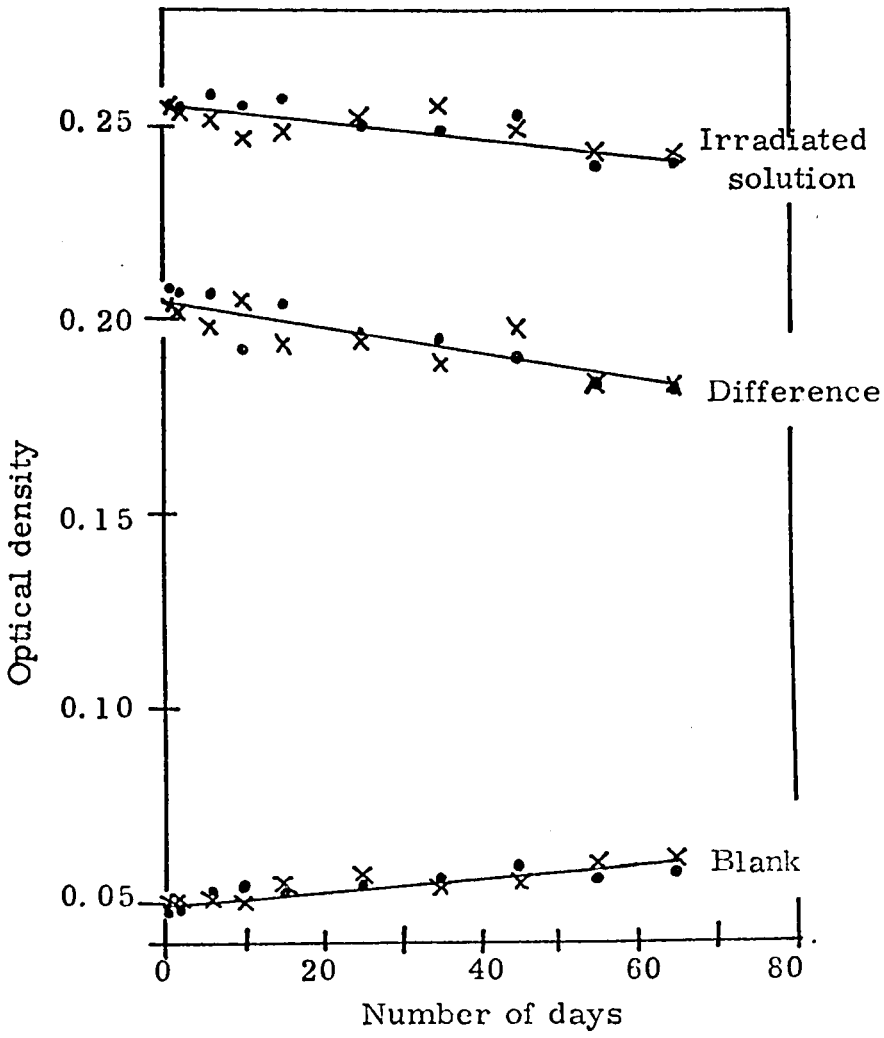

Fig. 20 : Change in absorbance of 1 and 0.1 millimolar ferrous sulphate solutions, on storage in polypropylene containers. • - 1 mM solution, and X - 0.1 mM solution. Optical density was measured at 304 nm, for absorbed doses of 2,000 rads of Co-60 γ-rays.

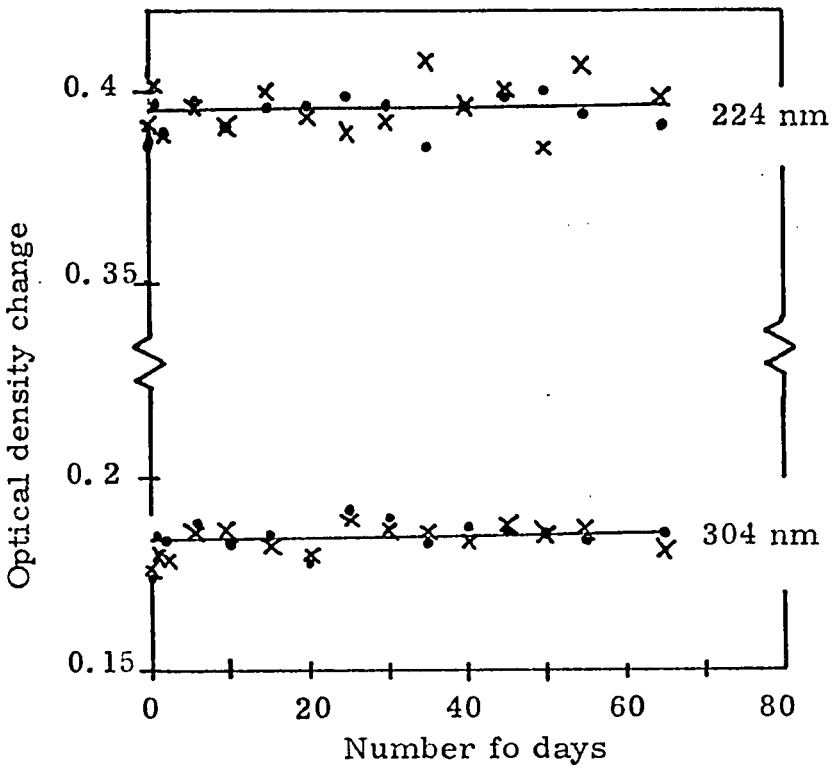

Fig. 21 : Effects of storage of 1 mM and 0. 1 mM ferrous sulphate solutions in pyrex bottles. ● - 1 mM solution and x - 0. 1 mM solution.

Fig.22 : Effects of storage of 1mM and 0. 1mM ferrous sulphate solutions in amber coloured bottles. ● - 1 mM solution, and x - 0. 1 mM solution.

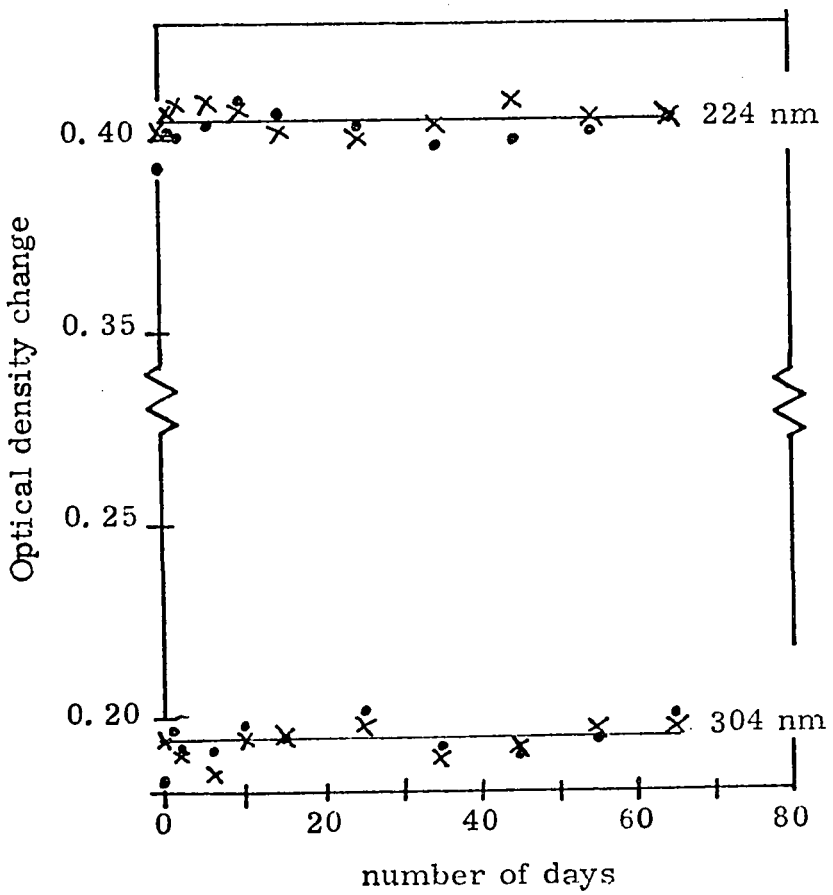

spontaneous oxidation is a thermal reaction rather than one induced by visible light.

Similar tests were performed with a dosimetric solution having a reduced ferrous sulphate concentration, to test the dependence of spontaneous oxidation on ferrous ion concentration. With a 0.1 millimolar solution identical results were obtained (Figs. 20, 21 and 22). Since the dose involved was small, the change in ferrous ion concentration by a factor of 10, would not be expected to show any change in dosimetric response. This is because the ferrous ions oxidized to ferric are only a small fraction of the total number present in either solution.

In all cases, less radiation induced oxidation resulted from the identical irradiation of freshly prepared solutions than those prepared even a few hours previously. This is in agreement with the original results reported by Fricke and Morse (33, 34).

3. Effect of Irradiation Containers

Many workers have observed that storage of the ferrous sulphate dosimetric solution in plastic containers resulted in an increase in the absorbance of the solution (21, 41, 54, 65, 68, 79 and 90). These effects may be explained as being due to the boundary effect, which are more dominant in plastics (23). The polystyrene cells used in these measurements were pre-irradiated in water to 500 kilorads and then stored in fresh distilled water (section II A - 1). Upon

filling with dosimetric solution, storage in these pre-irradiated cells still showed an increased absorbance, which saturated in 30 to 40 minutes. These results are given in Fig. 23.

4. Surface-to-volume Ratio

An increased absorbance was observed when dose measurements were made after irradiating the solution in pillboxes of 4.5 cm diameter and 0.1 cm deep. This effect was further investigated in the range of surface-to-volume ratios between 2.5 and 16 cm^{-1}. Fig. 24 shows the results of these experiments, where measured absorbances of irradiated and unirradiated solutions are given. After two hours of storage, both irradiated and unirradiated solutions showed an increased absorbance which increased linearly with the surface-to-volume ratio as a result of the surface phenomenon (23). When the pillboxes containing the dosimetric solution were stored for approximately 15 hours and then fresh solution was irradiated in them, the increase in absorbance was reduced considerably. The dashed curve in Fig. 24 represent the results of these measurements.

5. Comparison of Absorbance Measurements at 304 and 224 nm

Table IV contains the value of absorbance measured at 304 nm and 224 nm. In these experiments the dosimetric solution has been irradiated with 35 MeV electrons. The dose given was in the range between 250 and 5000 rads. Measurements were made employing

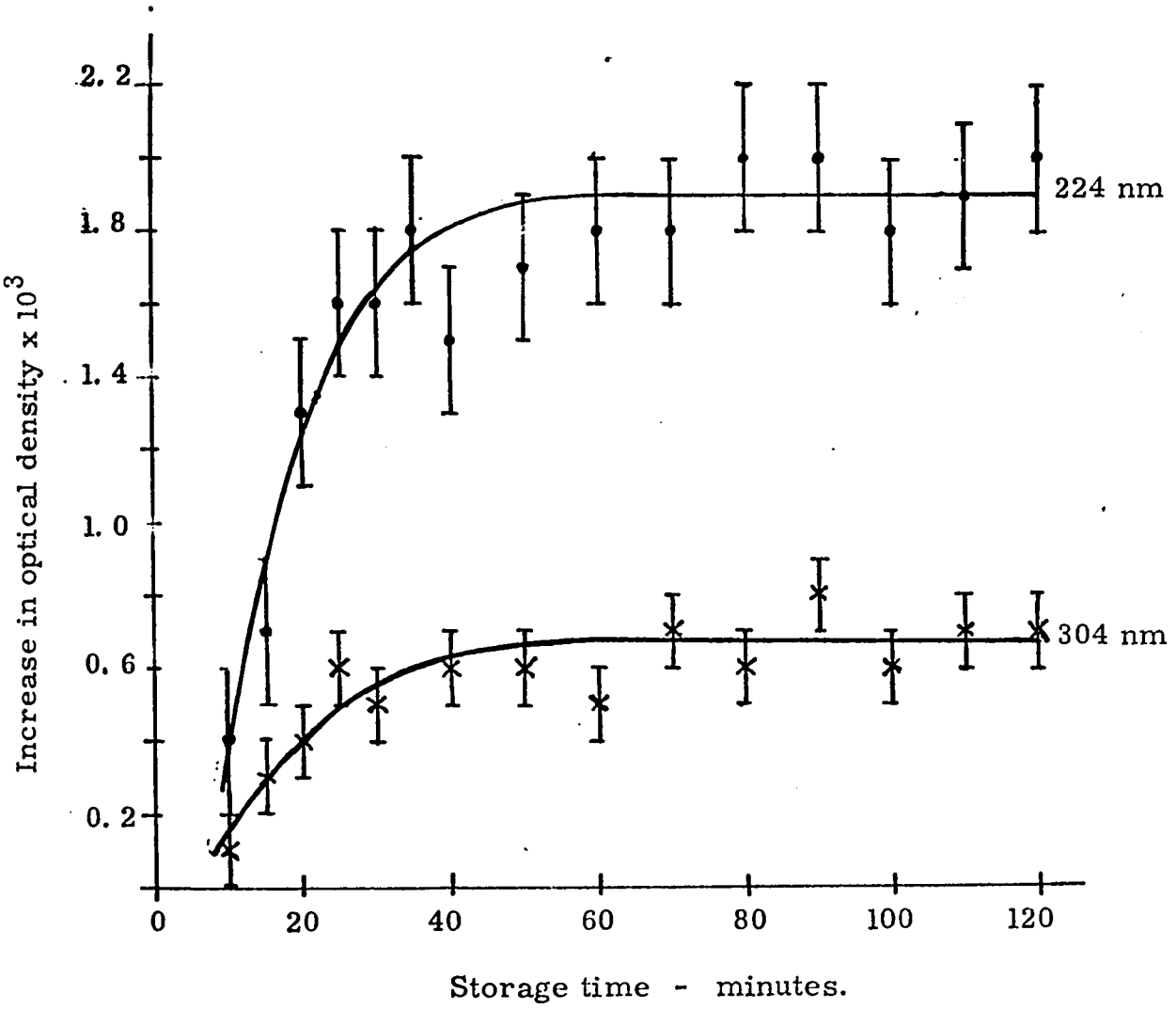

Fig. 23 : Effect of storage of ferrous sulphate solution in polystyrene irradiation containers. Optical density change of the stored, but unirradiated solution was measured at both 224 nm and 304 nm absorption peaks, with the 5 cm microcells.

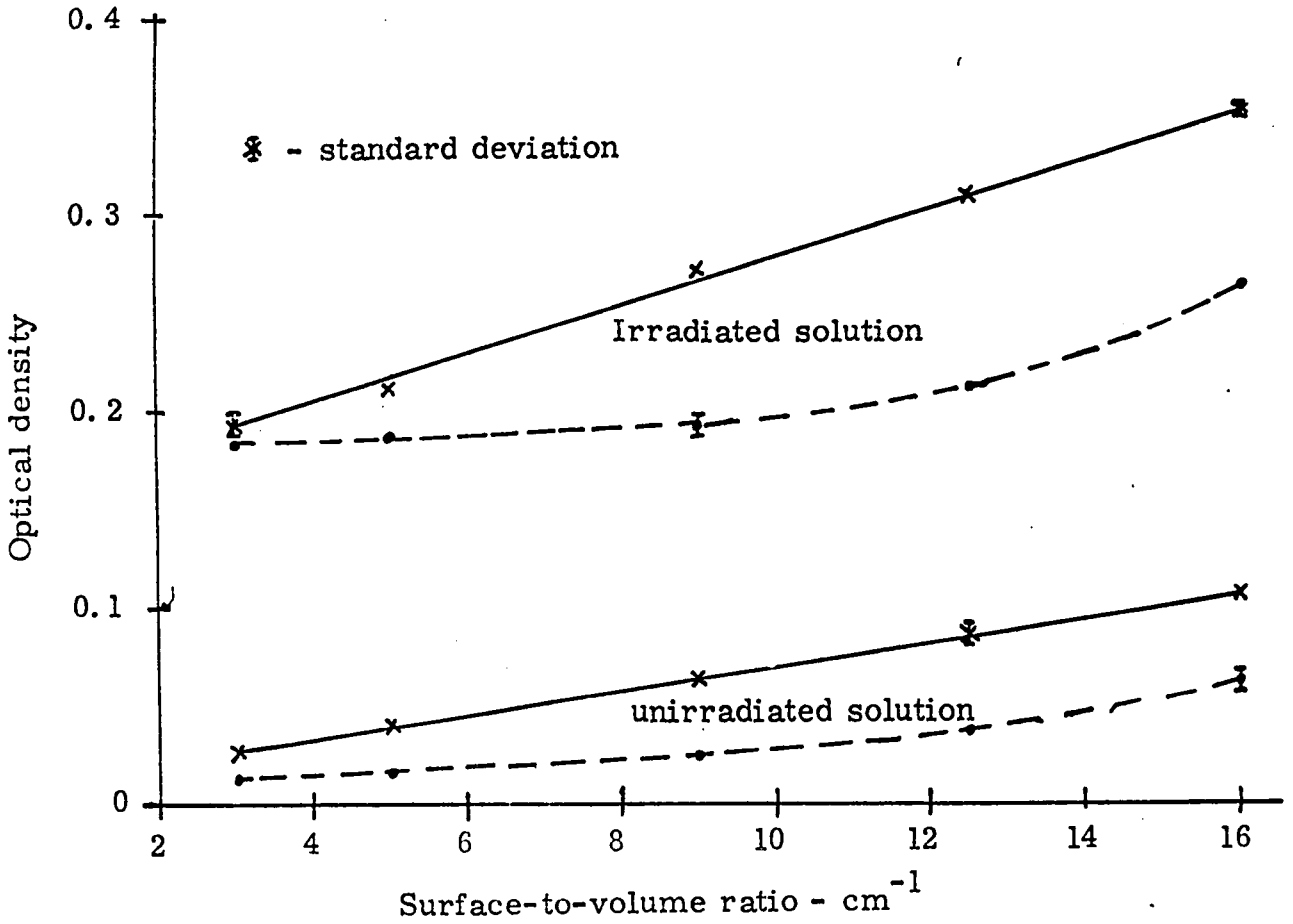

Fig. 24 : Increase of absorbance of ferrous sulphate solution stored and irradiated in polystyrene cells for approximately 2 hours. The absorbed dose given to the irradiated samples were 2,000 rads of 35 MeV electrons. X-Preirradiated pillboxes; and ● - preirradiated pillboxes treated with solution for about 15 hours.

TABLE IV

Results of Comparison Measurements of Ferrous Sulphate Solution at 304 and 224 nm Absorption Peaks. Samples were irradiated with 35 MeV electrons, at various doses-

Dose (rads)	Change in optical density at 304 nm (A)	224 nm (B)	Ratio B/A
	1 cm cell measurements		
250	0.011 ± .001	0.020 ± .001	1.82
500	0.021 ± .001	0.042 ± .001	2.00
1,000	0.043 ± .001	0.091 ± .002	2.12
2,000	0.089 ± .002	0.188 ± .002	2.11
3,000	0.131 ± .002	0.270 ± .002	2.06
4,000	0.178 ± .003	0.360 ± .003	2.02
5,000	0.223 ± .003	0.454 ± .003	2.04
	Microcell measurements		
250	0.054 ± .004	0.100 ± .006	1.85
500	0.102 ± .004	0.211 ± .006	2.07
1,000	0.212 ± .007	0.450 ± .008	2.12
2,000	0.446 ± .010	0.917 ± .010	2.06
3,000	0.654 ± .010	1.351 ± .012	2.07
4,000	0.888 ± .012	1.801 ± .014	2.03
5,000	1.114 ± .015	2.256 ± .017	2.03
		Average ratio	2.06 ± .04

the 1 cm cells and the microcells. These values are plotted in Fig. 25. For dose at and above 500 rads the absorbance measured at 224 nm is found to be 2.06 ± .04 times that measured at 304 nm absorption peak. This is in good agreement with the ratio 2.07, of the molar extinction coefficients at these absorption peaks (86). The deviation from this ratio at lower doses is explained by the larger error in the measurement of small changes in absorption.

In these experiments the dosimetric solution was irradiated in pyrex glass containers. The experimental uncertainty at the two peak wavelengths are very nearly the same. Hence the per cent standard deviation of measurements at 224 nm is approximately half that at 304 nm. When the dosimetric solution was irradiated in polystyrene containers the standard deviation of absorbance at 224 nm becomes 3%. In clinical dosimetry this loss of accuracy must be accepted, because glass vessels are not used because of the higher stopping power for radiation of all energies employed in radiation therapy. An additional advantage is that, because the temperature dependence of absorption at 224 nm is one-sixth of that at 304 (Appendix II, Fig. 55), measurement accuracy is less affected by slight changes in ambient temperature in 224 nm measurements.

6. Microdosimetry

A comparison of the results of absorption measurements in which commercial 1 cm path length absorption measurement cells

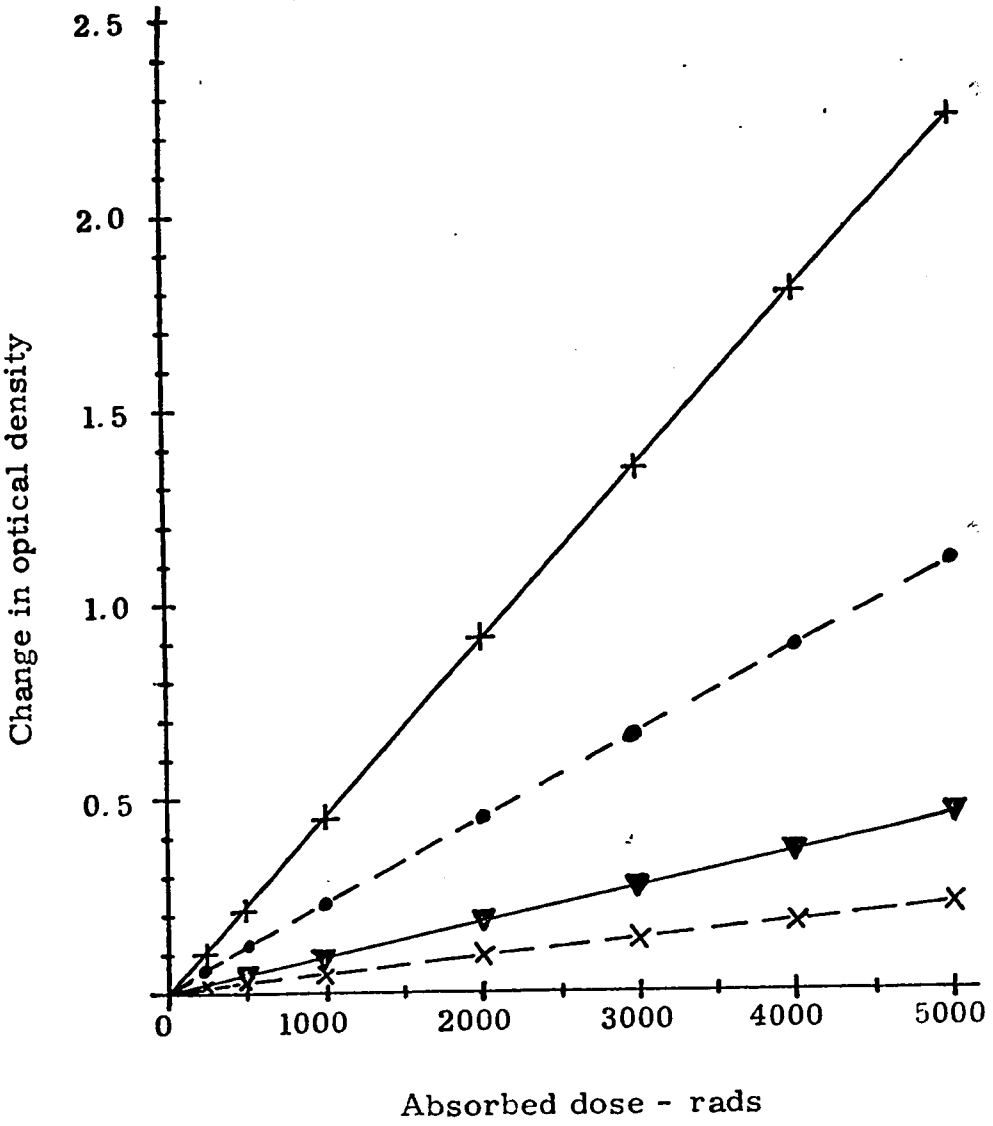

Fig. 25: Absorbance measurements of ferrous sulphate solution irradiated with 35 MeV electrons and measured with 1 cm and micro-cells, at 304 and 224 nm absorption peaks. x - 1 cm cell at 304 nm; ▼- 1 cm cell at 224 nm; ● - 5 cm microcell at 304 nm and + - 5 cm microcell at 224 nm.

and the newly designed 5 cm pathlength MICROCELLS are used, is illustrated in Fig. 25. Dosimetric measurements with the microcells require only 0.5 cm^3 of ferrous sulphate solution and an absorbed dose of the order of 500 rads; this technique is referred to as the MICRODOSIMETRY. Since the measured absorbance is a linear function of optical path length, methods of measurement using the 5 cm microcells are five times as sensitive as those using the 1 cm cells. The sensitivity can be increased further by measuring the absorbance at the 224 nm absorption peak, instead of the conventional 304 nm peak. Thus, by combining all these refinements, it has been proved possible to measure accurately absorbed doses down to 250 rads in an irradiated volume of 0.5 cm^3. The microdosimetric technique has the advantage that doses in the range of clinical application may be measured with the same accuracy as that attained with greater dosemeter volume, higher doses and using conventional techniques.

A comparison of results of microdosimetric and conventional techniques is given in Table V. Here the changes in absorbance are measured at 224 nm with microcells for exposures producing 500 clicks, and compared to those measured at 304 nm with the 1 cm cell for 5,000 clicks. The magnitude of the optical density changes are seen to be the same for the two techniques. The increased absorbance at higher energies is because the response of the monitoring ionization chamber decreases with electron energy.

TABLE V

Comparison of Microdosimetry with Conventional Measurement Technique, at Different Electron Energies

Electron energy (MeV)	Measured absorbance change Technique A	Technique B
10	0.175 ± .004	0.176 ± .005
15	0.172 ± .004	0.178 ± .005
20	0.180 ± .004	0.186 ± .005
25	0.187 ± .004	0.192 ± .005
30	0.203 ± .004	0.210 ± .005
35	0.233 ± .004	0.241 ± .005

Technique A - ferrous sulphate solution irradiated to 5,000 clicks and absorbance measured at 304 nm with 1 cm cells.

Technique B - ferrous sulphate solution irradiated to 500 clicks and absorbance measured at 224 nm with microcells.

7. Electron Dose Measurements

Electron output (in terms of rads per click) were measured in a transverse plane at 2 cm depth in a polystyrene phantom, as described in section II A - 2. The dose per click was measured for a few typical beam sizes (or field sizes). Those for 14 x 12 cm, employing the plastic applicator, and for 17 x 17 cm to the 50% dose (referred to as OPEN field) where no secondary collimation was provided, are listed in Table VI and are illustrated in Fig. 26.

The output in rads per click increases linearly from 10 to 25 MeV electron energy and then becomes super-linear beyond 25 MeV. This change indicates a dependence upon electron energy of the response of the monitor chamber (which produces the clicks).

The difference in the output measured using the 14 x 12 cm applicator and with an open beam is due to the scatter contribution from the walls of the secondary collimator.

Since this is the most nearly absolute method of dose measurement employed with the betatron to date, the "rads per click" values listed in Table VI are used as a basis for all other dosimetry techniques. Since other users of clinical betatrons employ the same basic dosimetric method, this affords a means of standardizing clinical dosimetry between treatment centers.

TABLE VI

Absorbed Doses (Rads) per Integrator "Click" Measured with the Ferrous Sulphate Dosemeter at the Depth of the Dose Maximum in Polystyrene

Accelerated electron energy (MeV)	Output-rads per click for 14 x 12 cm field	open field
10	0.91 ± .03	0.89 ± .03
15	0.96 ± .03	0.95 ± .03
20	1.01 ± .03	0.98 ± .03
25	1.06 ± .03	1.04 ± .03
30	1.16 ± .03	1.10 ± .03
35	1.25 ± .04	1.20 ± .03

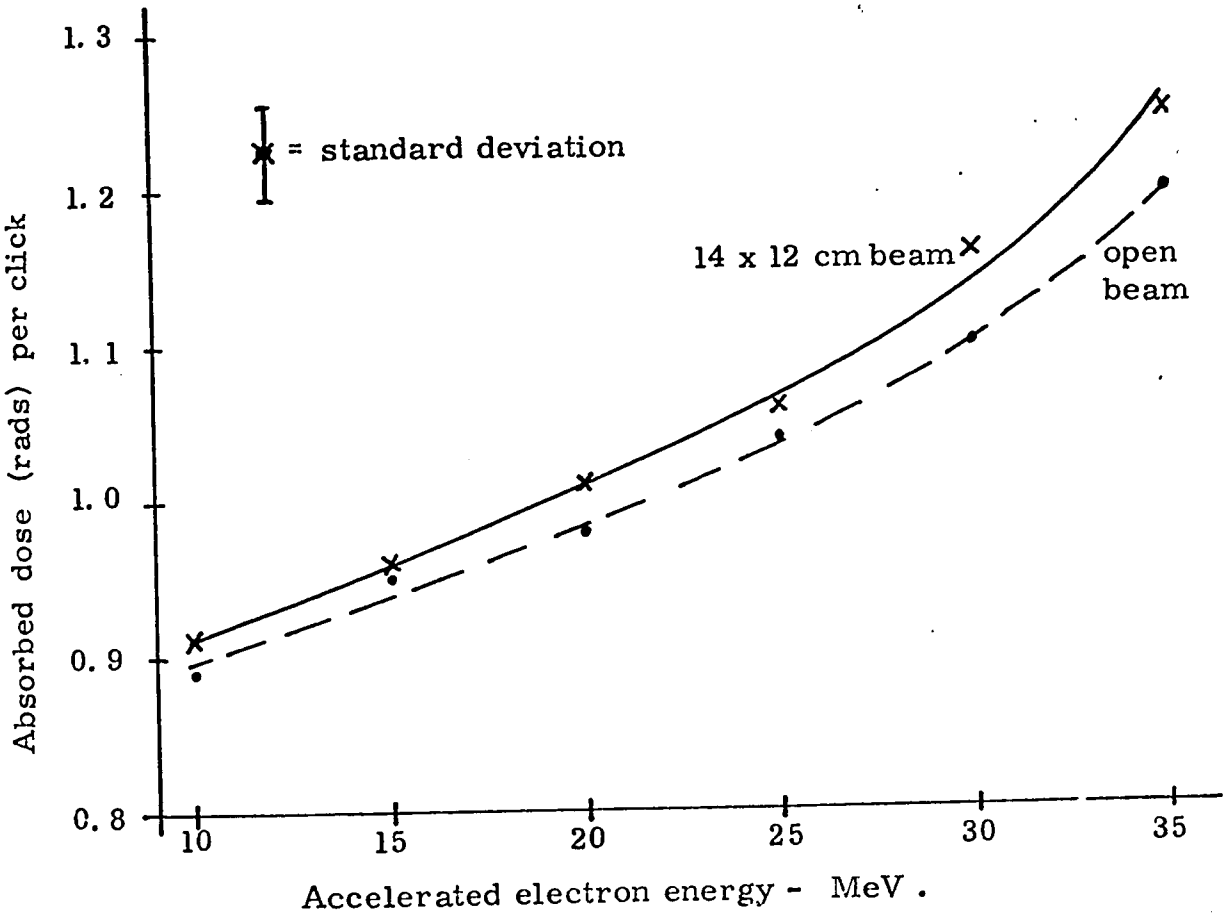

Fig. 26 : Electron output calibration , in rads per integrator click, with ferrous sulphate dosemeter. Measurements were taken at 2. 0 cm depth in a polystyrene phantom for two beam conditions.

B. THERMOLUMINESCENT DOSIMETRY (LiF)

1. Effects of Annealing and Storage

In TL dosimetry proper annealing of the thermoluminescent materials is of prime importance. A preliminary study of the light output of TLD-100 powder stored before and after irradiation showed that the magnitude of time-dependent fading is within experimental limits if the sample is properly annealed. On the other hand, a sample which had been annealed at 400°C for one hour and not annealed at the low temperature (Appendix III) showed an approximately 45% higher initial output than did the adequately-annealed sample. The glow curves in Fig. 27 illustrate the difference. The higher response is due to the presence of the low temperature peaks (curve A), the effects of which are added to that of the principal glow peak at 215°C. These low temperature peaks disappear after heating the powder at 80°C for 24 hours (curve B). An identical curve was obtained (curve C) when the 400°C annealed powder was stored for 60 days.

This fading with time was studied in detail; the results are shown in Fig. 28. Unlike the adequately-annealed TLD-100 samples, those which were annealed at 400°C only showed a continuous fading until the low energy traps had emptied spontaneously. Samples which were irradiated before storage exhibited different fading

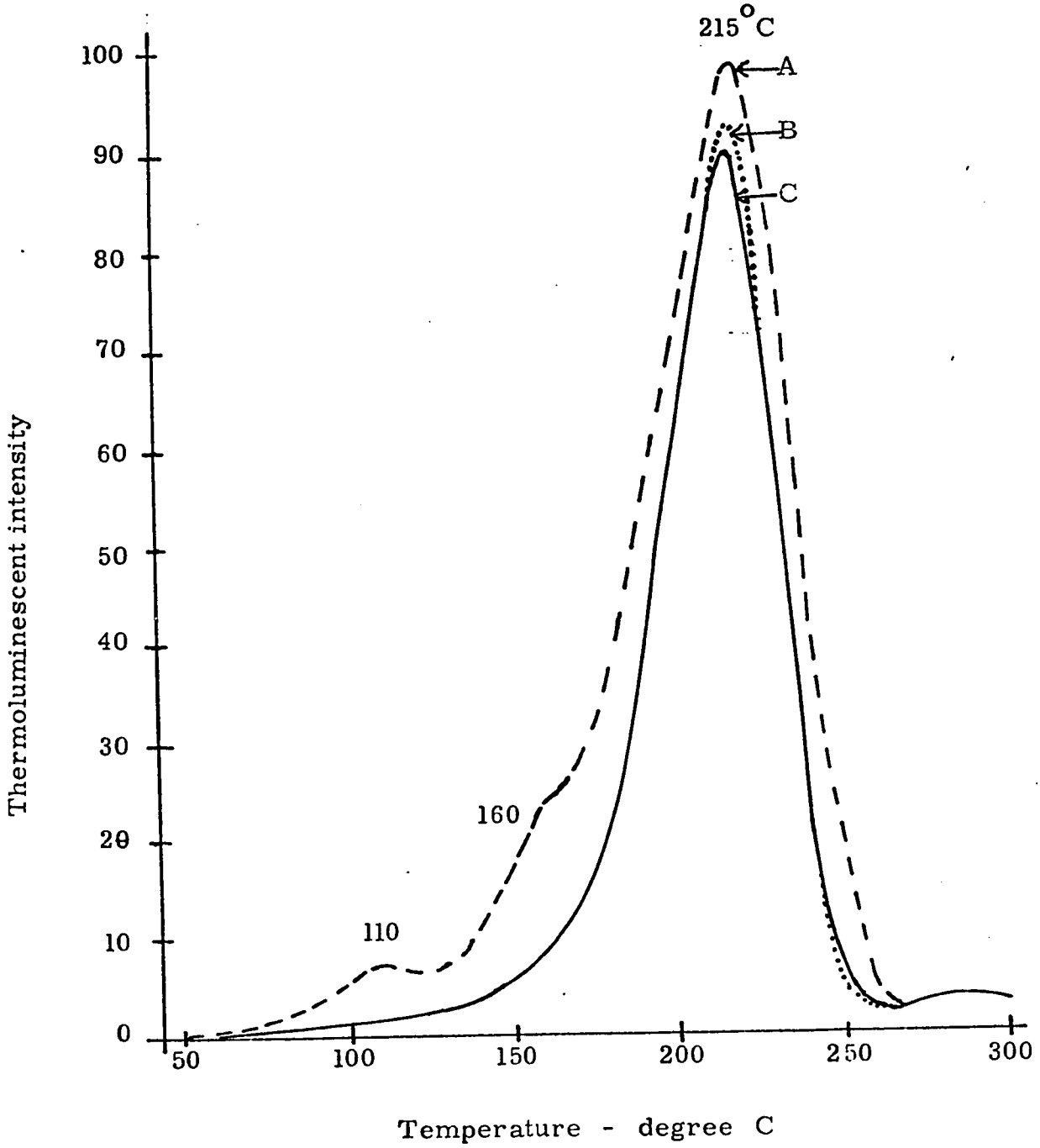

Fig.27 : Glow curves of TLD-100 powder. A - Initial output of sample annealed at 400 °C only; B - of adequately annealed sample; and C - output of 400 °C only annealed sample after storage of 60 days.

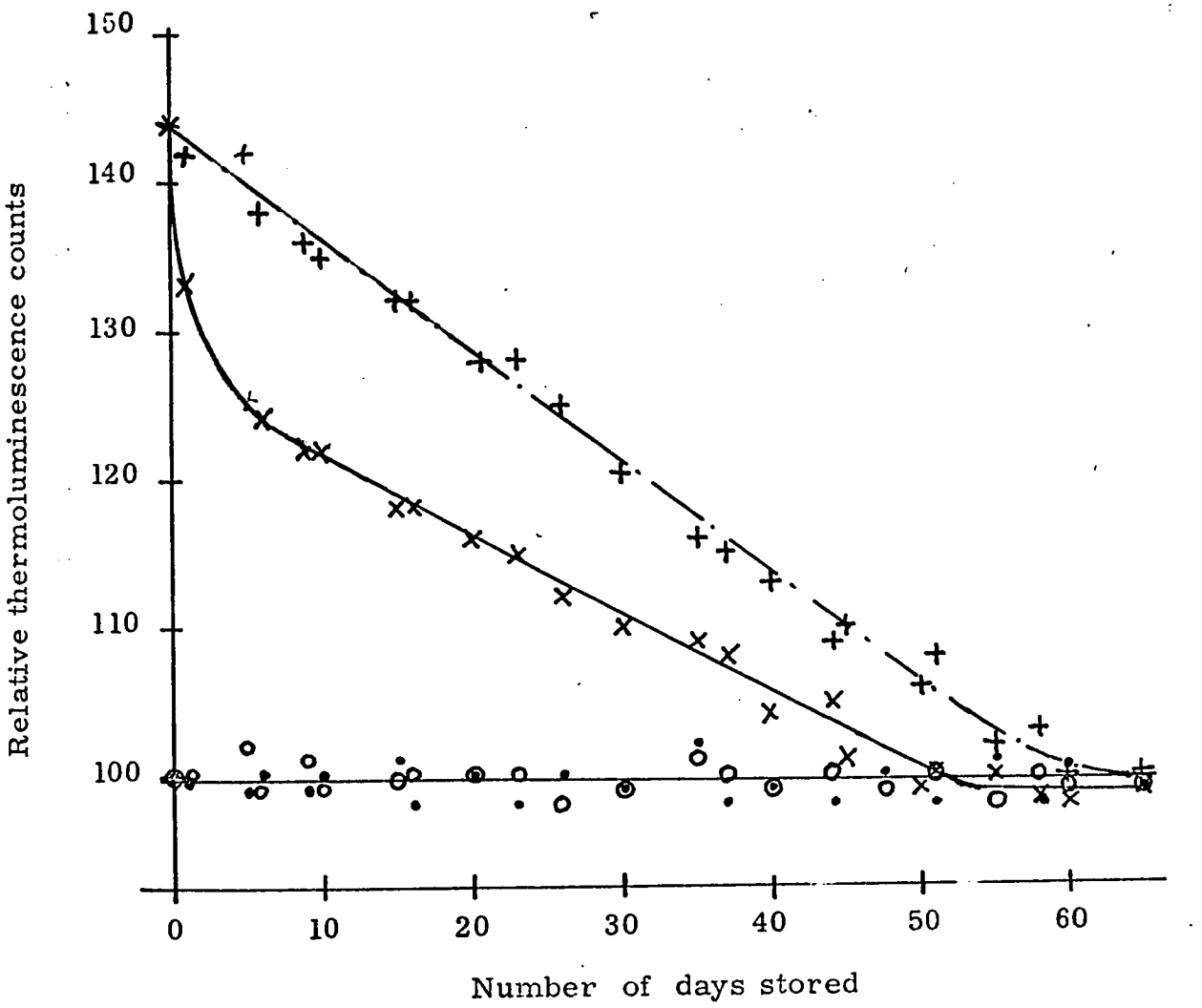

Fig. 28 : Dependence of fading on annealing and storage. O-adequately annealed powder, stored and irradiated just before measurement; •-adequately annealed, irradiated and stored; X- 400°C annealed, irradiated and stored; +-400°C annealed, stored and irradiated just before measurement. All were irradiated with electrons (30 MeV) to 200 rads and normalized to the initial reading of the adequately annealed TLD - 100 sample.

characteristics than those which were stored and then irradiated just before measurement. The former faded rapidly at first (approximately 15% in 10 days) and then at a slower rate. The samples which were stored and irradiated just before measurement showed a more uniform rate of fading throughout the period of study. This fading is due to the spontaneous emptying of the shallow traps in the TL crystals upon storage at room temperature. This same effect is achieved by heating at 80^{o}C for approximately 24 hours.

2. Effect of Crystal Size on Thermoluminescence

In the course of these experiments it was observed that the TL output of TLD-100 powder increased 5 to 8% after each annealing. A shipment from the supplier was found to contain crystal sizes between 100 and 200 mesh Tyler. After each annealing the crystal size was found to increase. More than half of the total quantity had attained crystal sizes between 50 and 100 mesh Tyler, after three annealing treatments.

At this stage the batch of crystals was separated into three groups. Crystals in the range 50 to 80 mesh were labelled TLD-50, those in the range 80 to 100 mesh were labelled TLD-80 and those between 100 and 200 mesh TLD-100. These samples were exposed to 25 MeV electrons (doses of 100 rads) and the TL output was compared. Results of these measurements are given in Table VII along with the

TABLE VII

Relative Thermoluminescent Response of Identical Volumes of Different Crystal Size Powder

Sample	Relative TL	Average weight per dispensed volume (mg)
TLD-100	1.00	30.7 ± 0.25
TLD-80	1.04	31.5 ± 0.25
TLD-50	1.10	31.9 ± 0.25
Mixture*	1.05	31.7 ± 0.25

* The TLD - sample after three annealing treatments (after receiving from the supplier) and before separating into TLD-100, TLD-80 and TLD-50.

average weight per dispensed volume. Both the weight and the TL response measured of the dispensed volume of the LiF crystals increased with increasing crystal size. The areas under the glow curves, shown in Fig. 29 confirm this increased thermoluminescent response.

Since the crystal size increases on annealing and the weight per dispensed volume increases with crystal size, the effective TL sensitivity of Harshaw Chemical's TLD-100 increases with each annealing. A similar increase in average weight of LiF crystals from another supplier was reported by Worton and Holloway (101). They observed an increase in weight of 3% in 18 months, under annealing conditions identical to those used in this work.

3. Measurements with monocrystalline Layers

Monocrystalline layers of TLD-100, described in section II B - 1, were used to measure the surface doses and the dose build-up with depth in a polystyrene phantom.

Table VIII shows the results of central-axis depth dose measurements in polystyrene for Co-60 γ-rays of different field sizes at 80 cm SSD, measured with the monocrystalline layers of TLD-100. The numbers in the brackets are the standard per cent depth dose values of the British Journal of Radiology, Supplement No. 10, which are measured in water. The agreement is within a maximum of 3%.

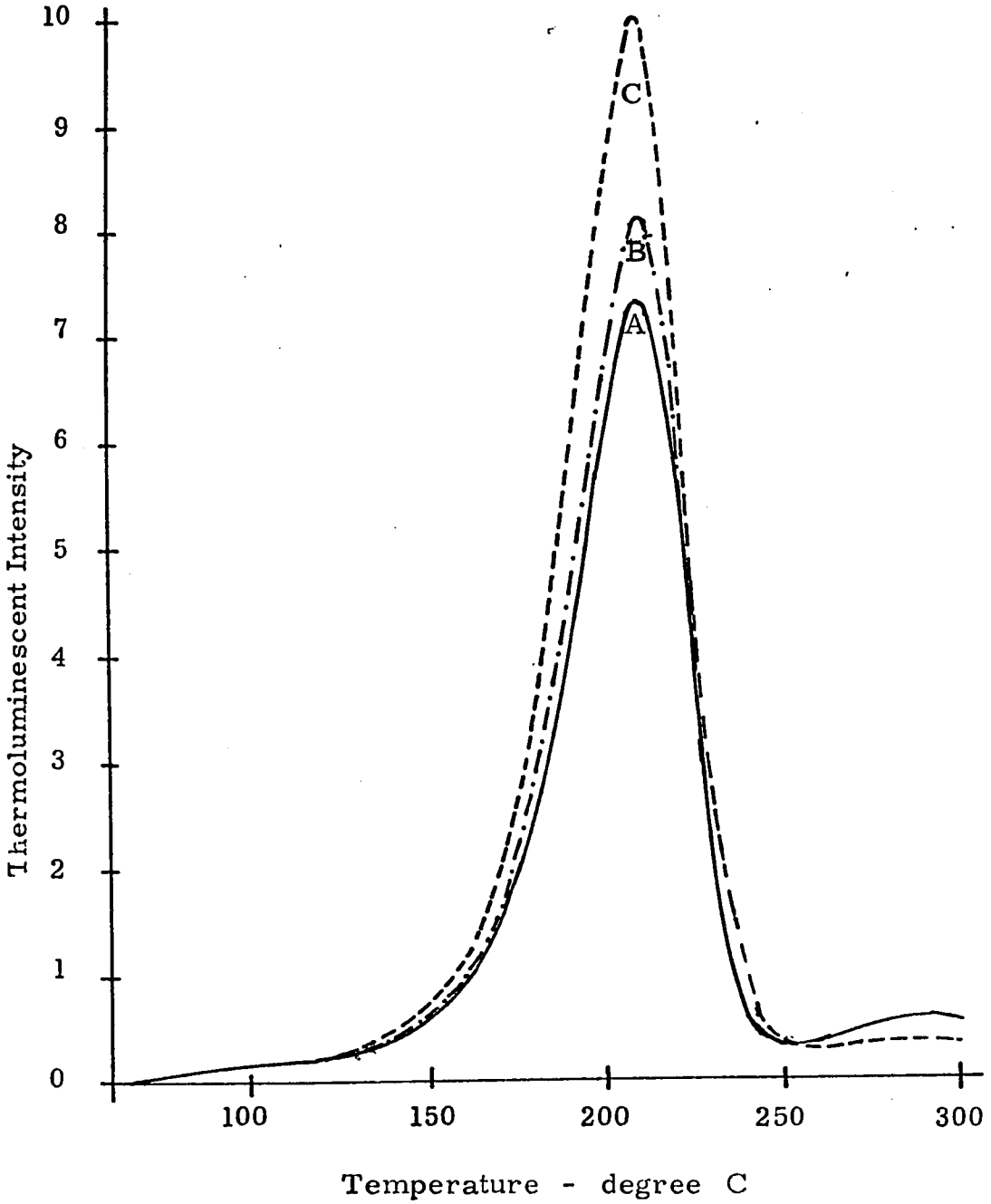

Fig. 29 : Glow curves of LiF - TLD powder as a function of crystal size. A - of TLD-100; B - of TLD-80; and C - of TLD-50.

TABLE VIII

Relative depth doses of Cobalt-60 γ-rays in polystyrene phantom, measured with monocrystalline layers of TLD-100, at various field sizes. The values quoted in the brackets are from British Journal of Radiology, Suppl. No. 10

Depth in polystyrene (cm)	Field Size (cm^2)			
	5 x 5	10 x 10	15 x 15	20 x 20
0.0	29.9	37.0	45.3	51.0
0.1	65.9	72.4	80.8	83.0
0.2	87.6	92.6	94.7	96.0
0.3	96.2	96.5	97.6	99.2
0.4	100.0	98.8	99.6	100.0
0.5	99.6 (100.0)	100.0 (100.0)	100.0 (100.0)	99.4 (100.0)
1.0	97.3 (97.0)	98.2 (98.2)	96.3 (98.4)	98.0 (98.4)
2.0	92.9 (91.3)	94.2 (93.3)	92.4 (93.0)	92.7 (94.0)
3.0	86.3 (85.6)	87.4 (88.3)	89.0 (89.3)	87.9 (89.6)
4.0	79.6 (80.2)	82.1 (83.4)	83.4 (84.7)	84.2 (85.2)
5.0	76.0 (74.8)	76.9 (78.5)	78.8 (80.1)	79.4 (80.8)

The surface doses, from Table VIII are plotted in Fig. 30 as a function of the field area. These measurements were done with Co-60 γ-rays, because no such data have been published for the electrons employed in this work. These experiments which give agreement with the published values, give confidence in the method.

The build-up curves for the electron beams from 10 to 35 MeV, for the 14 x 12 cm field size (using the fixed plastic applicator) are given in Fig. 31. The relative surface doses range from 90 to 93% of the maximum dose, and the dose maximum occurs between 1 and 4 cm. For all energies the dose is maximum at 2 cm depth.

In Fig. 32 the build-up curves for various beam sizes are given. The relative surface dose and the shape of the curve are dependent on the size and type of the applicator employed, because of the difference in low energy scattering produced. When no secondary collimation is employed the surface dose is a minimum and the build-up is slow (Fig. 32 A), especially at the lower energies. Results in Figs. 32 and 33 show a comparison of the build-up curves when the lucite applicator and the variable collimator are used.

The region of maximum dose is sharply defined in the case of the 4 x 4 cm variable applicator (Fig. 32 B), but is spread along a depth of approximately 1 cm by the 4 cm diameter lucite applicator (Fig. 32 A). This difference gets smaller at higher energies and is insignificant at 35 MeV. The difference in depth dose between

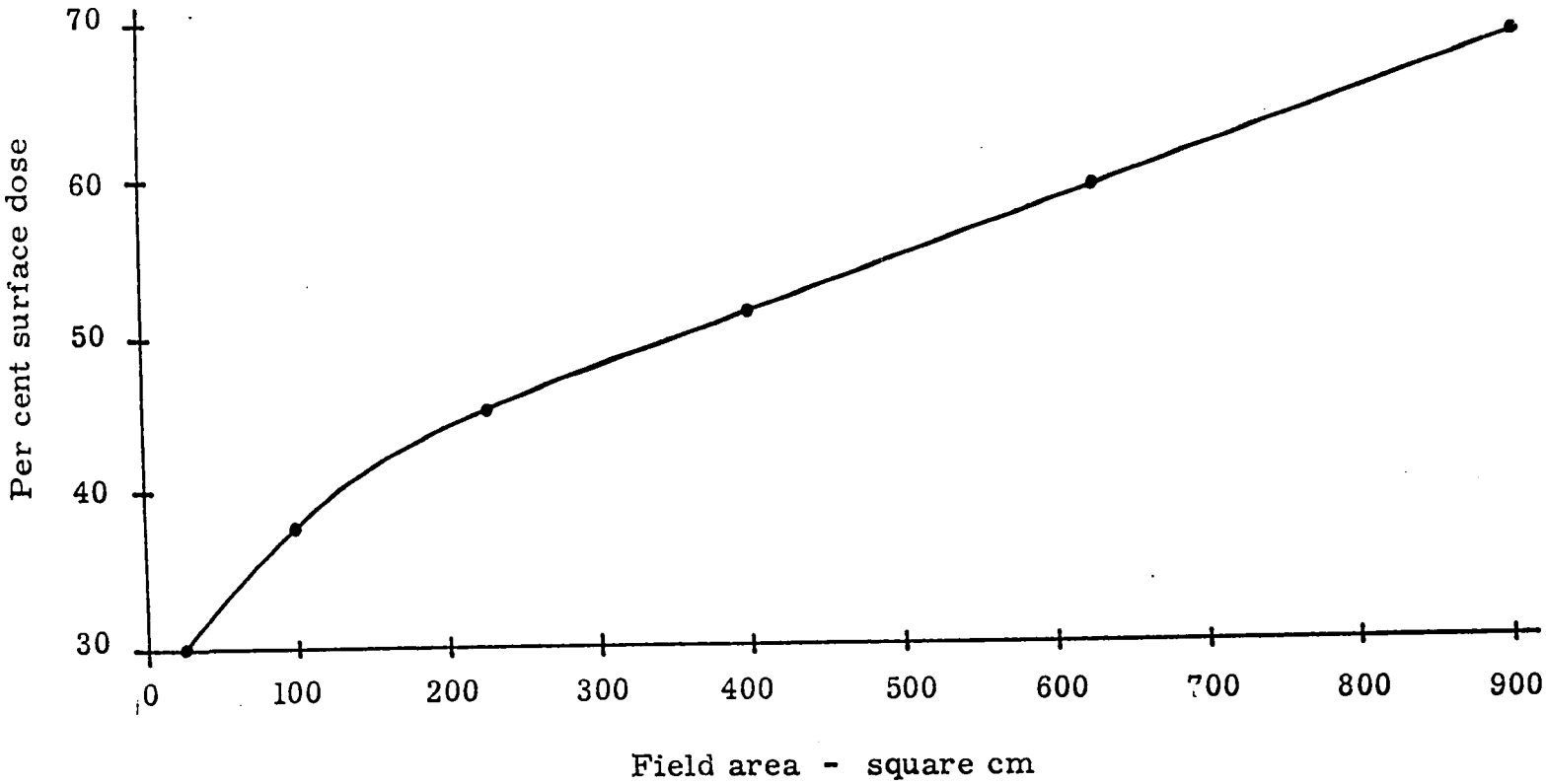

Fig. 30 : Dose at the surface relative to dose maximum, at different field sizes of Co-60 γ-rays (80 cm SCD), measured with monocrystalline layers of TLD-100 on polystyrene discs

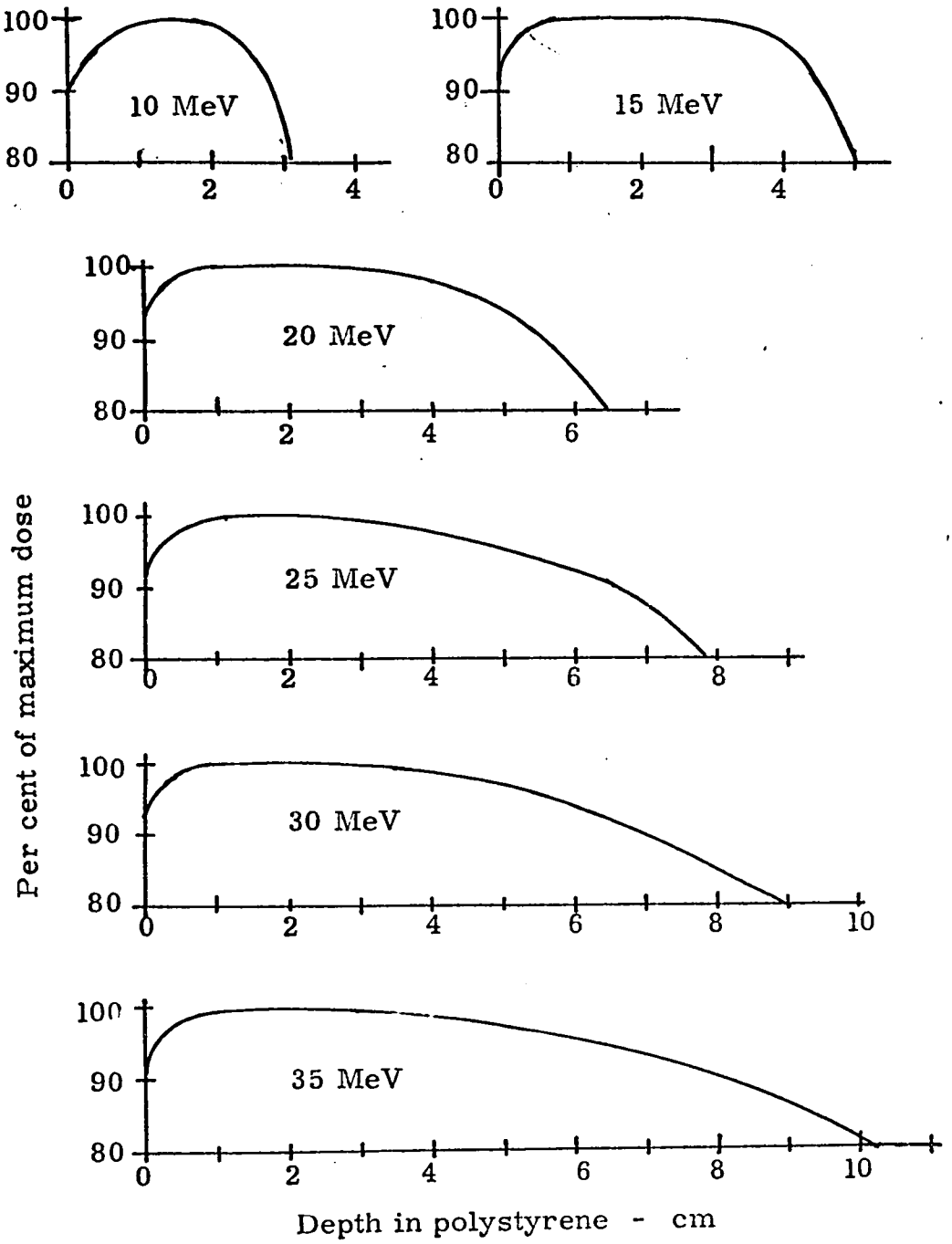

Fig. 31 : Build-up curves of 14 x 12 cm electron beam in polystyrene, measured with monocrystalline layers of TLD-100.

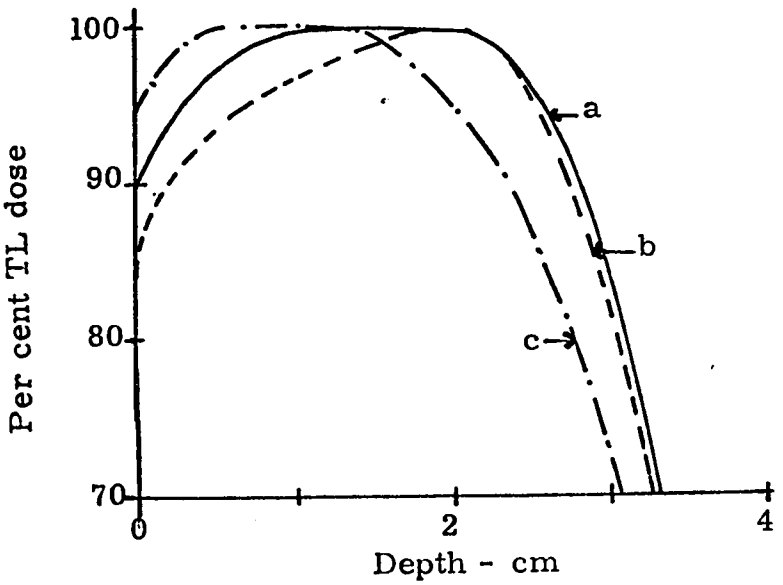

A

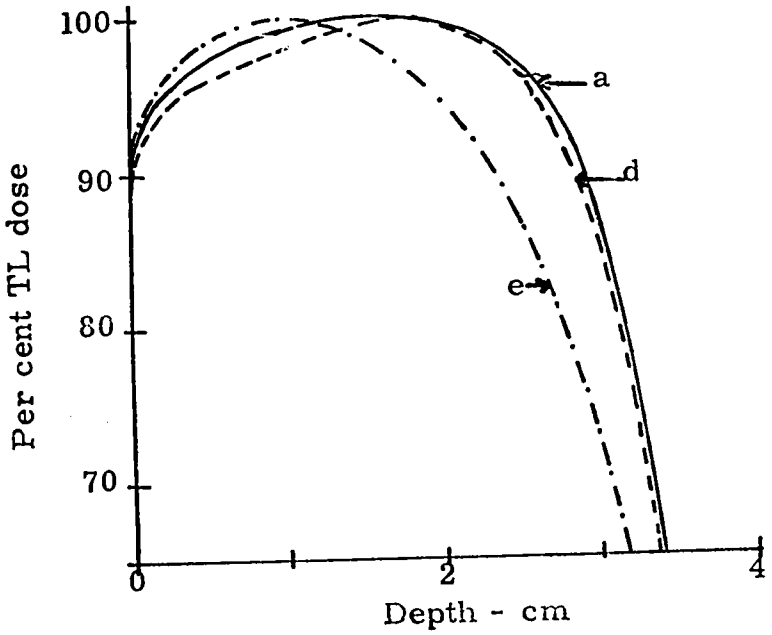

B

Fig. 32 : Build-up of 10 MeV electrons in polystyrene, measured with monocrystalline layers of TLD-100, at different beam size. a - 14 x 12 cm applicator; b - open beam; c - 4 cm diameter applicator; d- 14 x 12 cm variable collimator; and e - 4 x 4 cm variable collimator.

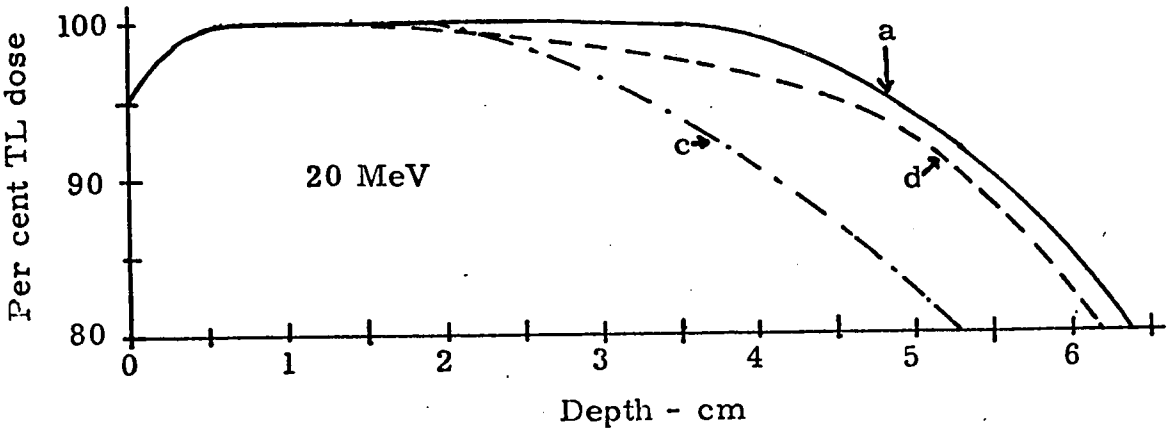

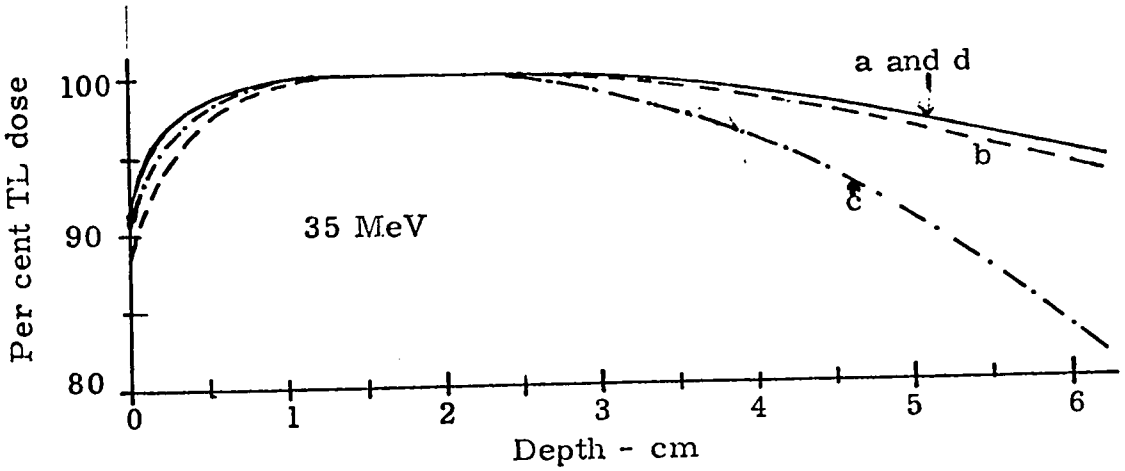

Fig. 33 : Build-up of electrons in polystyrene at different beam size, measured with monocrystalline layers of LiF. a - 14 x 12 cm applicator; b - open beam; c - 4 cm diameter circle applicator; d - 14 x 12 cm variable collimator.

the 14 x 12 cm fixed applicator (lucite) and an identical size variable collimator beam is also shown in these figures (i. e. 32 and 33). The difference in the build-up region is not significant. The difference beyond the maximum dose region is significant, but gets smaller at higher energies.

The scattering effect due to the plastic applicators and its influence on the peak dose region are illustrated in Fig. 34. The continuous curves represent the relative depth dose at the center of the field (curve A), at 3 cm (curve B) and at 6 cm(curve C) out towards the edge of the 14 x 12 cm beam, along the 14 cm side. The corresponding relative depth dose curve with no plastic applicator is shown in dashed lines. The difference between the two curves represents the contribution of scattered electrons to the dose by the walls of the plastic applicator. This scattering contribution is approximately the same throughout the transverse plane (i. e. plane perpendicular to the radiation beam) and is more significant at low energies.

The relative surface doses for electrons for five conditions of beam collimation are listed in Table IX. The values are relative to the maximum depth dose, individually normalized, and are averaged over 18 individual measurements. It is seen that the energy , the

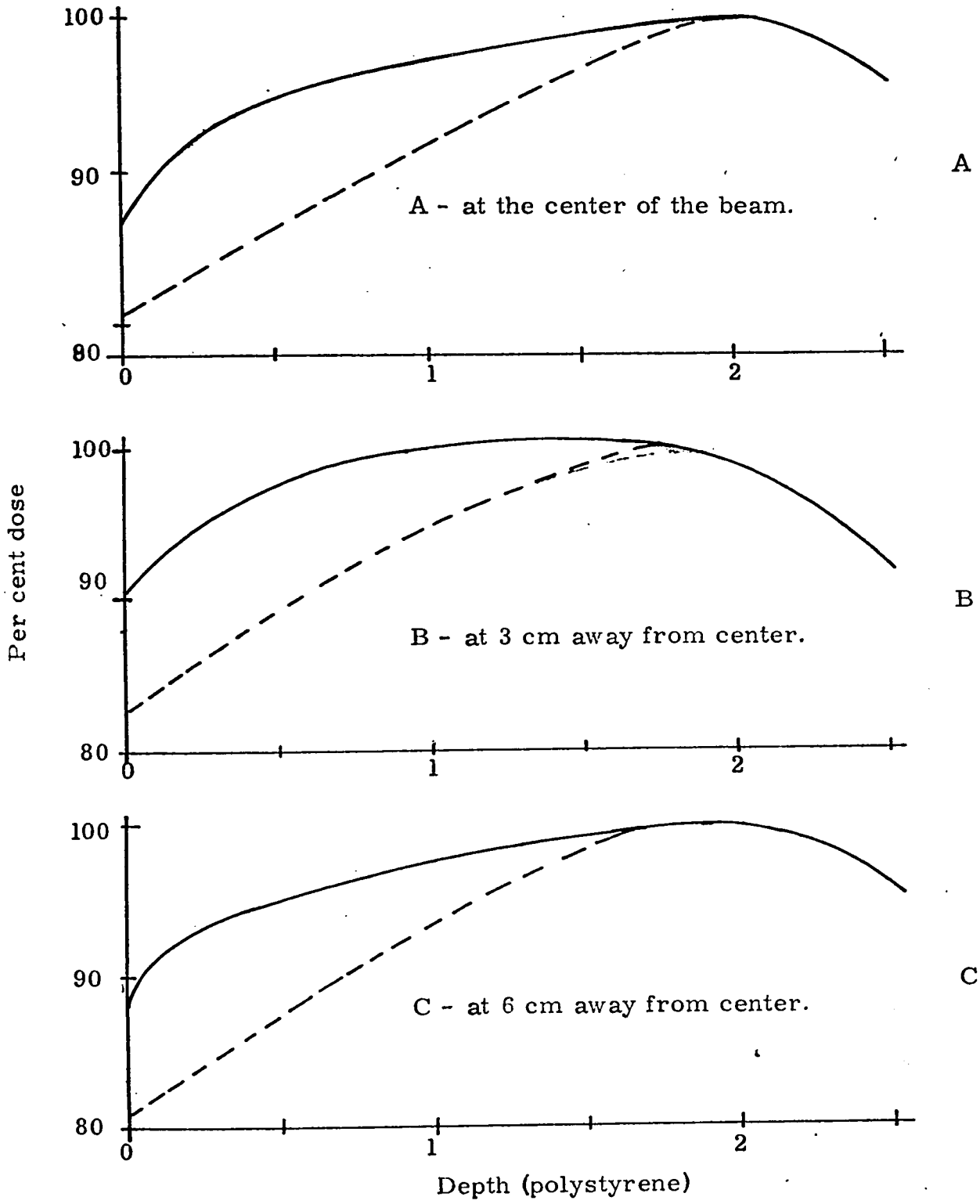

Fig. 34 : Build-up curves for 10 MeV 14 x 12 cm electron beam at different points in the field, measured with mono-crystalline TLD-100 (along the 14 cm side). Standard deviation : 1 per cent.

TABLE IX

Surface Doses as a Per Cent of the Dose Maximum, Illustrating the Effect of Beam Size and Method of Collimation

Accelerated electron energy (MeV)	Beam size and per cent surface dose: Plastic applicator 4 cm dia.	Plastic applicator 14 x 12 cm	Variable collimator 14 x 12 cm	Variable collimator 4 x 4 cm	No collimation open field
10	95	88	88	92	84
15	94	92	93	92	84
20	93	93	94	93	86
25	94	92	94	93	88
30	92	92	92	94	90
35	91	92	93	93	89

The standard deviation of measurement of all values listed is 1.5 per cent.

type of collimator, and the beam size have little influence upon the relative surface dose, but that for the open beam and for electron energy of 10 MeV.

4. Depth dose curves in Different Materials

The relative dose-dependence on depth has been found to be dependent on the atomic number and the density of the material. Fig. 35 shows the dependence of the build-up and the relative depth dose curves in homogeneous polystyrene, plaster of paris, magnesium, and copper absorbers. The measurements were made using mono-crystalline layers of TLD-100 placed at different depths in the material. The data are plotted against equivalent depth in water, i. e. corrected by the ratio of electrons per unit area of the material. Since (as discussed in Appendix I) the major portion of the energy loss is due to ionizing collisions with atomic electrons, the ratio of electron densities, N_d - given in Appendix IV, is used in comparing depths, rather than the mass-density ratio. The depth dose curves in all materials are normalized to 100% at the dose maximum in polystyrene. As expected the dose-maximum in copper is much higher (40%) than that in other materials.

5. Effects of Inhomogeneities in the Absorber

In the routine treatment of cancer with electron beams, the absorber is not a homogeneous medium. For this reason the effect

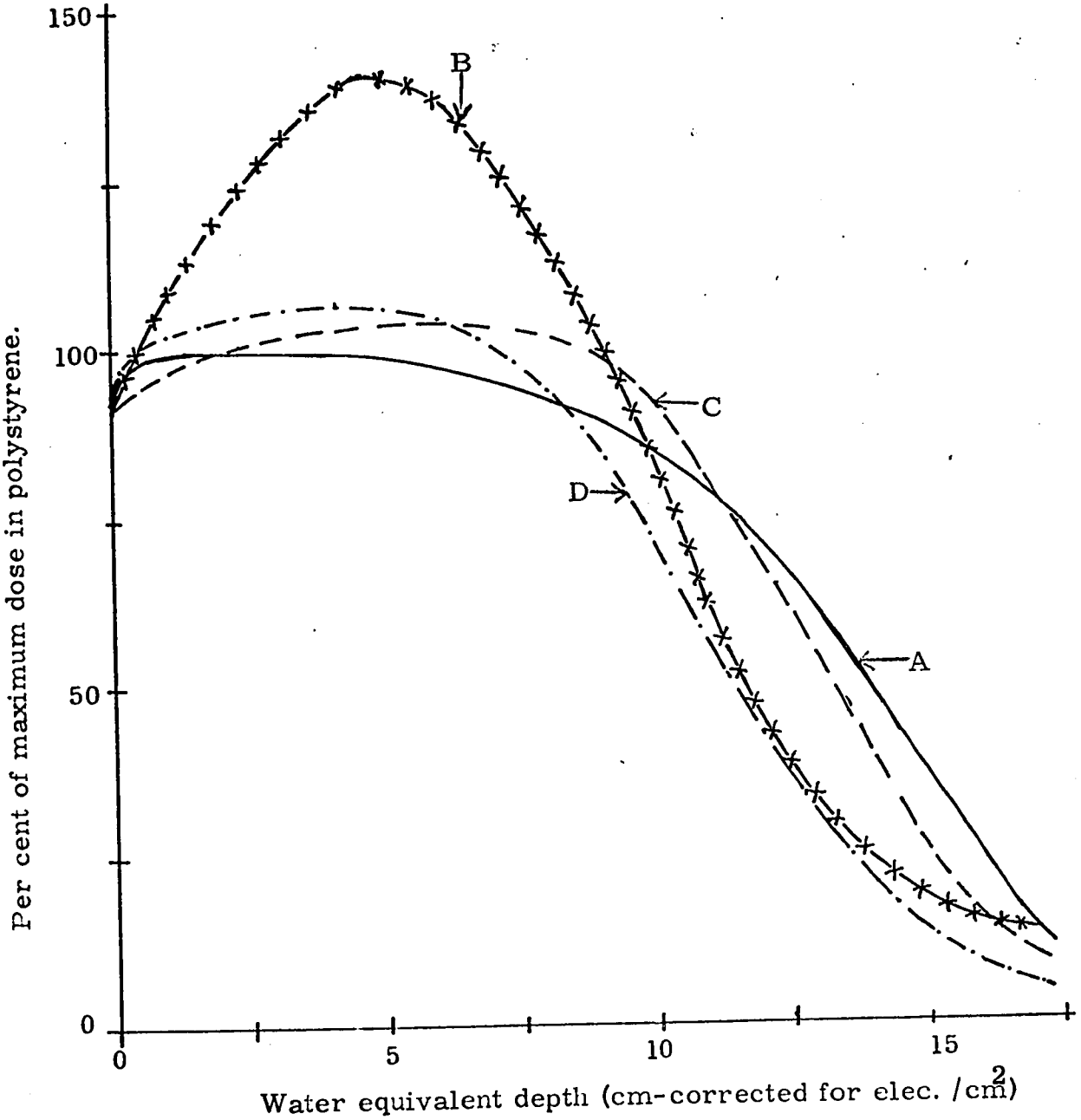

Fig. 35 : Build-up and depth-dose curve of 30 MeV electrons in different phantom materials 8 cm diameter circular field at 110 cm. Peak dose in polystyrene is taken as 100%. A - polystyrene $(C_6H_5CH:CH_2)_n$; B - Copper (Cu); C - Magnesium (Mg); and D - Plaster of Paris ($CaSO_4$-1/2 H_2O).

of the presence of high electron density material in the absorber was investigated. Bone is the material of high electron density that is encountered clinically; in terms of electron density its closest metallic simulant is magnesium. However, copper was used in these experiments to produce exaggerated, more readily measurable effect. Fig. 36 illustrates the effect of the presence of copper at two different depths in a polystyrene phantom. The electron beam employed is 8 cm diameter in size, of 30 MeV energy, and measurements were performed using monocrystalline layers of TLD-100. In both cases the dose due to back-scattered electrons from the copper is significant and extends over a depth of 0.5 to 1 cm in front of the copper. The build-up of dose inside the copper is in agreement with the copper depth dose curve shown in Fig. 36 (curve A). Due to the availability of more electrons in the absorber for interaction, the dose build-up is greater and the electron energy degradation of the primary beam is more rapid. Consequently, the relative dose immediately beyond the copper is increased and the effective range is decreased. The influence of these effects on the depth dose curve below the copper depends on its location. In Fig. 36 (curve D), where the copper is placed at a depth at which the average energy of the electron beam is high, the effects are more pronounced than in the case in which the copper intercepts a beam of lower average energy (curve C).

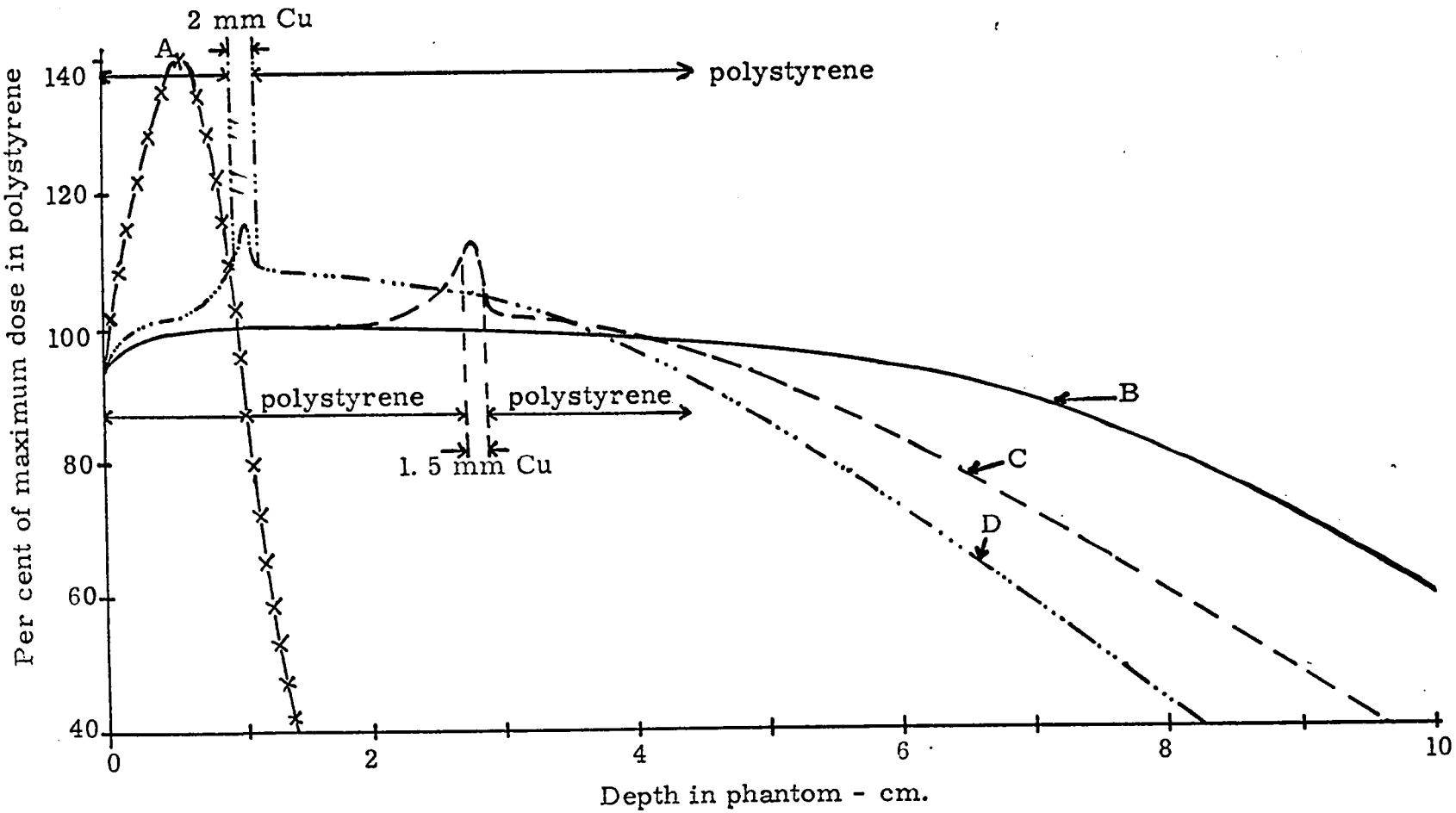

Fig. 36: The effect of the presence of copper in polystyrene phantom, in the maximum dose region and in the build-up region. A - depth-dose curve of 30 MeV (8 cm dia.) in copper; B - in polystyrene; C - in polystyrene with 1. 5 mm Cu at 3. 2 cm depth; D - in polystyrene with 2 mm of Cu at 0. 95 cm depth.

6. Electron Dose Measurements

TLD-100 is not an absolute dosemeter and must be calibrated with reference to the ferrous sulphate dosemeter. The TL emission of the irradiated samples has been measured at a suitable photomultiplier voltage (870 volts in this case), and the resulting recorded counts are related to ferrous sulphate rads (as discussed in section II C - 2). Table X shows the TL counts per rad determined as a function of energy, using the 14 x 12 cm plastic applicator. When the particular batch of TLD-100 powder has been so calibrated, it can be used for dose measurements with other beam sizes.

Figs. 37 and 38 illustrate the results of measurements of relative doses as a function of beam size, for the plastic applicators (Fig. 37) and the variable collimator (Fig. 38). All these measurements were made at the dose maximum, as determined from the build-up curves (described in section III B - 3). These values have been checked by ionization dosemeter measurements, and found to agree within a maximum of 2%.

7. Dependence of TL Response upon Electron Energy and Dose

The values of thermoluminescent counts per rads, given in Table X, are plotted in Fig. 39. These are averaged over 20 sets of independent measurements, and the standard deviations are given in the table. No energy dependence of the TL of TLD-100 is evident

TABLE X

Thermoluminescent Counts Relative to Integrator Clicks and to Ferrous Sulphate Rads, at Different Electron Energies

Accelerated electron energy (MeV)	Thermoluminescent counts per click	per rad
10	16.4 ± 0.2	17.8 ± 0.2
15	17.2 ± 0.2	17.9 ± 0.2
20	17.9 ± 0.3	17.7 ± 0.2
25	19.0 ± 0.3	17.9 ± 0.2
30	20.9 ± 0.4	18.0 ± 0.3
35	22.3 ± 0.5	17.8 ± 0.4

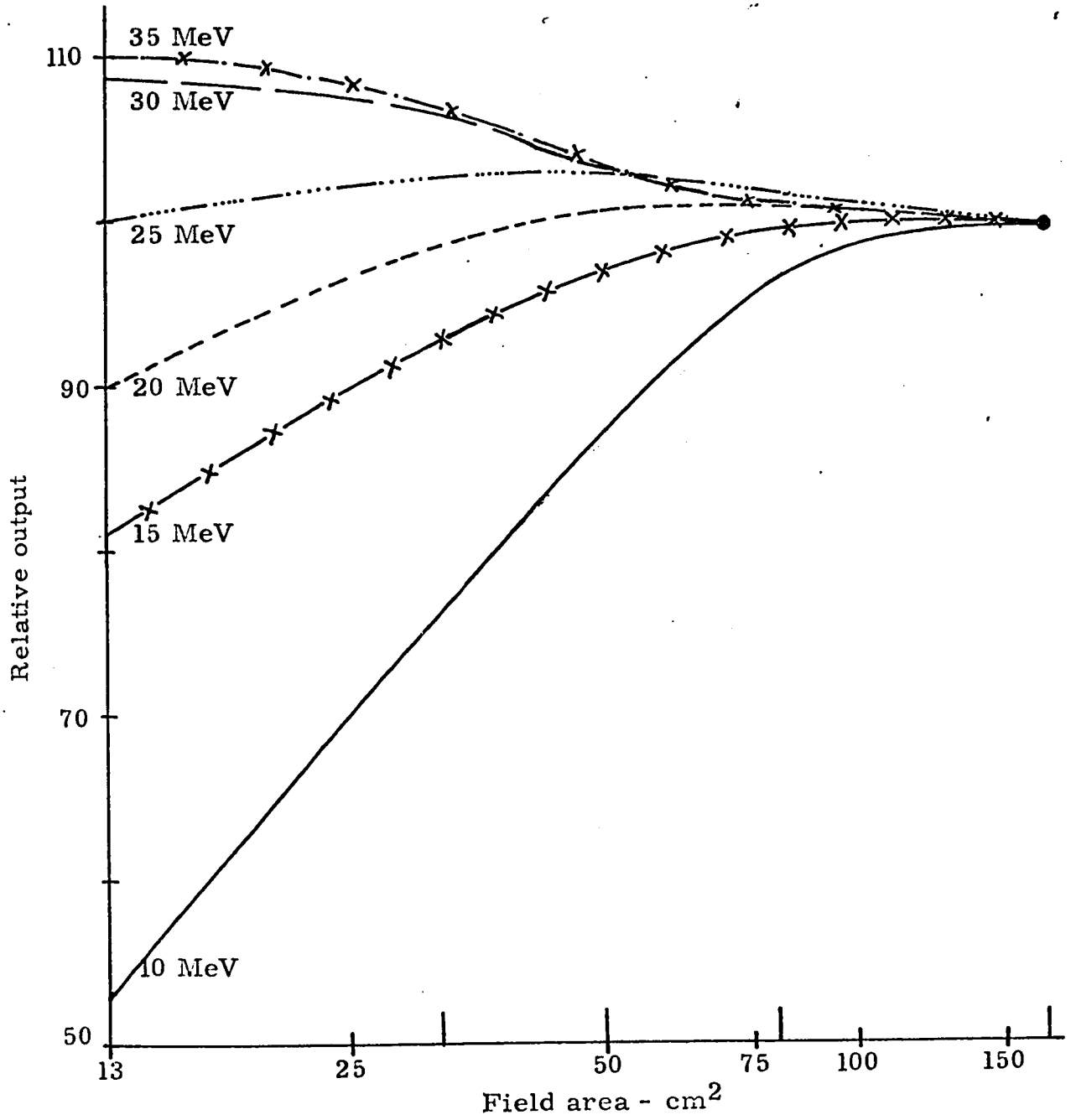

Fig. 37 : Relative output of electrons for the various plastic applicators, measured with TLD-100 (and ionization dosemeter).

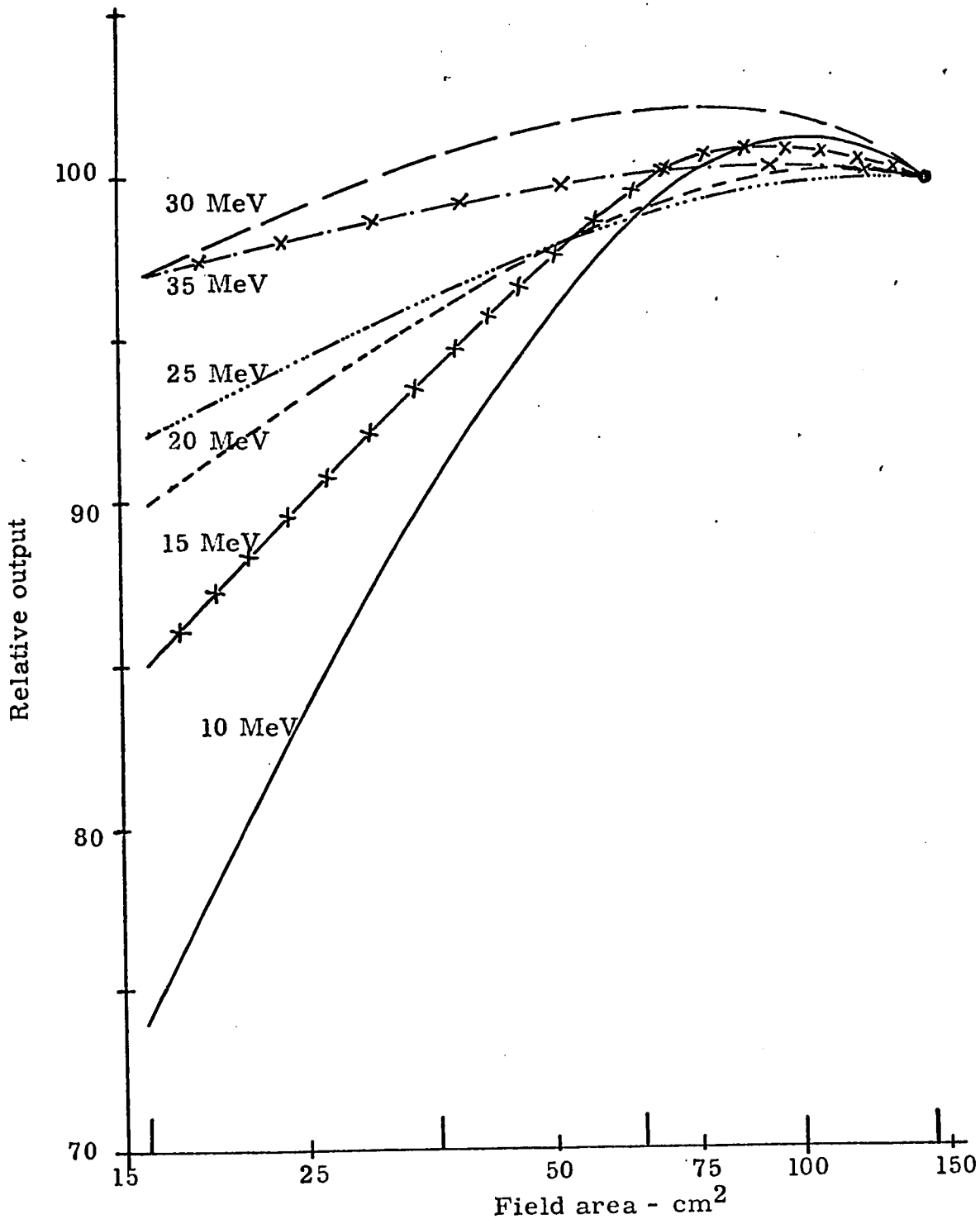

Fig. 38 : Relative output at various square field sizes, with the variable collimator, measured with TLD-100 (and ionization dosemeter) as a function of energy.

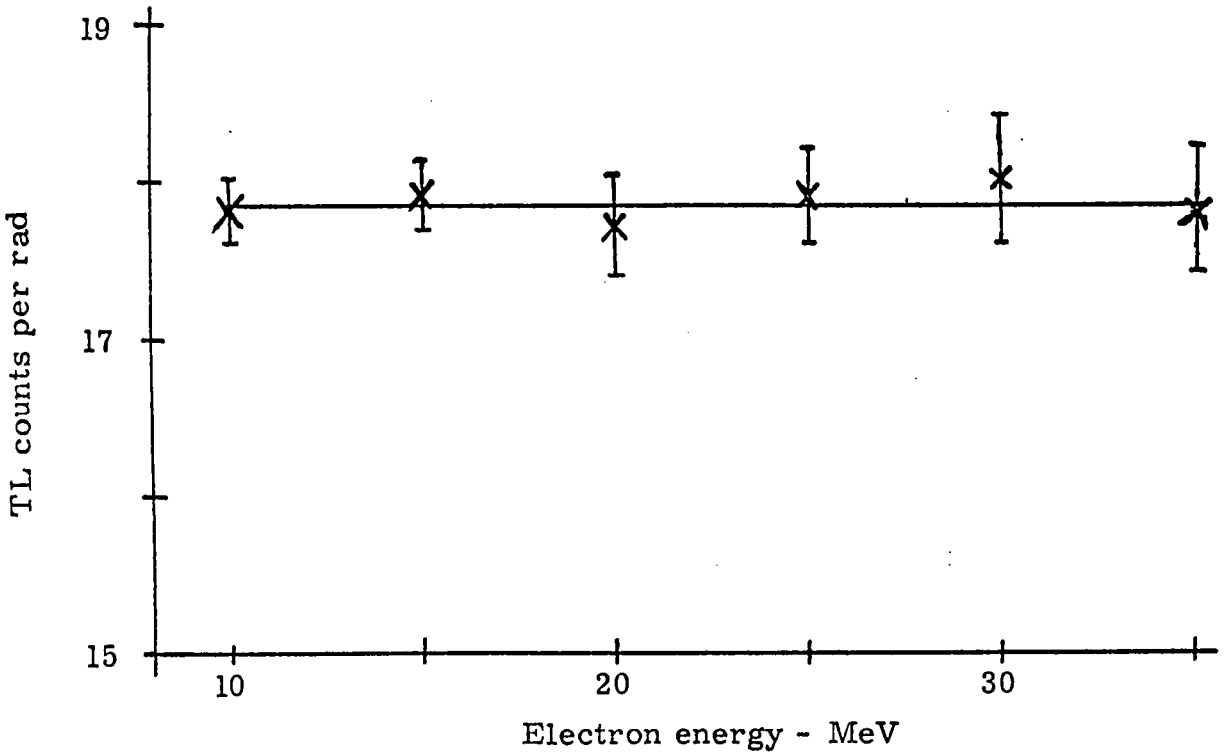

Fig. 39 : TL counts per rad at various electron energies.

in the range investigated (i. e. 10 to 35 MeV).

TLD-100 was irradiated in capsules (Fig. 7) to a dose of 100 rads in all cases. The scatter in the measured data increased with energy. This may be attributed to the short irradiation time associated with 100 rads ($\sim$ 20 seconds) at higher electron energies, compared to the order of 1 minute at 15 MeV, and 2 minutes at 10 MeV. The dose in the transverse plane varies with time, and so also the dose-rate. These are more pronounced at higher electron energies. When longer irradiation times are used the effective dose distribution and average dose-rate can be controlled more precisely. It is for this reason that the standard deviation of the results of the ferrous sulphate measurements is smaller and more consistant than that of the TL dosimetry data.

The dose dependence of the TLD-100 dosemeter is illustrated in Fig. 40, where the measured TL counts are plotted against absorbed doses in the range 10 to 5,000 rads. This dependence is the same within experimental limits at all electron energies between 10 and 35 MeV.

C. IONIZATION CHAMBER DOSIMETRY

1. Polystyrene Thimble Chamber

The ionization charge Q collected in the all-polystyrene ionization chamber described in section II C - 3, for an absorbed dose

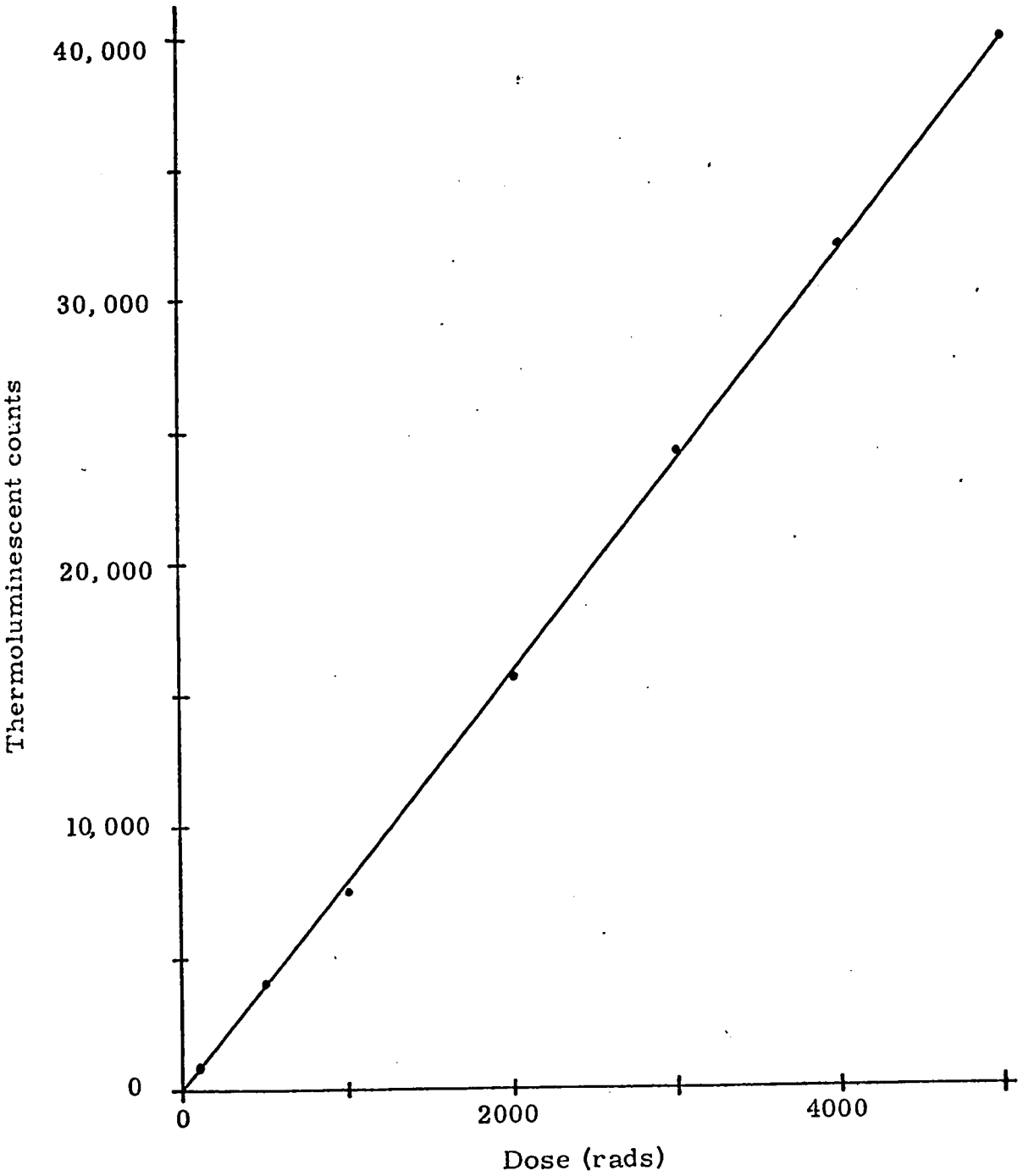

Fig.40: Dose dependence of TLD-100. TL measured at photomultiplier voltage 870 and heater settings of 55.

in the chamber wall of 100 rads, is plotted in Fig. 41. This charge, measured with a capacitor input electrometer circuit and an accurate voltmeter, is seen to increase between accelerated electron energies of 10 and 35 MeV. The increase is linear with energy, with a slope of approximately .6% per MeV. These measurements were made with the chamber in the maximum dose region of the polystyrene phantom. This energy dependence of the ionization measurements is in complete agreement with theory.

In Fig. 42 the results of similar ionization measurements are seen to have a linear dependence on dose, up to 200 rads at various electron energies. Less systematic measurements made at doses up to 600 rads display a similar dose dependence. The maximum dose attained (i. e. 600 rads) was determined by the resistance of the potentiometer in the electrometer circuit.

2. Baldwin-Farmer Thimble Chamber

The Baldwin-Farmer ionization chamber discussed in section II C - 2, is conventionally employed (94) for the measurement of absorbed dose in an electron beam, in the peak dose region of a polystyrene phantom. The range of the Mk2 Baldwin-Farmer dosemeter used in this work is only 0 to 60 roentgens when used to measure x-ray exposure. When this instrument is used to calibrate an electron beam, for which the roentgen (R) is not defined (57), we arbitrarily

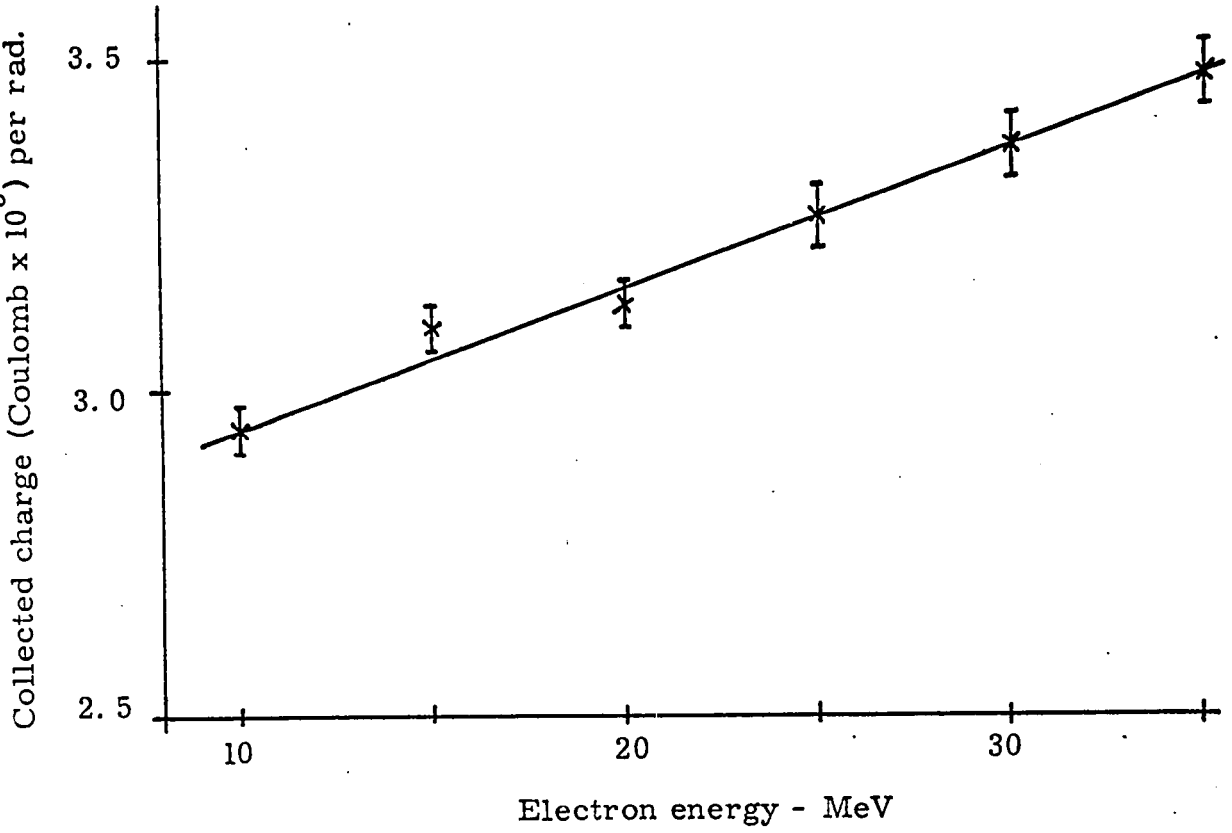

Fig. 41 : Electron energy dependence of ionization measurements with the polystyrene chamber.

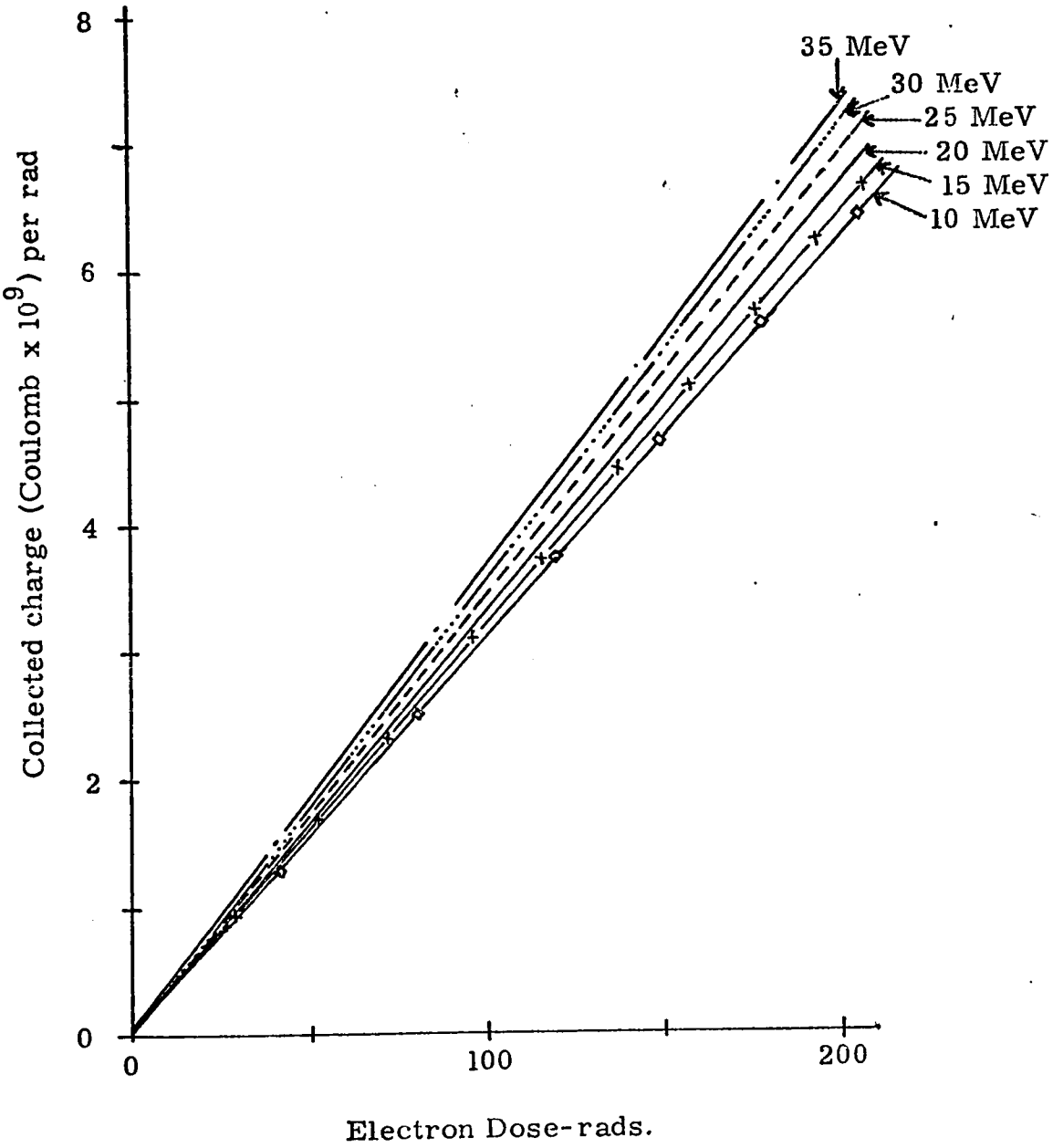

Fig. 42 : Electron dose dependence of ionization chamber mesurements with all polystyrene chamber, at various accelerated electron energies.

designate the scale divisions as "R". When this Baldwin-Farmer response has been calibrated against the ferrous sulphate dosemeter for a particular energy and set of irradiation conditions, it may then be used as a quick and accurate means of beam output measurement. The Baldwin-Farmer response in "R" per rad is listed in Table XI, as a function of energy and for two different irradiation conditions. The results show a uniform increase with accelerated electron energy, as seen in Fig. 43. The open beam output values are always greater than the corresponding 14 x 12 cm values, and the energy dependence in the latter case is more pronounced. We conclude that the effective energy of the open beam is always higher than that of the 14 x 12 cm beam.

When the plastic applicator is used, the scattering from its walls results in a reduction in the effective energy of the beam. Since the ferrous sulphate dosemeter has been found to be energy-independent (section III D - 1), the presence of lower energy electrons does not affect the measurement of dose (in rads) by this method. On the other hand, the ionization measurements will be affected because of the reduced polarization effect at lower electron energies. Thus the ionization per rad determined using the plastic applicator would be expected to be smaller than that for the open beam, where the low energy scatter contribution is a minimum. This is confirmed by the data of Fig. 43.

TABLE XI

Baldwin-Farmer "R" per rad Measured for the 14 x 12 cm Plastic Applicator and the the Open Beam, at Various Accelerated Electron Energies

Electron energy (MeV)	Baldwin-Farmer "R" per rad for 14 x 12 cm	open beam
10	1.03 ± 0.03	1.07 ± 0.03
15	1.05 ± 0.03	1.09 ± 0.03
20	1.08 ± 0.03	1.12 ± 0.03
25	1.09 ± 0.03	1.14 ± 0.03
30	1.11 ± 0.03	1.18 ± 0.03
35	1.12 ± 0.04	1.20 ± 0.04

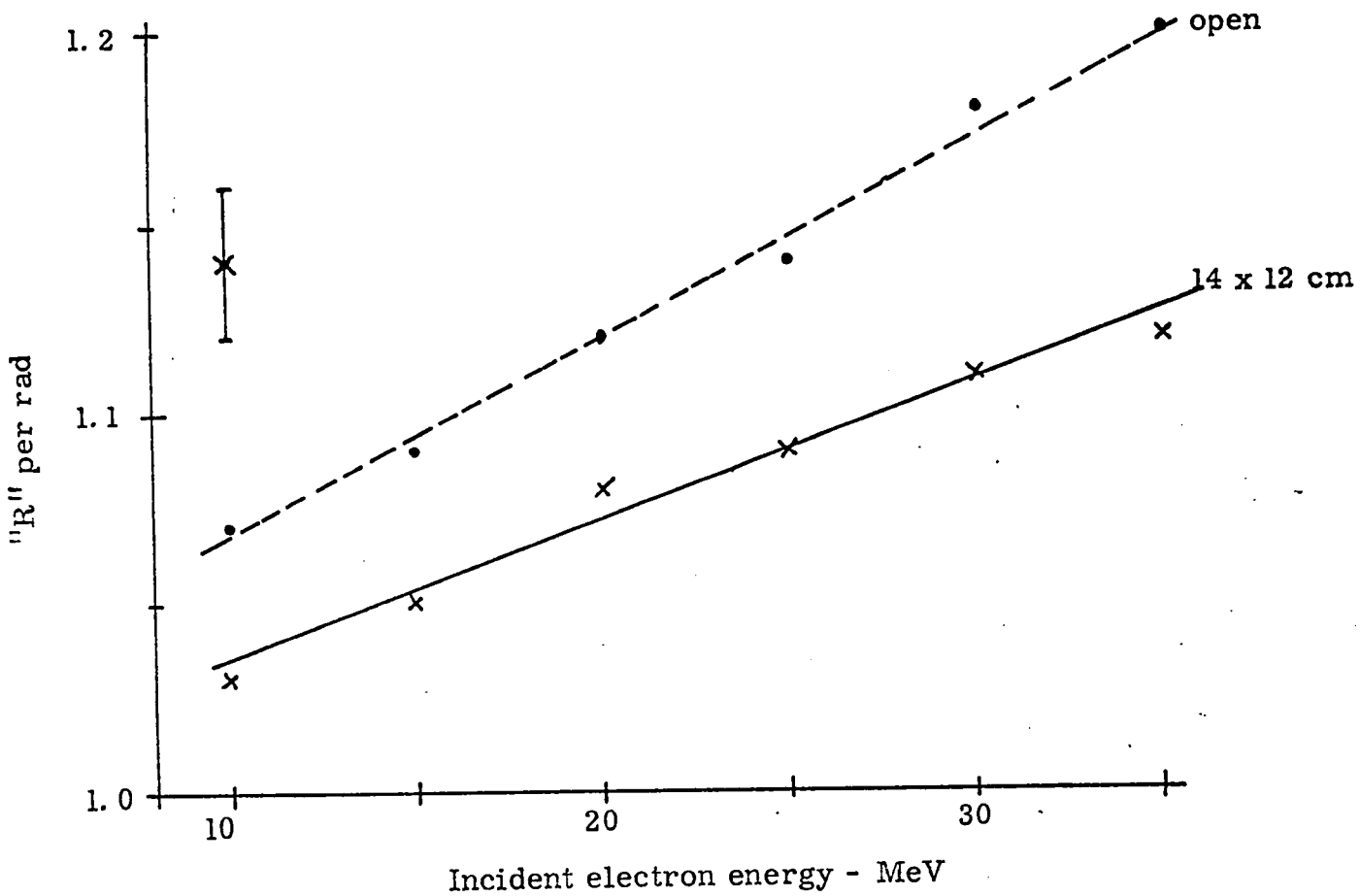

Fig. 43 : Baldwin-Farmer "R" per rad measured for the 14 x 12 secondary applicator and for open beams as a function of energy.

The response of the Baldwin-Farmer instrument may be converted to COBALT-CORRECTED "R" by multiplying it by the Co-60 quality factor as supplied by the National Research Laboratories for that particular instrument. The results may then be compared with the corresponding ferrous sulphate dose in rads to determine the applicable C_F factors (section II C - 2) for this chamber. The magnitudes of these absorbed dose conversion factors C_F depend upon the incident electron energy and on the depth at which the measurements are made.

Average values of 10 to 12 independent sets of measurements to compare ferrous sulphate dose (rads) and Baldwin-Farmer "Cobalt-corrected R" are listed in Table XII. These measurements have been made at 2 cm depth in a polystyrene phantom. Comparison measurements of dose (in rads) with the ferrous sulphate solution in the pillbox shaped irradiation cells with those using the cylindrical irradiation cells (Fig. 3) of size and shape identical to the Baldwin-Farmer cavity showed agreement within a standard deviation of 1%. All values given in Table XII are for the 14 x 12 cm beam size, using the plastic applicator. The cobalt quality factor used is 1.07. The values of C_F are presented in a graphical form in Fig. 44. The theoretical and experimental values of Almond (5) and the experimental values of Svensson and Pettersson (93) are also shown for comparison. The theoretical values have been calculated from the equation (v), on the assumption that the ionization chamber behaves as a Bragg-Gray cavity (section II C - 2) for electron

TABLE XII

C_F Values for Electrons from 10 to 35 MeV Accelerated Energy. The Values were Measured at 2.0 cm Depth in Polystyrene Phantom and are Average of 10 to 12 Independent Sets of Measurements. The beam size is 14 x 12 cm, using the Plastic Applicator

Electron energy (MeV)	Cobalt corrected "R" per click	rads per click	C_F rads per "R"
10	1.00 ± 0.02	0.91 ± 0.03	0.91 ± 0.03
15	1.08 ± 0.02	0.96 ± 0.03	0.89 ± 0.03
20	1.16 ± 0.02	1.01 ± 0.03	0.87 ± 0.03
25	1.24 ± 0.02	1.06 ± 0.03	0.85 ± 0.03
30	1.38 ± 0.02	1.16 ± 0.04	0.84 ± 0.03
35	1.50 ± 0.02	1.25 ± 0.05	0.83 ± 0.04

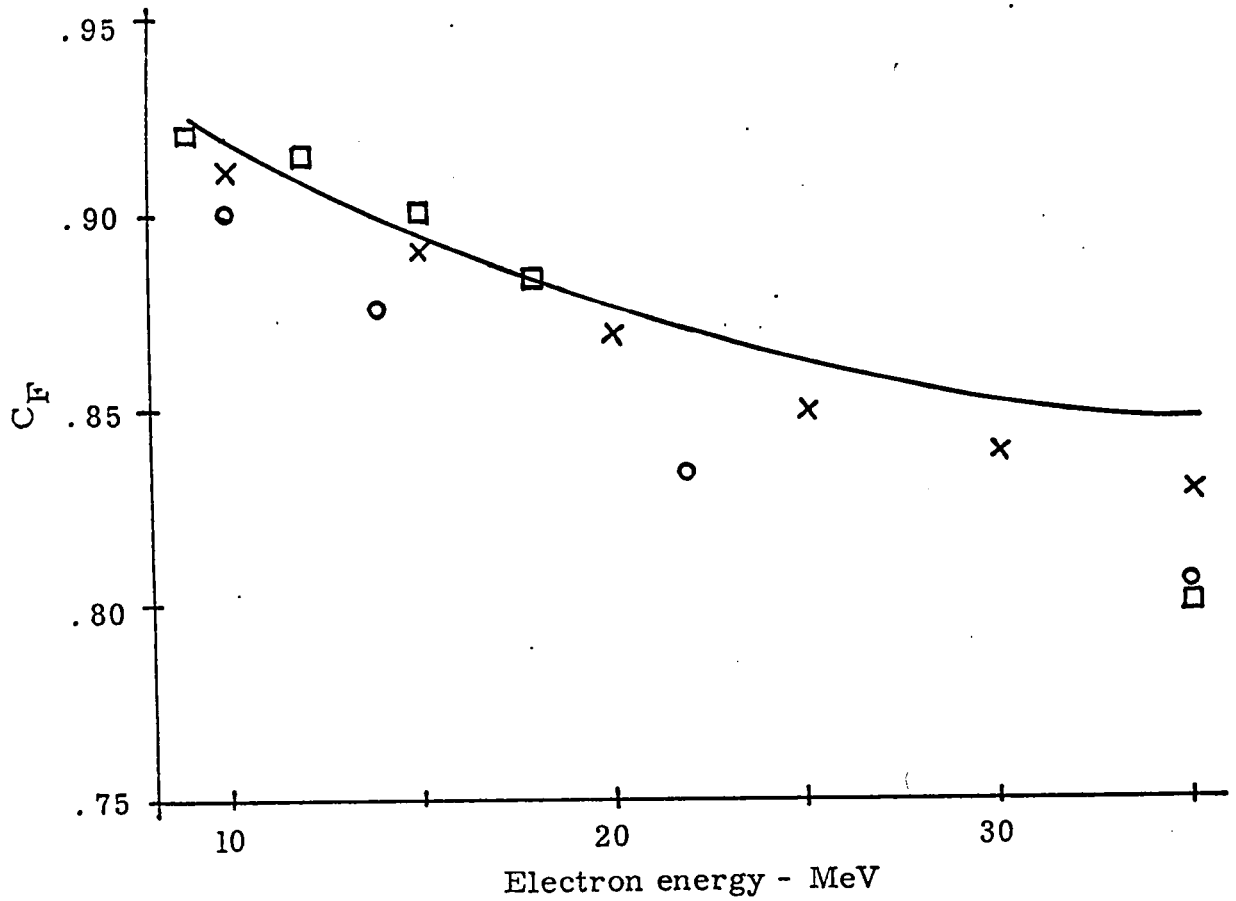

Fig. 44: Theoretical and experimental values of C_F; curve shows the theoretical values and experimental values - □ - Almond; o - Svensson and Pettersson; x - this work.

measurements. Our experimental results agree with the theoretical value within 1/2% at 10 MeV, but the difference increases with energy to 2% at 35 MeV. Compared to the experimental values of Almond, Svensson and Pettersson, our results are in better agreement with the theory.

3. Variable Volume Ionization Chamber

Once calibrated, the pillbox-shaped parallel-plate ionization chamber (section II C - 3) can also be used to determine the absorbed dose in a medium irradiated with electrons. With the chamber connected to the electrometer by a 50 foot cable, ionization measurements were made in esu per cm^3. The volume of the ionization chamber was varied in steps between 0.25 and 1.25 cm^3, to study the effect of the size of the cavity on the ionization measurements. The collected charge, stated in esu cm^{-3} rad^{-1} at the dose maximum of the uncollimated electron beam (i. e. open beam), is given in Table XIII. It is apparent that the ionization produced per unit volume is unaffected by the cavity dimensions within the range investigated. The average values from Table XIII are shown in graphical form in Fig. 45.

In the measurements with the pillbox chamber, it was observed that the results obtained when collecting negative ions were numerically greater than those when collecting positive ions (Table XIV), except at very high electron energies. Further this difference was

TABLE XIII

Esu per cc per Rad as a Function of Collecting Volume as Measured with a Pillbox-shaped Chamber at Various Electron Energies. These Values are Averages of those Obtained when Collecting Positive Ions and Negative Ions. Measurements were made at a Depth of 2.2 cm in a Polystyrene Phantom under Open Field Conditions

Cavity volume (cc)	esu per cc per rad at electron energies (MeV)					
	10	15	20	25	30	35
0.25	1.34	1.39	1.42	1.50	1.55	1.58
0.50	1.38	1.36	1.41	1.48	1.51	1.54
0.75	1.35	1.37	1.40	1.49	1.52	1.58
1.00	1.35	1.36	1.40	1.48	1.55	1.58
1.25	1.32	1.39	1.43	1.51	1.54	1.54
Average	1.34	1.38	1.41	1.49	1.53	1.56

Standard deviation 0.02

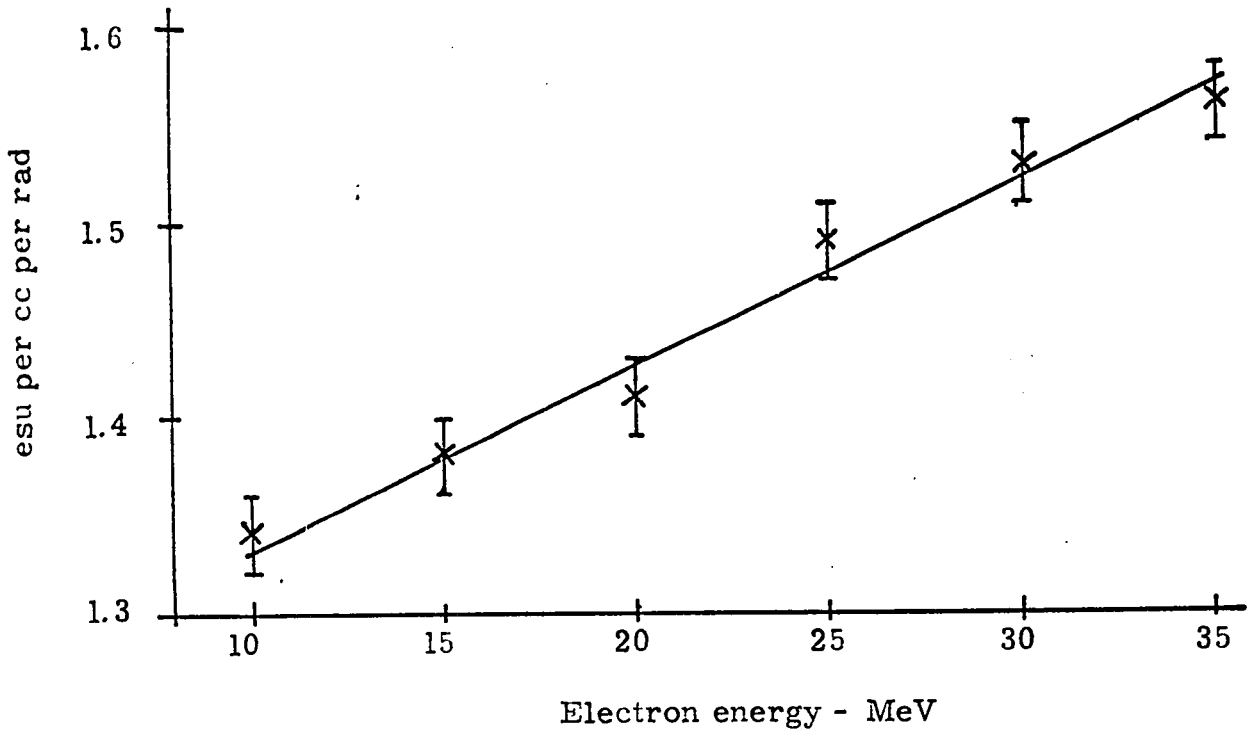

Fig. 45: Energy dependence of the dosimetric response of the pillbox-shaped parallel plate ionization chamber.

TABLE XIV

Average esu per cc per Rad Measured with Opposite Polarities of the Collecting Electrode, taken at a Depth of 2.2 cm in a Polystyrene Phantom; Average of Values Measured with Different Collecting Volumes. The Value when Positive Ions were Collected is called P and those when Negative Ions were Collected are called N.

Ions collected \ MeV	esu per cc per rad for open field					
	10	15	20	25	30	35
P	1.38	1.42	1.44	1.51	1.55	1.57
N	1.29	1.33	1.38	1.48	1.53	1.55
N/P	1.07	1.07	1.04	1.02	1.01	1.01

Standard deviation 0.02

observed to decrease with increasing electron energy. This effect is superficially similar to that observed in the absorbed dose build-up region of a Co-60 γ-ray beam by Aspin et al (7). It may be explained by a consideration of the effect of the electrons which come to rest in the collecting electrode.

As electrons lose their kinetic energy and come to rest in a dielectric absorber, a build-up of negative charge occurs which is centered at a depth of approximately 0.8 R_p (where R_p is the practical range). Close to the surface, a net positive charge remains because of the loss of electrons in the region which have been propelled to greater depths. The theoretical charge distributions produced by electron beams of energy 10, 20 and 35 MeV, as a function of depth, are shown in Fig. 46 (63). When the pillbox chamber is placed in the phantom at any depth $< 0.8\ R_p$ the deeper electrode will be surrounded by a region of more excess negative charge than will the one nearer to the surface. In the region beyond 0.8 R_p, according to Laughlin's theory, the opposite will prevail.

To examine this theory, an experiment was performed in which the measurements to determine the esu cm^{-3} rad^{-1}, were repeated at depths of 0.2, 2.2 and 3.9 cm, with electron beam energies of 10, 20 and 35 MeV. The depth 3.9 cm was chosen because it is beyond 0.8 R_p for the 10 MeV electron beam. The results of this experiment are given in Table XV.

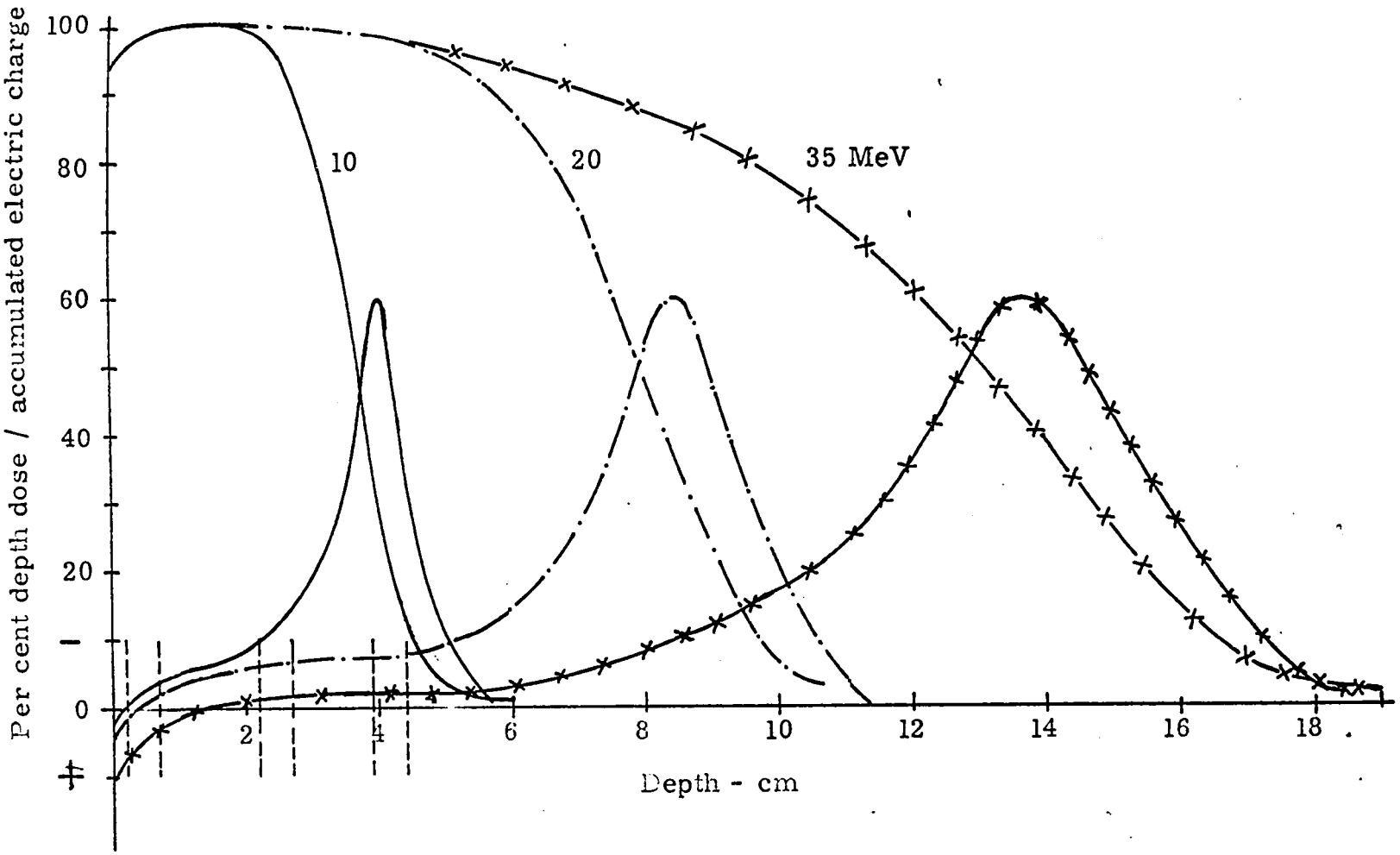

Fig. 46 : Central axis depth-dose curve and charge distribution as a function of depth produced by 10, 20, and 35 MeV electron beams in polystyrene [The latter adapted from Laughlin, J. S., In: Symposium on high energy electrons, Springer-Verlag, New York (1965), p. 11.]

TABLE XV

N/P Ratios Measured at Depths of 0.2, 2.2, and 3.9 cm in Polystyrene, using Electrons of Beam Energy 10, 20 and 35 MeV

Electron energy (MeV) \ depth (cm)	The ratio N/P		
	0.2	2.2	3.9
10	1.01	1.07	1.11
20	0.99	1.04	1.04
35	0.97	1.0.	0.99

N - collecting electrode positive to collect negative ions.

P - collecting electrode negative to collect positive ions.

We see that, with 35 MeV electron beam, the N/P ratio is close to unity at the 2.2 and 3.9 cm depths, and indicates an excess positive charge at 0.2 cm, in confirmation of the curve in Fig. 46. At 20 MeV, the excess positive charge at 0.2 cm depth has virtually disappeared, and the N/P ratio exceeds unity at the other two depths because of the positive slope of the charge distribution curve at these points. When the electron energy is decreased to 10 MeV, the ratio increased at all three depths. This is in quantitative agreement with the theoretical curve in Fig. 46, except for the value at 3.9 cm depth. The large value of the ratio N/P for 10 MeV electrons, at the depth of 3.9 cm (which is greater than 0.8 R_p) indicates that the peak value of the charge distribution curve (Fig. 46) occurs at depths greater than the theoretical value of 0.8 R_p.

Upon confirmation of this theory, it was decided to average the N and P values to eliminate the error due to the additional charge collected by the deposition of charge at the electrode by the electron beam in the dielectric.

D. INTERCOMPARISON

1. Absorbed Dose at a Point

The results of electron dose measurement using the three dosimetric systems, at 2.0 cm depth in the polystyrene phantom and

for the 14 x 12 cm beam (using plastic applicator) will first be compared. The response of the dosemeters per integrator click, normalized to 1.0 at 10 MeV are plotted in Fig. 47. The ionization results increase more rapidly with electron energy than do those of ferrous sulphate and TL dosemeters. This is due to the polarization effect discussed in section II D - 1.

Several workers have reported in the literature a number of conflicting values of $G_{Fe^{+++}}$ when the ferrous sulphate dosemeter is used in conjunction with high energy electron beams; these are summarized in Table XVII in Appendix II, and are plotted in Fig. 48. On the assumption of linearity a trend line has been drawn, which shows an increase of $G_{Fe^{+++}}$ with electron energy, although this conclusion is by no means unambiguous.

The electron doses measured by the ferrous sulphate method were calculated so far on the basis of a constant G-value of 15.5 ions per 100 eV. Values calculated on the basis of the varying G-value as given by the trend line of Fig. 48, have also been plotted in Fig. 47. Upon the assumption of a constant G-value, the results of ferrous sulphate measurements are less than those measuring LiF thermoluminescence. When a constant G-value is assumed, the relative doses calculated are in close agreement with the theory. Thus, this experimental evidence favours a constant value of $G_{Fe^{+++}}$ for the electron energy range investigated in this work.

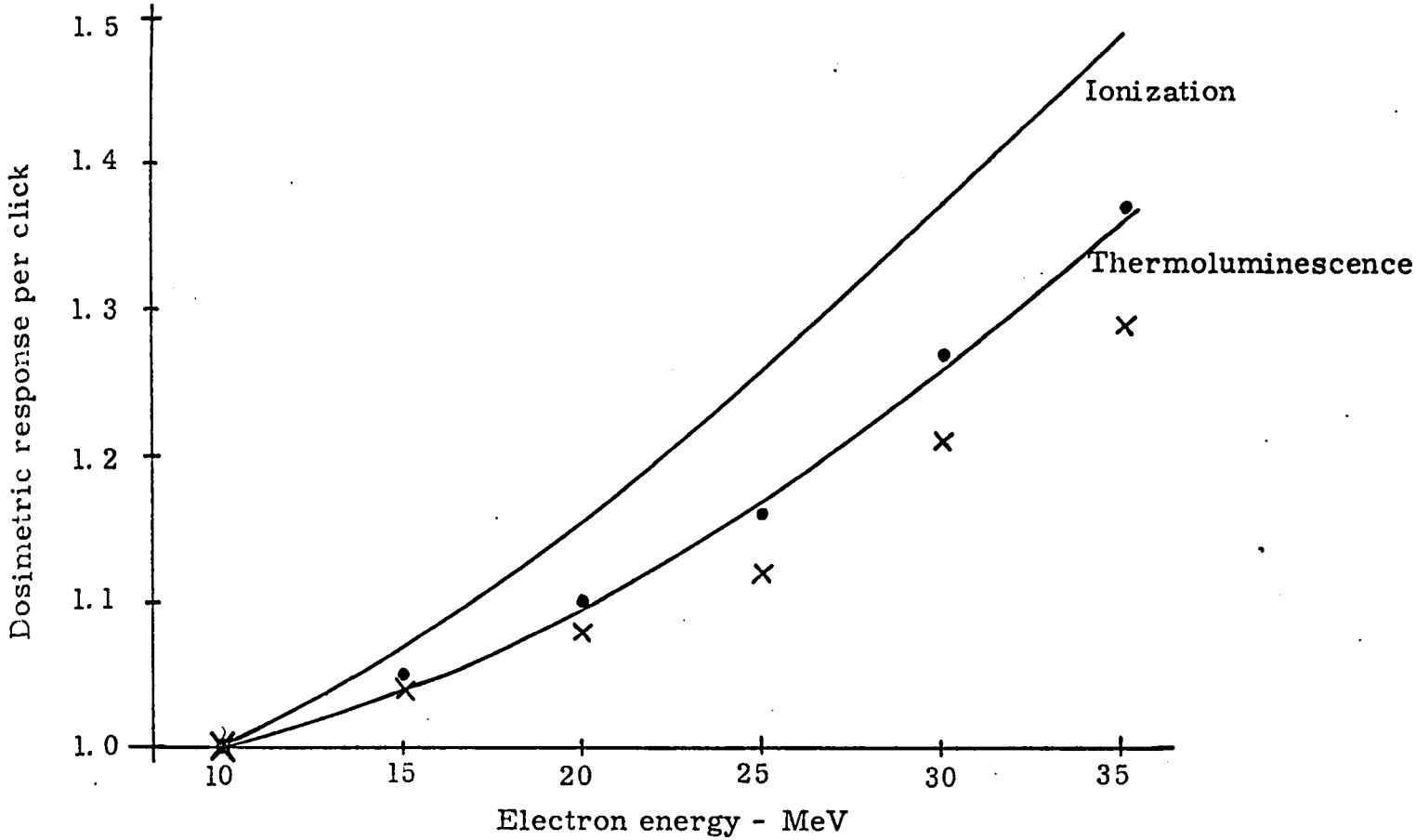

Fig. 47 : Relative response of ionization chamber, ferrous sulphate dosemeter, and TLD-100, normalized to that at 10 MeV. Ferrous sulphate values plotted are: ⊙ - for a constant G-value, and ✕ -for a varying G-value

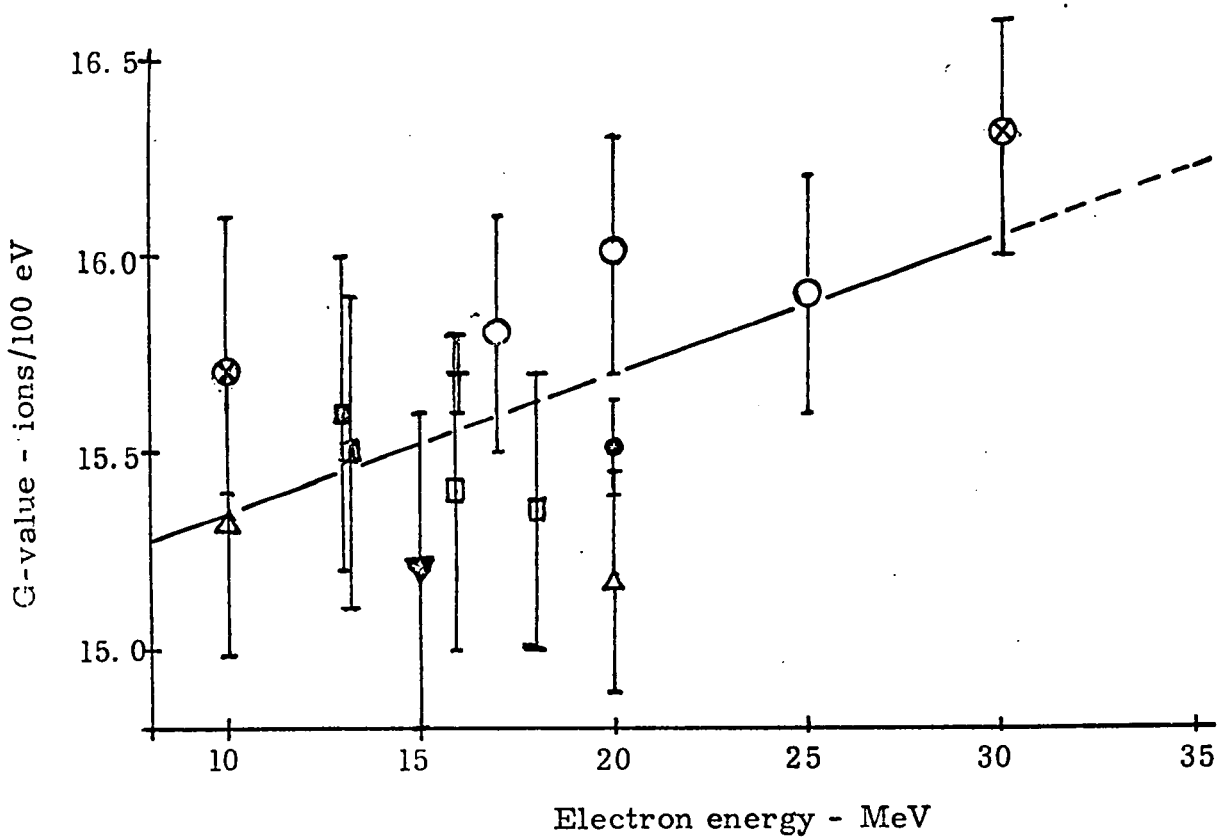

Fig. 48 : The electron G-values collected from the literature: - ▣ - Thomas and Hart; ✕ - Minder; ⊙ - Liesem and Pohlit; Δ - Geisselsoder et al.; ◻ - Almond; ● - Pettersson and Hettinger; ▽ - Anderson and +- Zsula et al.

2. Central Axis Response Curves

The dose distributions along the cental axis of the electron beam of 10, 15, 20, 25, 30 and 35 MeV energy, were measured with the ferrous sulphate dosemeter (section II A - 2), with TLD-100 (section II B - 3), and with the all-polystyrene thimble ionization chamber (section II C - 2). Two typical sets of results are plotted, for a beam size of 14 x 12 cm using the plastic applicator, in Fig. 49, as percentages of the dose maximum. Each of these data points is an average of 15 measurements, and it is seen that the relative values measured with the three different dosimetric systems agree at all energies, within the standard deviation of measurements.

The agreement shown by the ionization chamber values with the other two is most important. Hettinger et al. (52) concluded from their experimental observations that when the center of the thimble chamber is selected as the measurement point, the ionization dose ratio has to be corrected for displacement of the phantom material by the air cavity. On the other hand, Loevinger et al. (68) found that this correction is unnecessary when ionization thimble chambers are employed in measuring electron doses. The results of the present work do not settle this controversy, since the radius of the ionization chamber used is only 0.15 cm, and the difference would thus be less than the accuracy of measurement.

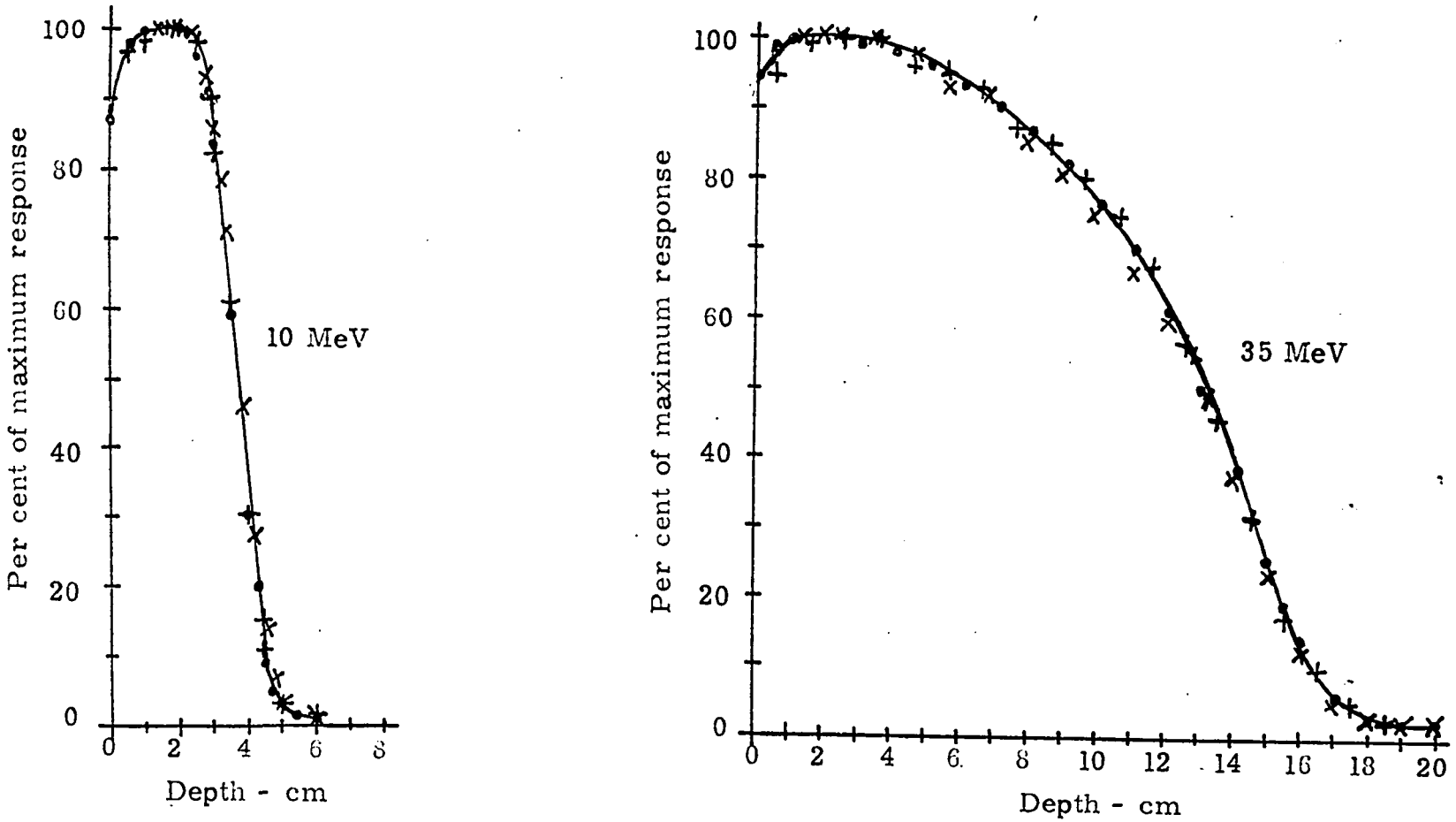

Fig. 49: Central axis depth dose measured in polystyrene, by the three dosimetric systems - ● - TLD-100; + - ferrous sulphate dosemeter; and x - polystyrene ionization chamber. Standard deviation : ferrous sulphate 3%; ionization and TLD 1%.

3. Iso-response Curves

Films and ionization thimble chambers are usually employed in the measurement of the iso-response curves used in radiation therapy. In Fig. 50, a typical set of curves measured with the Baldwin-Farmer ionization chamber is illustrated. This corresponds to the distribution in the plane including the central-axis of the electron beam and the accelerating orbit. The beam size used was 14 x 12 cm (plastic applicator), and the distribution was measured along the 12 cm side. The set of isodensity curves was measured on Kodaktype R film after exposure in the same plane as described in Appendix III B. The percentage contours are obtained by measuring the relative optical density of the film with the densitometer. These isodensity curves are shown in continuous lines in Fig. 50.

When measuring the optical density of the film, the net value is obtained by subtracting the background optical density of the film from the measured density. The maximum net optical density along the central-axis has been taken as 100% in determining the relative values. The agreement between results obtained by film and ionization measurements are good, except for the 95% iso-response curves. This is attributed to the large standard deviation inherent in the photographic dosimetry. Since, in electron therapy the tumour volume is generally made to include in the 80% isodose volume, this disagreement is not significant.

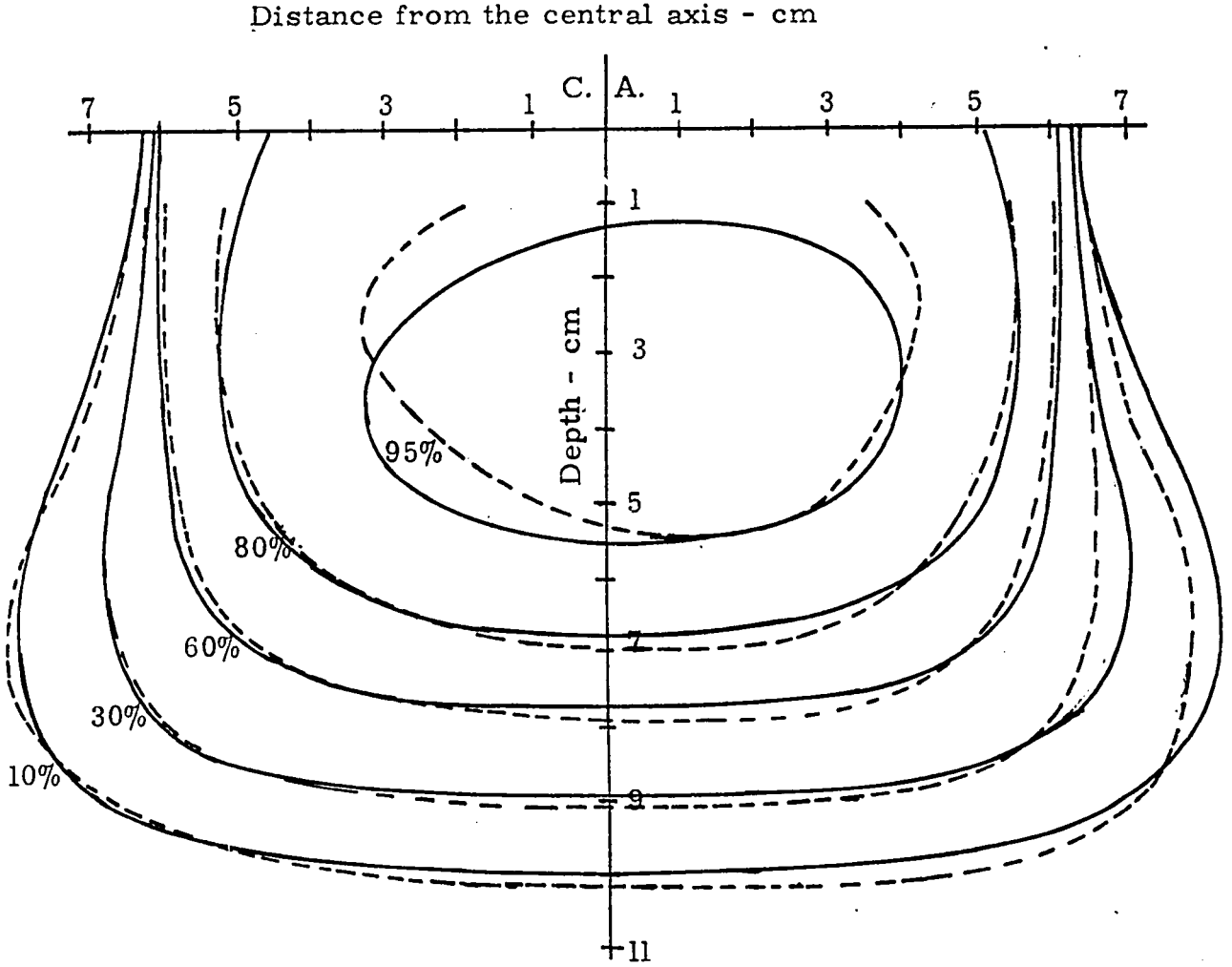

Fig. 50 : Iso-response curves for 20 MeV electrons, 14 x 12 cm applicator beam, along the 12 cm side. Continuous curves are those measured with photographic film, and dashed curves are those measured with the Baldwin-Farmer ionization chamer.

4. Polarization Correction

In the determination of absorbed dose produced by Co-60 γ-rays, a thimble ionization chamber, which has been calibrated to read in roentgens for Co-60 radiation, is introduced into the medium at the point in question. The reading obtained with this instrument may be then converted to absorbed dose in rads, using the Bragg-Gray relation (equation i). It would be desirable to be able to use such an ionization chamber in the determination of absorbed dose in a medium irradiated with high energy electrons. A simple conversion factor analogous to that of the Bragg-Gray relation must take into account the effects of polarization of the medium. Zsula et al. (102) have calculated theoretical values of the polarization correction for water and polystyrene (relative to air) for a few electron energies up to 20 MeV. However, no experimentally determined values for these correction factors have been reported previously.

In experiments described in section II D - 2, we wished to determine this polarization correction, so that ionization chamber instruments can be used to determine the electron absorbed dose in a tissue-equivalent medium. Table XVI gives the average value of the ratio R_T in rads per esu cm^{-3}, along with the ratio R_T/R_o, which is plotted in Fig. 51; $(1 - R_T/R_o)$ gives the per cent polarization correction. The electrons lost approximately 8% of its energy in

TABLE XVI

Ratio (R_T) of the Dose Measured by Ferrous Sulphate Dosemeter (in rads) and the Ionization Measured by the Parallel-Electrode Chamber (in esu cm^{-3}), at Different Electron Energies. The Ratio R_o for Co-60 X-rays is 0.796 Rads per esu cm^{-3}.

Electron energy T (MeV)	Ratio R_T (rads per esu cm^{-3})	Ratio R_T / R_o
4.7	0.747	0.938
9.5	0.728	0.915
14.1	0.709	0.891
18.9	0.672	0.844
23.1	0.655	0.823
28.0	0.636	0.799

Standard deviation 0.021

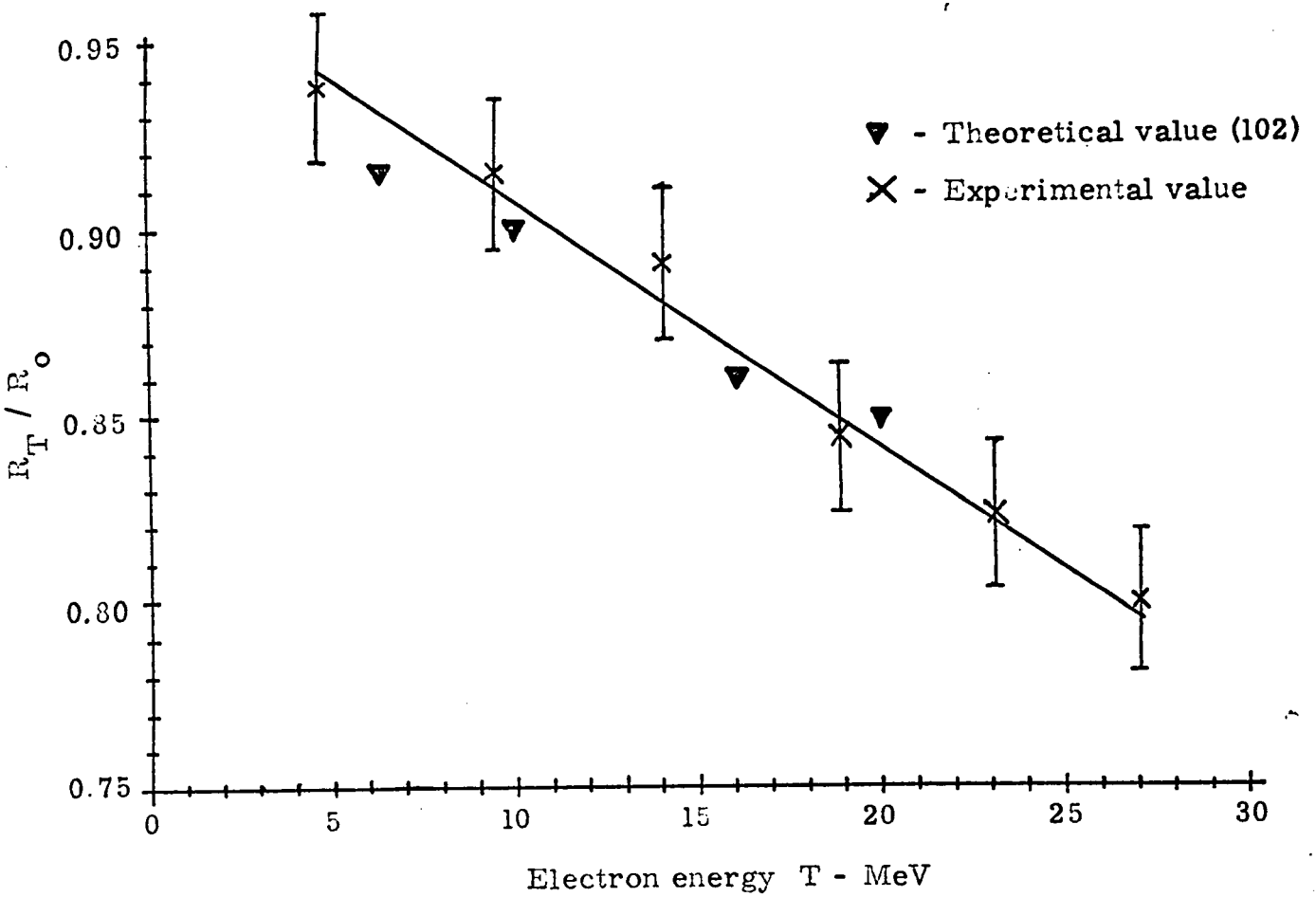

Fig. 51: Effects of polarization on absorbed dose in water relative to air.

traversing the donut wall, the scatterer and the transmission ionization monitoring chamber. In addition, the electron penetrated 2 cm of polystyrene (and ferrous sulphate solution) before reaching the center of the dosemeter. In order to calculate the effective energies at this point, a complete knowledge of the spectral distribution, at this point, is necessary. Since such data were not readily available, calculation was based on other published data (45, 77). The electron energies T, given in Table XVI, have been calculated from these data.

The theoretically calculated values (102) are plotted in Fig. 53, along with our experimental values for comparison. It shows that the per cent polarization corrections calculated theoretically agree with those determined experimentally, within experimental limits.

CHAPTER IV.

SUMMARY AND CONCLUSION

CHAPTER IV

SUMMARY AND CONCLUSION

The Asklepitron 35, which was employed as the source of high energy electrons in this work, was designed primarily for the radiation therapy of cancer. While dosimetric techniques are well established for use with ortho- and mega-voltage x-ray therapy, this is not true in the case of the therapeutic use of high energy electrons.

Conventional dosemeters are routinely calibrated against national standards at all x- and γ-ray energies that are employed in medicine. Below 1 MeV the calibration standard is a free-air ionization chamber; above this energy it is a Co-60 or radium source of known activity. At the present time, no national standards exist for high energy electron dosimetry. Consequently, physicists concerned with the treatment of cancer using high energy electrons must rely on dosimetric systems calibrated in their own laboratories. None of the available dosimetric systems are completely understood as regards their response to electron irradiation. Because of this,

investigations similar to that reported in this thesis are under way at several other laboratories.

The fundamental problems in dose evaluation are the determination of absorbed dose D_d in the measurement system, and the calculation of absorbed dose D_m in the surrounding medium from the knowledge of D_d. A conversion factor is involved in the determination of D_d from the results of measurements with any dosemeter. In the case of calorimeters, this factor converts the measured temperature increase in the absorbing element to dose D_d. In ferrous sulphate dosimetry, this conversion factor, which depends principally on the G-value, is used to convert absorbance measurements to dose D_d. In ionization dosimetry the amount of charge collected must be converted to dose D_d through the use of some factor such as C_F, which has been discussed in section III C - 2. In each case the conversion factor must be universally accepted, so that the measurements at all institutions are made in identical dose units, within the prevailing experimental uncertainties. For measurements in high energy electron beams, none of the available dosimetric systems have yet reached the final stage of development in which these conversion factors are well-established. The results reported in this thesis bring this stage closer in the cases of ferrous sulphate and ionization dosimetry.

When the dose D_d in the dosemeter has been determined, the dose D_m in the surrounding medium can be calculated from it by

the use of a factor which depends upon the materials of the dosemeter and absorber and upon the energy spectrum of the electrons. The relationship between D_d and D_m is readily obtainable in the presence of electron equilibrium (i. e. when the number of electrons entering the dosimetric element is equal to the number leaving it) and when the electron fluence is unchanged by the introduction of the dosemeter into the absorbing medium. Under these conditions

$$D_m = (S_d / S_m) D_d , \qquad (vi)$$

where $S = 1/\rho \, (dE/dx)$ is the total mass stopping power of the material, ρ being its density. This ratio of mass stopping powers is dependent on the primary electron energy.

The problem at hand is to be able to state the magnitude of the absorbed dose in rads, at a point in the irradiated volume within the patient under treatment. The direct and precise calorimetric measurement of radiation energy locally absorbed in tissue is impracticable with present techniques, and so indirect methods of determining the dose must be employed. A study of the present status of electron dosimetric techniques indicates that more experimental data are required on topics such as broad beam attenuation, secondary electron spectra at all points in the irradiated media and polarization-corrected stopping powers.

When an accurate radiation calorimeter is not available, the ferrous sulphate dosemeter has proven to be the most reliable system upon which to base the determination of electron dose. The microdosemeter developed in this work (section III A - 6) increases the value of this system by extending the lower limit of the useful dose range to 500 - 1000 rads, instead of 4000 - 5000 rads required in the conventional technique. A further advantage is the small volume ($< 0.5\ cm^3$) of dosimetric solution required which approximates point dosimetry. The introduction of this small quantity of nearly tissue-equivalent solution into a tissue-equivalent phantom distorts the particle flux only slightly, when the containers of the solution are of the same material as the phantom. This microdosimetric technique has a reproducibility of $\pm$ 3%, most of which is introduced by the use of polystyrene irradiation containers.

At present the principal indeterminancy associated with the realization of absorbed dose in rads using ferrous sulphate dosimetry arises from an uncertainty in the G-value for electrons. Available data show a maximum spread of 7.5% in the calorimetrically-determined values, and an even greater spread of 12% if all the values listed in Table XVII are considered. The calorimetrically-determined values are constant within the quoted experimental limits. However, no calorimetrically-determined G-values are available for electron energies above 20 MeV. On the other hand, the G-values determined

by the ionization method include the polarization correction, which increases with increasing electron energy. An analysis of the experimental results reported in this work supports the choice of a constant G-value, rather than one increasing with electron energy. The existence of a constant G-value above 20 MeV is justified by the experimental data and by the published G-values determined by calorimetric methods at energies below 20 MeV.

The high sensitivity of the ferrous sulphate dosimetric solution to organic impurities is a disadvantage of the method. Careful cleaning and handling the dosemeter, and the use of analytical reagent chemicals cannot completely eliminate this, especially when the solution has to be transported from place to place. In addition, the skill and experience of the operator is a factor in the accuracy of the measurements, and limits its usage as a routine dosemeter.

Ionization chambers are very useful for beam monitoring and for routine dose-rate measurements. The chambers and their associated equipment are widely used for x- and γ-ray dosimetry, so the actual measurement techniques are familiar and the reproducibility is excellent. However, the theory involved in the determination of the absorbed dose from ionization measurements of high energy electrons is not yet completely understood. The ionization chamber can only be a sub-standard dosemeter, and must be calibrated against

some absolute system. The conversion factors C_F given in section III C - 2 provide the necessary calibration for commercial x-ray dosemeters used in the determination of electron doses. These factors combined with the calibration factor of the individual instrument at Co-60 γ-ray energies provide a basis for ionization measurements of absorbed dose of electrons.

Ionization chambers of one type could show consistent behaviour, and yet have different energy dependence arising from factors other than wall attenuation, stopping power and particle equilibrium. Experiments comparing the performance of a commercial Baldwin-Farmer ionization chamber and an all-polystyrene chamber, built to give a minimal wall attenuation (section III C - 1), showed no essential difference.

The energy dependence of the effects due to polarization is a significant factor in dose determinations using ionization chambers. The polarization corrections calculated in this work (section III D - 4) provide the data necessary for determining absorbed dose from ionization chamber measurements. The results of this work verify the theoretical values obtained by Zsula et al. (102) up to 20 MeV, and extend them up to incident electron energies of 28 MeV. Since most therapeutic betatrons now produce electrons up to 35 MeV, this is very useful information in high energy electron dosimetry.

The polarization data and the related C_F factors obtained

in this work make possible the use of air-ionization chamber instruments in clinical electron dosimetry. The good agreement between the C_F values obtained from these experiments and from the theory based on the Bragg-Gray cavity principle (section III C - 2) justifies the use of commercial ionization dosemeters in electron dosimetry. This brings output measurements of high energy electron sources to the same level of complexity as those of conventional x-ray machines and cobalt units. The results of the measurements can be converted, by means of the factors discussed above, into clinically useful dose data. Furthermore, since the accuracy of the dose data depends upon the precision of the C_F factors, it can be upgraded as more information provides greater precision.

Electron irradiation of an absorber results in the deposition of electrical charge within the absorber. In tissue and other conducting media, this charge is rapidly distributed by conduction. There is no indication whatever that the concentration or conduction of charge is sufficient to be biologically effective. In insulating media, such as polystyrene, Laughlin's theory of charge deposition from electron irradiation (63) can be experimentally verified. The experimental results using the pillbox-shaped ionization chamber, given in section III C - 3, provide the first experimental verification of the theory, other than that reported by Laughlin himself. The data indicate that the peak value of the deposited charge occurs beyond

0.8 R_p, as predicted by the theory.

These results also explain the difference in ionization charge collected with opposite polarities of the chamber collecting electrode. When a parallel plate ionization chamber is used to measure electron dose, the results reported in section III C - 3 show that the average of the values when collecting positive and negative ions is more accurate than is either single value.

TLD-100 LiF has not been employed as an absolute dosemeter in this work. This dosimetric system has proved to be very convenient for relative dose determinations in a phantom (section III B) and for intracavitary measurements in clinical applications. The thermoluminescent output can be measured at any convenient time after irradiation. The dosimetric response of the TLD-100 is independent of electron energy and can be reproduced within a standard deviation of 1%. On the other hand, the dosemeter requires careful handling and annealing, and the measurement is time consuming. With the automated reader developed in this work (section II B - 5) the measurements are facilitated, although some measurement accuracy has been lost. However, in the medical application of radiation dosimetry, the increased standard deviation of 2.6% can be accepted in order to achieve greater flexibility of use.

The photographic method has proven to be useful in field-mapping of high energy electron beams (section III D - 3). In this

work no special attempts were made to control the processing conditions to permit quantitative interpretation of the results of densitometry. Rather, the technique was used only to provide rapid, qualitative information preparatory to more precise measur ements using the other dosimetric methods.

How are the results of this investigation applied in the treatment of patients suffering from cancer? Reports from other treatment centers, coupled with experience gained in previous cases, provide the physician with a considered optimal dose to be administered in a specific number of daily fractions. His knowledge of the extent of the tumour governs his choice of field size and electron energy (since this latter factor determines the depth of the high dose zone). The dose distributions discussed in section III D - 2 and 3 are necessary for this purpose.

He then needs to know the number of integrator "clicks" that will result in the delivery of the desired daily dose at the depth of the dose maximum. This "click per rad" datum is found in the manner described in section III A - 7 using the ferrous sulphate dose-meter. The Baldwin-Farmer instrument, periodically calibrated against the ferrous sulphate dosemeter (section III C - 2) is used routinely to check the constancy of the integrator.

Where possible, TLD-100 dosemeters (section III B) are placed on the skin and in accessible bodily cavities to check the

accuracy of dose administration. When new therapeutic techniques are considered, the dose distributions are first measured in humanoid phantoms, using both TLD-100 and photographic densitometry (section III D - 3).

The existing theory describes in a satisfactory way the interaction of pencil electron beams with matter. Under broad beam conditions, however, the theory fails to describe adequately the observed patterns of energy dissipation in a phantom. This is borne out by the work described in this thesis which shows clearly that scaling of depth dose data with electron density NZ from one absorber to another is not feasible.

An adequate theory would predict the energy spectrum and the particle fluence at any point in a medium irradiated with a broad beam of electrons. It would provide scaling laws which would make possible the prediction of depth dose data for all absorbing materials and therapeutically-useful incident electron energies. One approach to the realization of such a theory would be through an experimental investigation of the energy spectrum of electrons at each point in a material irradiated under the conditions of interest in therapy. Such a study would provide the necessary data upon which to extend the existing theory to cover broad beam conditions.

APPENDIX I

APPENDIX I

THEORY OF INTERACTION OF HIGH ENERGY ELECTRONS WITH MATTER

The response characteristics of any type of radiation-measuring device depends upon the interaction of charged particles with its sensitive elements. A moving electron loses kinetic energy, or is deflected from its original path, through elastic and inelastic collisions with atomic electrons and nuclei. In the study of the energy absorbed from a beam of fast electrons under the conditions of interest in this work, the interactions of primary importance are ionizing and radiative collisions.

A. IONIZING COLLISIONS

In inelastic collisions between fast moving electrons and atomic electrons, the kinetic energy transfer may be large enough to eject an atomic electron. This type of interaction is called an IONIZING COLLISION, because a primary ion pair results. In some

such events, the target electrons may receive kinetic energy of the order of 1 keV or more, and will then produce additional ion pairs while being brought to rest. These high energy secondary electrons are called δ-rays (27).

The energy loss by a moving electron through ionizing collisions has been the subject of much theoretical study (10, 14, 15, 16, 17, 35, 70, 71, 73, 74 and 99). The parameter of interest in the present work is the so called "stopping power" of an absorber as a function of electron energy. The magnitude of the stopping power for relativistic electrons in a homogeneous absorber of atomic number Z is given by the Bethe-Bloch relation (11, 14):

$$\left(\frac{dT}{dx}\right)_{ion} = \frac{2\pi e^4}{m_o v^2} NZ \left[\ln \frac{m_o v^2 T}{2 I^2 \gamma^2} - (2\gamma - \gamma^2) \ln 2 + \gamma^2 + \frac{1}{8}(1-\gamma)^2\right], \quad \text{MeV/cm} \qquad \text{I - 1}$$

where e and m_o are the charge and rest mass respectively of the electron, T is the kinetic energy of the incident electron of velocity v, $\gamma = 1 - \beta^2$ ($\beta = v/c$, where c is the velocity of light), N is the number of atoms of the absorber per cm^3, and I is the ionization potential of the target atoms (27).

For very high-energy electrons ($T \gg m_o c^2$, $\beta \sim 1$) the stopping power equation becomes:

$$\left(\frac{dT}{dx}\right)_{ion} = \frac{2\pi e^4}{m_o c^2} NZ \left[\ln \frac{T^3}{2m_o c^2 I^2} + \frac{1}{8}\right], \text{ MeV/ cm} \qquad \text{I - 2}$$

B. POLARIZATION

In the derivation of the Bethe-Bloch formula, the perturbation of the field of the passing electron which arises from the electric polarization of the surrounding atoms has been neglected. In fact, the effective electric field of the incident electron is decreased by this polarization. Since the energy transfer by ionization is through Coulomb interactions, this is also reduced. Obviously, this polarization effect is greater in dense absorbers, such as liquids and solids, than in gaseous media. Thus the polarization correction term Δ which must be inserted into the Bethe-Bloch equation is negligible for gases, but is significant in dense media. It results in a reduction in the magnitude of the stopping power which is given by (29, 44, 92, and 98):

$$\Delta = \frac{2\pi e^4}{m_o v^2} NZ \left[\ln \frac{4\pi e^2 \hbar^2 NZ}{m_o I^2 \gamma^2}\right], \text{ MeV/cm} \qquad \text{I - 3}$$

where $\hbar = h / 2\pi$ and h is planck's constant.

Compared to the magnitude of the ionization losses, the value of Δ is negligible below 1 MeV, and then increases with electron energy T and atomic number Z of the absorber, as shown in Fig. 52.

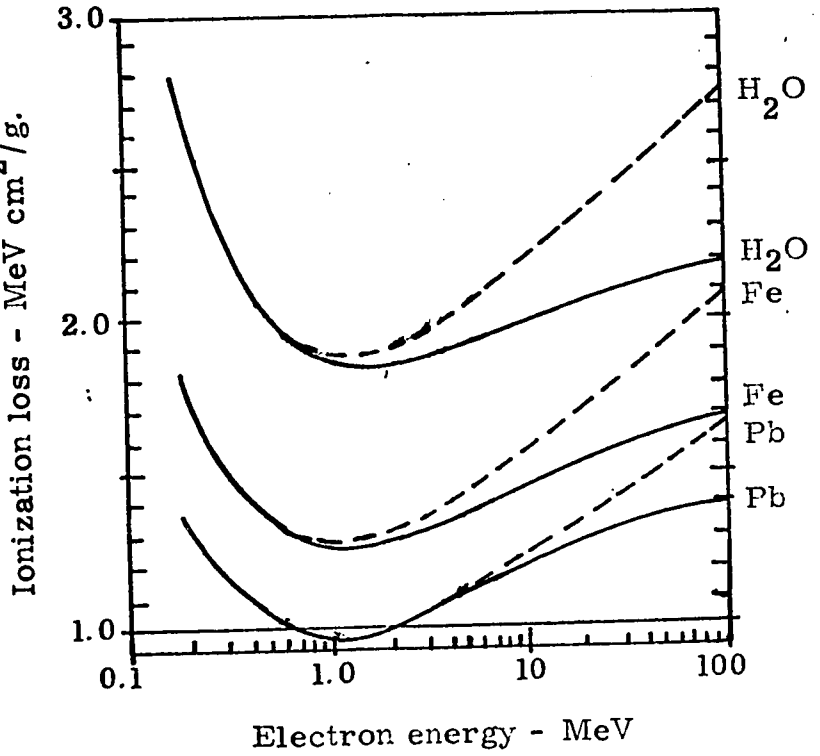

Fig. 52: The theoretical ionization losses for electrons in condensed materials (44).

—— No polarization correction

---- Polarization correction included.

For electrons of the energies involved in this work the Bethe-Bloch formula I - 2 takes the form:

$$\left(\frac{dT}{dx}\right)_{ion} = \frac{2\pi e^4}{m_o c^2} NZ \left[\ln \frac{T^3}{2m_o c^2 I^2} + \frac{1}{8} - \delta \right] , \text{ MeV/cm} \qquad I - 4$$

where $\delta = \ln \frac{4\pi e^2 h^2 NZ}{m_o \gamma^2 I^2}$.

C. RADIATIVE LOSSES

When an electron of kinetic energy T passes through the field of an atomic nucleus, a probability exists that it will be deflected from its original path. In some of these collisions between moving electrons and nuclei, quanta of radiation (BREMSSTRAHLUNG) are emitted. The energy radiated in these events can have values between zero and a maximum of T. The radiative loss by a fast electron in these circumstances is given by (10, 12, 13, 48 and 97):

$$\left(\frac{dT}{dx}\right)_{rad} = NE \frac{Z(Z+1)}{137} r_o^2 \left(4 \ln \frac{2T}{m_o c^2} - \frac{4}{3}\right), \text{ MeV/cm} \qquad I - 5a$$

for $m_o c^2 << T << 137\, m_o c^2\, Z^{-1/3}$

and for $T >> 137\, m_o c^2\, Z^{-1/3}$

$$\left(\frac{dT}{dx}\right)_{rad} = NT\,\frac{Z(Z+\zeta)}{137}\,r_o^{\,2}\,\left(4\ln\frac{183}{Z^{1/3}}+\frac{2}{9}\right),\ \text{MeV/cm} \qquad \text{I - 5b}$$

where $E = (T + m_o c^2)$ is the total energy of the electrons, ζ is a "shielding factor" which accounts for the effect of screening of the nuclear charge by the atomic electrons, and r_o is the Bohr radius.

An approximate relation between the magnitudes of the ionization and radiative losses is given by (13):

$$\left(\frac{dT}{dx}\right)_{ion} \Big/ \left(\frac{dT}{dx}\right)_{rad} \approx \frac{800}{TZ} \qquad \text{1 - 6a}$$

Thus the radiative and ionization losses become of equal importance at a CRITICAL ENERGY given by:

$$T_c \approx \frac{800}{Z}\ \text{MeV} \qquad \text{I - 6b}$$

This critical energy for water is 92 MeV (77). The theoretical values of ionization and radiative losses in water for electrons of energy between 2 and 100 MeV are given in Fig. 53. The polarization correction estimated from the theory is also included.

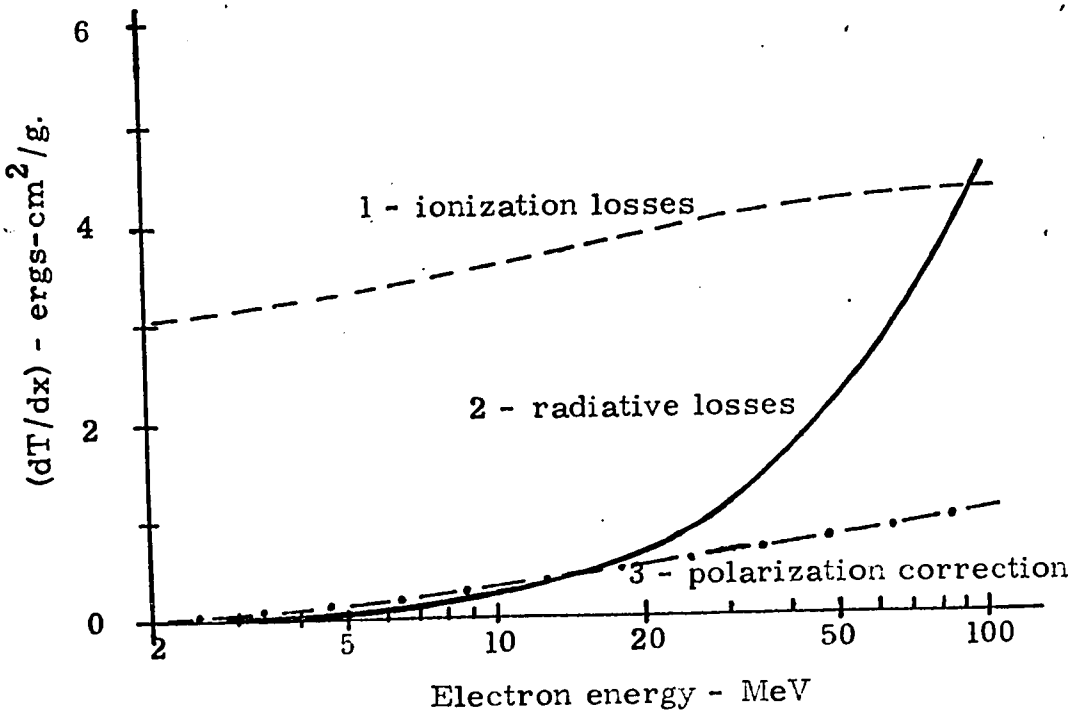

Fig. 53: Ionization and radiative losses of electrons in water (Theory). Curve 3 gives the polarization correction for water. H. E. Johns and J. S. Laughlin, In: Radiation dosimetry, G. J. Hine and G. L. Brownell (Ed.), Academic Press, 1958.

D. TOTAL STOPPING POWER

In the case of electrons of kinetic energy T, traversing a material of electron density NZ electrons per cm^3, the total stopping power can be obtained from equations I - 4 and I - 5. However, the quantum-mechanical approach employed in the derivation of these equations results in a statistically - averaged value for the stopping power. Thus one may expect both a variation in the energy lost per unit path traversed and a variable path length for a given amount of energy loss. These phenomena are referred to as energy and range STRAGGLING. They are more pronounced when light particles, such as electrons, traverse an absorber, and they increase with incident electron energy.

The Bethe-Bloch equation and radiative-loss equation have been found to agree with the results of experiments employing pencil beams of monoenergetic electrons (42). However, they cannot be expected to predict the results of measurements under the conditions of broad beam geometry of interest here. Thus, for dosimetric purposes, the theory is of little value, and reliance must be placed on experimental observations.

APPENDIX II

APPENDIX II

THEORY OF FERROUS SULPHATE DOSEMETER

A. FERROUS-TO-FERRIC OXIDATION

Interaction of fast electrons with water molecules results in radiolysis of H_2O:

$$H_2O \xrightarrow{\text{irradiation}} H,\ OH,\ H_2,\ H_2O_2 . \qquad \text{II - 1}$$

In pure water or in aqueous solutions of inert substances, the molecular hydrogen is attacked by the OH radical and reverted to H_2O. On the other hand, in aqueous solutions of ferrous sulphate or ferrous ammonium sulphate, the ferrous ions react with the OH radicals, preventing this recombination.

The secondary reactions may be summarized:

$$OH + Fe^{++} \longrightarrow Fe^{+++} + OH^- \qquad \text{II - 2a}$$

$$H + O_2 \longrightarrow HO_2 \qquad \text{II - 2b}$$

$$HO_2 + H^+ + Fe^{++} \longrightarrow Fe^{+++} + H_2O_2 \qquad \text{II - 2c}$$

$$H_2O_2 + Fe^{++} \longrightarrow Fe^{+++} + OH^- + OH \qquad \text{II - 2d}$$

$$HO_2 + Fe^{+++} \longrightarrow Fe^{++} + O_2 + H^+ \qquad \text{II - 2e}$$

The last reaction, which results in a decrease in ferrous oxidation, may be inhibited when the ferrous sulphate solution is prepared in 0.8 N H_2SO_4 (1).

In the absence of dissolved oxygen (or air), the reactions II - 2 are:

$$H + H^+ + Fe^{++} \longrightarrow Fe^{+++} + H_2 \qquad \text{II - 3a}$$

$$OH + Fe^{++} \longrightarrow Fe^{+++} + OH^- \qquad \text{II - 3b}$$

$$H_2O_2 + Fe^{++} \longrightarrow Fe^{+++} + OH^- + OH \qquad \text{II - 3c}$$

As ferric sulphate builds up in the oxygen-free solution, the rate of oxidation falls, slightly in 0.8 N H_2SO_4 solution and quite rapidly at lower acidities (2). This reduction is due to the competition of Fe^{+++} for H atoms:

$$Fe^{+++} + H \longrightarrow H^+ + Fe^{++} \qquad \text{II - 3d}$$

which has the same consequences as that due to equation II - 2e.

The number of ferric ions produced in solution of ferrous ammonium (or ferrous) sulphate in 0.8 N H_2SO_4 is proportional to the amount of energy absorbed from the radiation beam. Thus it can be employed as a radiation dosimetric system (33, 34).

B. DOSE-RATE DEPENDENCE

The yield of ferric ions in aerated solution of ferrous (or ferrous ammonium) sulphate has been found to be independent of dose-rate up to 10^9 rads per second (6, 64, 80, 85 and 95). Above this dose-rate the ferric ion yield in the dosimetric solution decreases with increasing dose-rate. The lower limit for this dose-rate independence is 10^{-1} rad per second (87).

C. EFFECTS OF PULSED BEAM

The effects of pulsed radiation beams have been investigated in the range of frequencies between 1 to 750 pulses per second, with pulse durations ranging from 0.4 to 5 microseconds (95). No pulse rate dependence was observed in the ferric ion yield in a one millimolar aerated solution of ferrous sulphate in 0.8 N H_2SO_4.

The pulse frequency of the electron beam employed in the present work is 60 pulses per second, and the maximum dose-rate is approximately 10^6 rads per second. Consequently the rate of oxidation and hence the ferric ion yield may be considered to be uniform.

D. ABSORBED DOSE DETERMINATION

The calorimetry is the best method for the absolute calibration of the ferrous sulphate dosemeter in terms of the absorbed dose. However, other methods, such as ionization and power input have been employed.

Originally Fricke (33, 34) determined the amount of ferrous-to-ferric oxidation by titration. The technique generally employed at present is the spectrophotometric method, first introduced by Hardwick (46). He showed that the number of ferric ions formed could be determined by measuring the increase in light absorption in the wavelength region between 303 to 305 nm, where the absorption is a maximum (Fig. 54). The concentration M of the ferric ions is given by:

$$M = \frac{A}{L\{\Sigma(Fe^{+++}) - \Sigma(Fe^{++})\}} = \frac{A}{L\Sigma(Fe^{+++})} \text{ moles/liter,} \qquad \text{II - 4a}$$

where A is the difference in absorbance between the irradiated and unirradiated dosimetric solutions, L is the path length of the solution in cm, and $\Sigma(Fe^{++})$ and $\Sigma(Fe^{+++})$ are the MOLAR EXTINCTION COEFFICIENTS (discussed in the following section), in liter per mole per cm of ferrous and ferric ions respectively. It has been shown that $\Sigma(Fe^{++})$, at the absorption maxima of 304 nm, is negligible compared to $\Sigma(Fe^{+++})$ (83). Hence $\Sigma(Fe^{+++})$ is referred to as Σ in what follows, and equation II - 4a may be written as

$$M = \frac{A}{\Sigma L} \quad \text{moles/liter} \qquad \text{II - 4b}$$

The quantity M may be converted into units of energy by introducing G - the number of ions produced per 100 eV (discussed in section F of this Appendix), to give the absorbed energy E_m:

$$E_m = N_o \times 1.6 \times 10^{-10} \quad \frac{A}{LG\Sigma} \text{ ergs/liter} \qquad \text{II - 5}$$

where N_o is Avogadro's number (6.02×10^{23}). Hence, the dose D_m in rads is:

$$D_m = \frac{9.63 \times 10^8 \ A}{LG \ \Sigma \rho} \text{ rads,} \qquad \text{II - 6}$$

where ρ is the density of the ferrous sulphate solution, which has been measured to be $1.015 \pm .002$ g/cm^3, at 25°C.

E. MOLAR EXTINCTION COEFFICIENT

From Lambert's and Beer's laws the MOLAR EXTINCTION COEFFICIENT Σ is defined as the absorbance per unit path length of a molar solution (26), and is expressed in liter per mole per cm. It is a function of wavelength, as shown in Fig. 54. The existence of a stronger absorption peak of ferric sulphate at 224 nm has been observed (86). Here also $\Sigma (Fe^{++})$ is negligible compared to $\Sigma(Fe^{+++})$.

Fig. 54 illustrates both these characteristic absorption peaks.

Several values of Σ at the 304 nm absorption peak have been reported (9, 21, 47, 50, 53, 65, 66, 86, 87, 91 and 102), and the value range between 2149 and 2240 liter $mole^{-1}$ cm^{-1}. The weighted average of these values of Σ_{304} is 2197 ± 23 liter $mole^{-1}$ cm^{-1} at 25°C. The molar extinction coefficient at 224 nm has been investigated by Scharf and Lee (86) only; their value is 4565 ± 6 liter $mole^{-1}$ cm^{-1} at 25°C.

The temperature dependence in the range 20 to 30°C of Σ_{304} and Σ_{224} are illustrated in Fig. 55. In this range Σ increases linearly with temperature; Σ_{224} by 0.13% per C° and Σ_{304} by 0.69% per C° (86). Because the density of the solution also changes with temperature, the measured change in absorbance is also temperature dependent. Briefly, between 20 and 30°C:

at 224 nm

$$\Sigma(t) = \Sigma(25) \left\{1 + 0.0013\,(t-25)\right\} \qquad \text{II - 7a}$$

$$A(t) = A(25) \left\{1 + 0.001\,(t-25)\right\} \qquad \text{II - 7b}$$

and at 304 nm

$$\Sigma(t) = \Sigma(25) \left\{1 + 0.0069\,(t-25)\right\} \qquad \text{II - 8a}$$

$$A(t) = A(25) \left\{1 + 0.0065\,(t-25)\right\} \qquad \text{II - 8b}$$

The molar extinction coefficient also shows a dependence

on the H_2SO_4 concentration. This dependence is less significant at 224 nm than at 304 nm (61).

F. G-VALUE

The "G-value", which is defined as the number of ferric ions oxidized as a result of an energy absorption of 100 eV, is an essential part of the calibration factor of the ferrous sulphate dosemeter. Various high energy electron G-values have been reported; those for energies of 10 MeV and higher are listed in Table XVII. Those obtained by calorimetric measurements are seen to be nearly independent of electron energy. However, there are no calorimetric values reported for electrons above 20 MeV. The values obtained by power-input and ionization methods show an increase with energy. The SCRAD (94) recommends a constant G-value of 15.5 ions per 100 eV for electrons, independent of energy. This is in agreement with the weighted average calculated by Almond (4), Pettersson and Hettinger (79) and Pinkerton(81). Since the results reported in section III D - 1 favour a constant G-value, the SCRAD-recommended value of 15.5 ions per 100 eV has been used in this work.

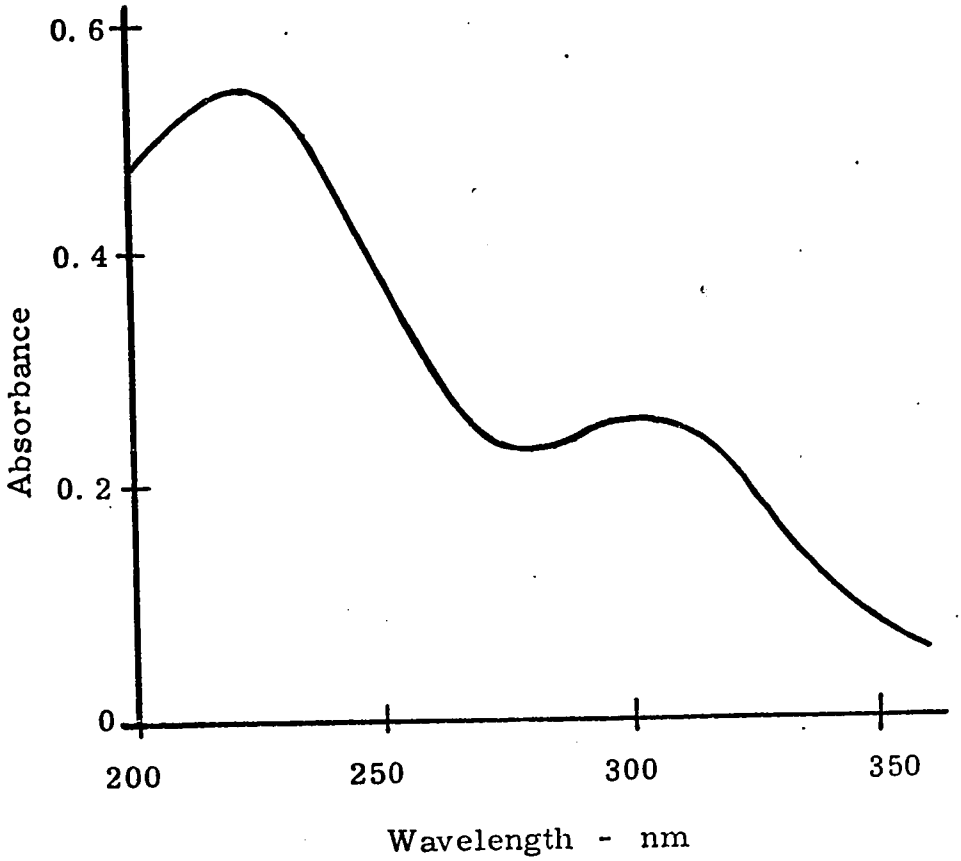

Fig. 54: Absorption spectra of a 0.1 millimolar solution of ferric sulphate solution in 0.8 N H_2SO_4, measured with a Hitachi Perkin-Elmer spectrophotometer and 1 cm silica cells.

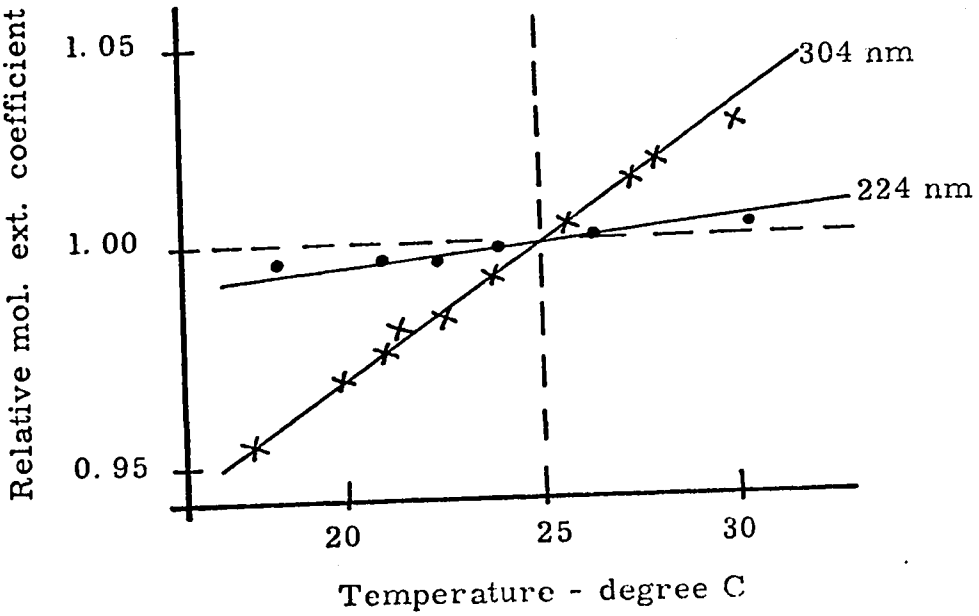

Fig. 55: Temperature dependence of molar extinction coefficient of ferric ions in 0.8 N H_2SO_4, at 304 and 224 nm absorption peaks. Values are relative to those measured at 25°C. [Scharf, K., and Lee, R. M., Rad. Res., 16:119 (1962)]

TABLE XVII

Published G-Values for Electrons of Energies at and more than 10 MeV

Electron energy (MeV)	G-value ions/100 eV	Method of determination
10	15.32 ± 0.34 (36)*	calorimetry
20	15.17 ± 0.28 (36)	..
15	15.20 ± 0.40 (6)	..
13.25	15.49 ± 0.40 (4)	..
15.9	15.4 ± 0.40 (4)	..
18	15.35 ± 0.35 (4)	..
20	15.51 ± 0.12 (79)	..
Average	15.35 ± 0.35	
10	15.7 ± 0.3 (69)	power-input
30	16.3 ± 0.3 (69)	..
13	15.6 ± 0.4 (95)	..
10	15.7 ± 0.3 (67)	ionization
17	15.8 ± 0.3 (67)	..
20	16.0 ± 0.3 (67)	..
25	15.9 ± 0.3 (67)	..
30	16.3 ± 0.3 (67)	..
16	15.7 ± 0.1 (102)	..
Grand average	15.65 ± 0.47	

* References

APPENDIX III

APPENDIX III

A. THEORY OF THERMOLUMINESCENT DOSIMETRY

1. Radiothermoluminescence

Energy absorbed by a solid from ionizing radiations may be dissipated as heat or as thermoluminescence. If the electrons involved in the absorption transitions return to the ground state instantaneously (i. e. in $\leq$ 1 microsecond), the resulting emission is termed fluorescence, otherwise phosphorescence.

A phosphor can be considered a pure insulating crystal, made luminescent by the introduction of a small portion of impurity atoms, whose valence is different from that of the host crystals. These crystals are said to contain an ALIOVALENT impurity, which upsets the electrical neutrality condition and modifies the thermal equilibrium defect concentrations. Impurity atoms or LATTICE DEFECTS give rise to localized electron states (such as D, E, and F. in Fig. 56) with narrow energy levels, which may occur in the forbidden band. The levels such as F are normally empty, and are called TRAPS. These traps may capture electrons excited into the

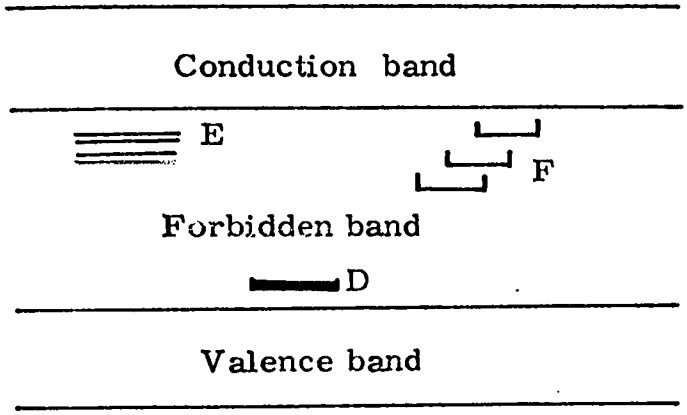

Fig. 56 : Energy levels in phosphors. D, E, and F are localized electron states due to lattice defects. Randall, J. T., and Wilkins, M. H. F.(84).

Fig. 57 : TL process in impurity activated alkalihalide crystals leading to luminescence characteristic of the impurity.

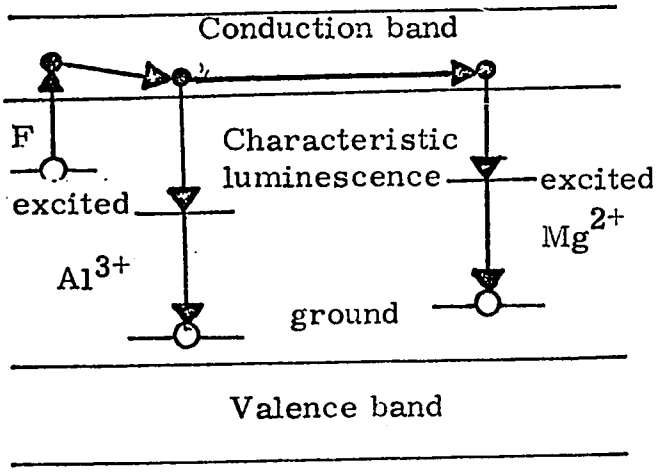

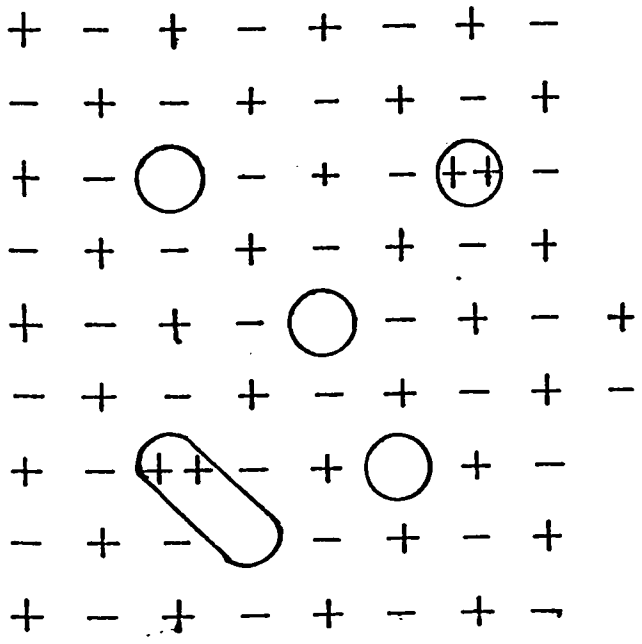

Fig. 58: Schematic representation of vacancies ◯ , substitutional divalent action impurity ⊕⊕ , and vacancy impurity complexes ⊖⊕ , in alkalihalides.

conduction band on irradiation. Electrons bound to these traps may be released by external influence, such as pressure, light and heat. Release of trapped electrons by thermal agitation gives rise to delayed luminescent emission; this phenomenon is called THERMO-LUMINESCENCE (TL).

In alkalihalides these traps (called COLOUR CENTERS) exist at points in the crystal lattice, where a negative ion (i. e. halide ion) is missing (75). Real crystals very seldom attain the normal structure, but have small proportions of impurities. For alkalihalides the principal F-center* absorption band lies in the visible region of the spectrum.

The mechanism of TL is still imperfectly understood, but the explanation given is in terms of lattice defects. Alkalihalides can be doped with known luminescent ions or activators to ensure that the luminescent transitions are radiative processes, and to control the emission spectrum. Figs. 57 and 58 show the effect of the presence of such activators. On irradiation of a doped crystal, electron trapping leads to F-center formation and the "hole" is trapped by the activator ion. On heating, the electron is ejected from the F-center and recombines with the hole at the activator, thus exciting luminescence characteristic of the activator.

* F-centers are electron trapped Schottky defects. When alkali ions and halide ions are missing from the crystal lattices, it is said to have Schottky defects.

Radiation dosimetry utilizing TL has been studied in detail by various investigators (19, 37, 38, 55, 62, 72, 76 and 88). The electrons trapped in the crystal lattice imperfections, as a result of irradiation, remain trapped for long periods at room temperature. If the temperature is raised, the electrons are released, resulting in TL emission. The total amount of TL emission can be measured and related to the absorbed dose. The principal advantage of TL dosimetry over other solid state systems is its higher sensitivity and its wide useful range (Table XVIII).

2. Annealing for Reuse

The TLD-100 may be reused. The used powder, however, shows a higher response, as illustrated in Fig. 27, and fades rapidly on storage. This enhanced response is a consequence of radiation damage in the crystal as well as of the shallow traps from which arise the low temperature peaks.

On exposure to high energy radiation, some atoms in the crystal are ejected into an interstitial site. This radiation damage increases the lattice defects in the crystals, upsets the thermal equilibrium, and consequently increases its TL efficiency. After very high doses the crystal may crumble. Such permanent damage in TLD-100 has been observed at a dose of 3×10^4 rads (8).

The radiation damage can usually be corrected by proper

TABLE XVIII

Thermoluminescent Dosemeters and Their Characteristics

TLD		Dose Range (rads)	Fading at Room Temperature
$CuSO_4$: Mn	(62)*	10^{-1} to 10^5	severe
CaF_2 : Mn	(37)	10^{-2} to 10^5	10% in 16 hrs. then 1% per day to 66%
LiF : Al_2O_3	(19)	10^{-1} to 10^5	none up to 50°C
TLD-100 (LiF)	(20)	10^{-1} to 10^5	none
$Li_2B_4O_7$: Mn	(89)	10^{-1} to 10^5	none

* References

annealing. Annealing at temperature near its melting point allows the atoms ejected into the interstitial sites to return to their equilibrium positions. All the filled traps will not be emptied in the process of measurement. These filled traps add to the TL light output in the successive measurements.

A standard annealing procedure devised by Cameron (20) has been employed to obtain the used TLD-100 for accurate reuse. This consists of maintenance of the powder at 400°C for 1 hour, followed by heating at 80°C for 24 hours. The 400°C annealing completely de-excites all traps in the phosphor and lets the crystals recover from radiation damages. The 80°C annealing affects the trap distribution, eliminating low temperature glow peaks (section II B - 4).

B. PHOTOGRAPHIC DOSIMETRY

Photographic films provide a rapid method of determining electron dose distribution for clinical applications. A film irradiated in any given plane inside a phantom, homogeneous or inhomogeneous, gives useful information about the energy dissipation in that plane. Provided the relationship between the film density and the absorbed dose is known, photographic dosimetry has the advantage that a complete set of dose data in one plane can be obtained in a single short exposure. Fig. 59 illustrates two such films taken, one at 10 MeV and the other at 35 MeV electron energy, showing the depth dose data in a plane

Figure 59

Electron dose distribution measured in the plane parallel to the accelerating plane and to the direction of the beam, recorded on photographic films.

A - of 35 MeV electrons; and E - of 10 MeV electrons, along the 14 cm side using a 14 x 12 cm plastic applicator.

Figure 59

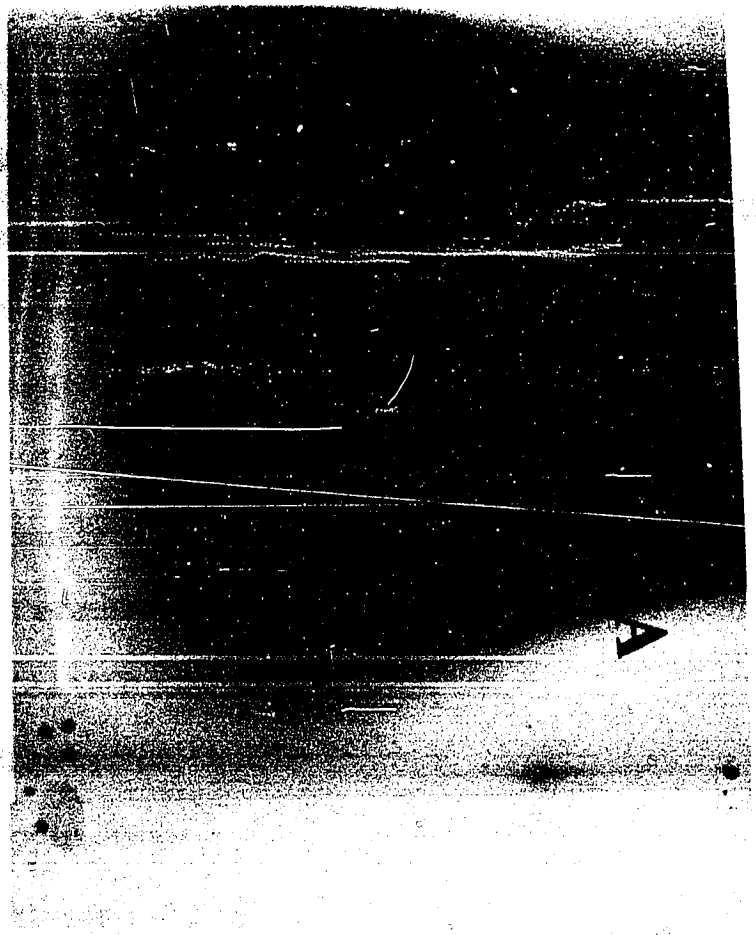

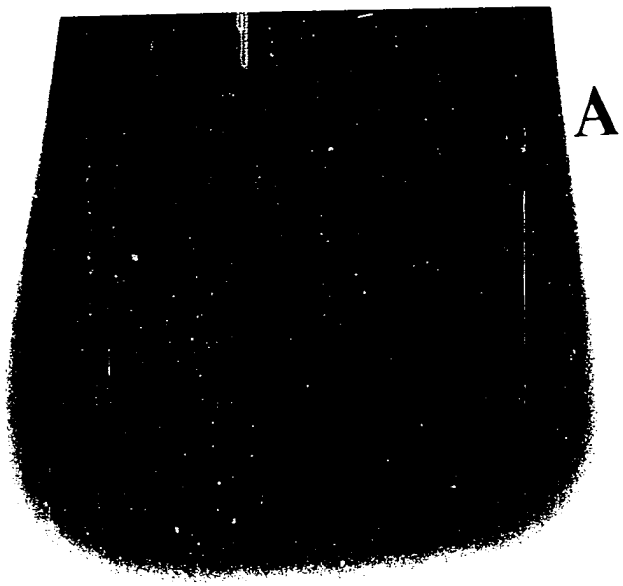

A

E

parallel to that of the accelerating orbit. Even though the error of these measurements is 5 to 10% (59) the technique is widely used.

When evaluating films for dosimetric purposes, special calibration measurements must be made to establish the dose-optical density relationship. Kodak type R single coated x-ray film, under controlled conditions of exposure and development, has been shown to yield a linear dose-optical density relationship up to doses of 150 rads and optical density of 3.0 (shown in Fig. 60). This is in agreement with reported results with other film types : Kodak type AA (78); Kodak microtex (51); and Kodak type M (68).

The optical density response of photographic emulsions in dosimetric applications depend upon a number of parameters. Those of interest here are 1) type and energy of the incident radiation, 2) development conditions, 3) angle between beam axis and film, 4) atomic number of the phantom material and 5) pressure on the film during irradiation. In dosimetric irradiations films were exposed at a slight angle of 3^{o} to the beam axis, sandwiched in polystyrene phantom. The films were developed at a temperature of $20^{o}C$.

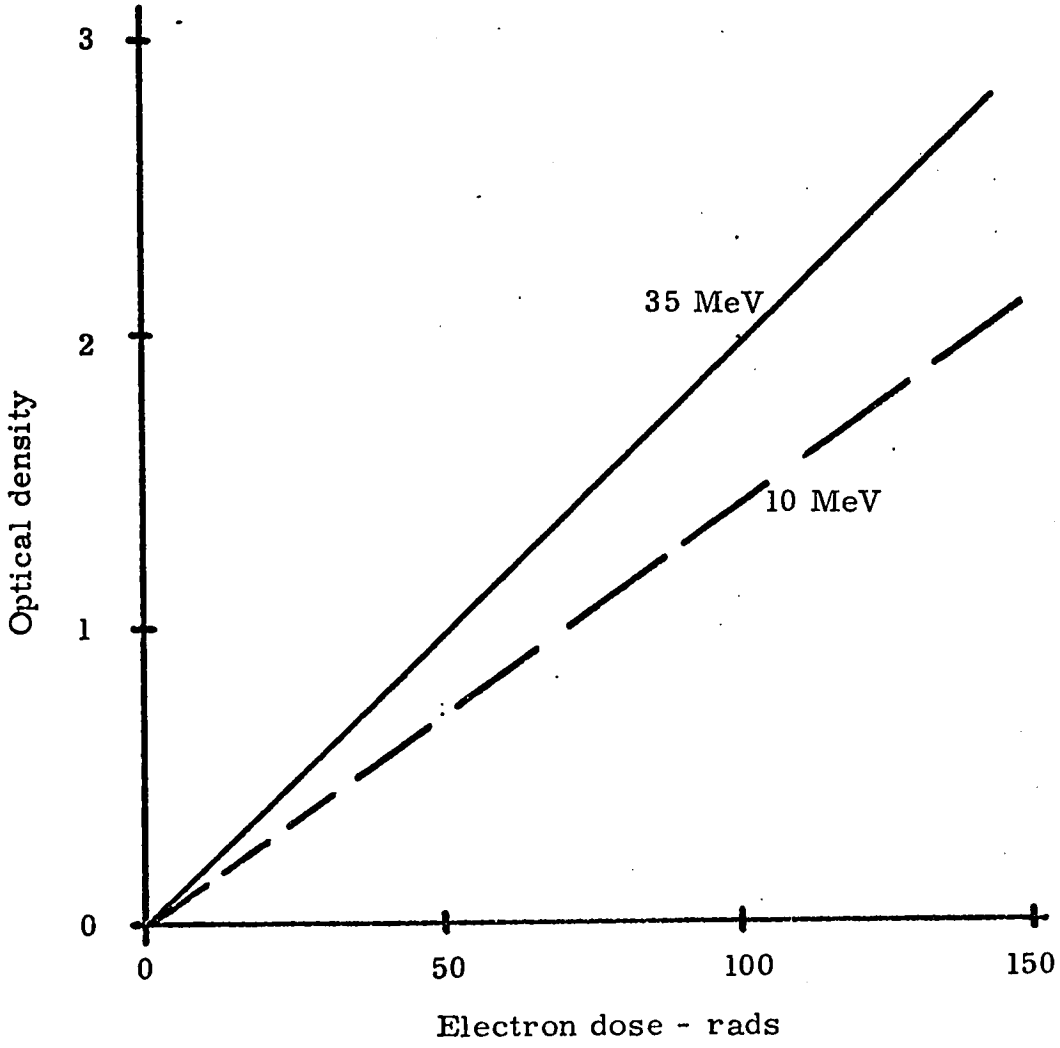

Fig. 60 : Dosimetric response of Kodak Type R film to 10 and 35 MeV electrons.

APPENDIX IV

TABLE XIX

Number of Electrons per gram (ELECTRON DENSITY) N_e, and the Number of Electrons per cm^3 (N_d) of Different Materials Employed in the High Energy Electron Dosimetry Work

Material	Chemical symbol	Z	A	Density g/cm^3	$N_e \times 10^{-23}$ electrons/g	$N_d \times 10^{-23}$ electrons/cm^3	Ratio
water	H_2O	10	18.016	1.000	3.344	3.344	1.000
polystyrene	$C_6H_5(CH{:}CH_2)$	56	104.14	1.044	3.240	3.383	1.012
lucite (methyl methacrylate)	$CH_2 : C(CH_3)\text{-}COOCH_3$	54	100.11	1.15	3.250	3.737	1.118
polyethylene	$CH_2 : CH_2$	16	28.05	0.934	3.437	3.210	0.960
teflon (tetrafluoroethylene)	$CF_2 : CF_2$	48	100.02	2.20	2.891	6.360	1.902
lithium fluoride	LiF	12	25.94	2.33	2.788	6.495	1.942
plaster of paris	$CaSO_4 \cdot 1/2H_2O$	73	145.15	1.14	3.030	3.454	1.033
graphite	C	6	12.011	2.25	3.010	6.773	2.025
magnesium	Mg	12	24.32	1.74	2.973	5.173	1.547
aluminum	Al	13	26.98	2.903	2.903	7.835	2.343
copper	Cu	29	63.54	8.94	2.750	24.585	7.352
lead	Pb	82	207.21	11.35	2.384	27.058	8.092

$N_e = N_o(Z/A)$, where N_o is the Avogadro'd number, Z is the number of electrons per atom, and A is the atomic (or molecular) weight.

BIBLIOGRAPHY

1. Allen, A. O., Proc. Internat. Conf. Peaceful Uses of Atomic Energy, Geneva 1955, 7: 513, 1956.

2. Allen, A. O., "The Radiation Chemistry of Water and Aqueous Solutions", Van Nostrand, Princeton, N. J., 1961.

3. Allen, A. O. and Holroyd, R. A., J. Am. Chem. Soc., 77: 5852, 1955.

4. Almond, P. R., Phys. Med. Biol., 12: 13, 1967.

5. Almond, P. R., Private Communications.

6. Anderson, A. R., J. Phys. Chem., 66: 180, 1962.

7. Aspin, N. et al., J. Can. Assoc. Radiol., 8: 72, 1957.

8. Attix, F. H., U. S. Naval Res. Lab. Report 6145, 1964.

9. Baarli, J. and Borge, P., Acta Radiol., 47: 203, 1957.

10. Bethe, H. A., Ann. Phys., 5: 325, 1930.

11. Bethe, H. A., Z. Physik., 76: 293, 1932.

12. Bethe, H. A., Proc. Camb. Phil. Soc., 30: 524, 1934.

13. Bethe, H. A. and Heitler, W., Proc. Roy. Soc. (London), A146: 83, 1934.

14. Bloch, F., Ann. Phys., 16: 285, 1933.

15. Bloch, F., Z. Physik., 81: 363, 1933.

16. Bohr, N., Phil. Mag., 25: 10, 1913.

17. Born, M., Z. Physik., 38: 803, 1926.

18. Bragg, W. H., Phil. Mag., 20: 385, 1910.

19. Cameron, J. R. et al., Science, 134: 333, 1961.

20. Cameron, J. R. et al., Health Phys., 10; 25, 1964.

21. Cormack, D. V. et al., J. Chem. Phys., 22: 6, 1954.

22. Crosby, E. H. et al., Phys. Med. Biol., 11: 131, 1966.

23. Davies, J. R. and Rideal, E. K., "Interfacial Phenomena", Academic Press, New York, 1963.

24. Davies, J. V. and Law, J., Phys. Med. Biol., 8: 91, 1963.

25. Dewhurst, H. A., Tras. Farad. Soc., 48: 905, 1952.

26. Dyer, J. R., "Application of Absorption Spectroscopy of Organic Compounds", Prentice-Hall, New York, 1965.

27. Evans, R. D., "The Atomic Nucleus", McGraw-Hill, New York, 1955.

28. Farmer, F. T., Brit. J. Radiol., 28: 304, 1955.

29. Fermi, E., Phys. Rev., 57: 485, 1940.

30. Fowler, J. F., Phys. Med. Biol., 8: 1, 1963.

31. Fricke, H. and Glasser, O., Am. J. Roentgenol., 13: 453, 1925.

32. Fricke, H. and Hart, E. J., In: Radiation Dosimetry", Vol. II, F. H. Attix and W. C. Roesch (Ed.), Academic Press, New York, 1966.

33. Fricke, H. and Morse, S., Am. J. Roentgenol., 18: 430, 1927.

34. Fricke, H. and Morse, S., Phil. Mag., 7: 129, 1929.

35. Gaunt, J. A., Proc. Camb. Phil. Soc., 23: 732, 1927.

36. Geisselsoder, J. et al., Rad. Res., 20: 423, 1963.

37. Ginther, R. J., J. Electrochem. Soc., 101: 248, 1954.

38. Ginther, R. J. and Kirk, R. D., Report of NRL Progress, Sept. 1956.

39. Glasser, O., Radiol., 37: 221, 1941.

40. Glasser, O. et al., Am. J. Roentgenol., 20: 505, 1929.

41. Glocker, R. et al., Z. Physik, Chem., N. F., 14: 129, 1958.

42. Goldwasser, E. L. et al., Phys. Rev., 88: 1137, 1952.

43. Gray, L. H., Proc. Royl Soc., A122: 648, 1929 and A156: 578, 1936.

44. Halpern, O. and Hall, H., Phys. Rev., 57: 459, 1940 and 73: 477, 1948.

45. Harder, D., In: "Symposium on High Energy Electrons", Springer-Verlag, New York, p. 26, 1965.

46. Hardwick, T. J., Can. J. Chem., 30: 17, 1952.

47. Hart, E. J., J. Am. Chem. Soc., 73: 68, 1951.

48. Haybittle, J. L. et al., J. Chem. Phys., 25: 1213, 1956.

49. Heitler, W. and Sauter, F., Nature, 132: 892, 1933.

50. Henderson, C. M. and Miller, N., Rad. Res., 13: 641, 1960.

51. Hettinger, G. and Svensson, H., Acta Radiol., 6: 74, 1967.

52. Hettinger, G. et al., Acta Radiol., 6: 61, 1967.

53. Hochanandal, C. J. and Ghormley, J. A., J. Chem. Phys., 21: 880, 1953.

54. Holloway, A. F. and Froese, G., Radiol., 85: 729, 1965.

55. Houtermans, F. J. et al., Ann. Phys., 20: 283, 1957.

56. Huffmann, R. E. and Davison, N., J. Am. Chem. Soc., 78: 4836, 1956.

57. International Commission on Radiological Units, London 1950, Radiol., 56: 117, 1951.

58. International Commission on Radiological Units, Copenhagen 1953, Radiol., 62: 106, 1954.

59. International Commission on Radiological Units, Report 10b, N. B. S. (U. S.) Handbook 85, 1964.

60. Karzmark, C. J. et al., Phys. Med. Biol., 9: 273, 1964.

61. Katzin, L. and Gebert, E., Report ANL 4457: 4, 1950.

62. Kossel, W. et al., Naturwissen, 41 (9): 209, 1954.

63. Laughlin, J. S., In: "Symposium on High Energy Electrons", Springer-Verlag, New York, p. 11, 1965.

64. Laughlin, J. S. et al., Radiol., 60: 165, 1953.

65. Lazo, R. M. et al., J. Chem. Phys., 22: 1370, 1954.

66. Lefert, M. and Tarrgo, X., J. Phys. Chem., 63: 883, 1959.

67. Liesem, H. and Pohlit, W., Z. Physik. Chem., N. F., 35: 351, 1962.

68. Loevinger, R. et al., Radiol., 77: 906, 1961.

69. Minder, W., In: "Selected Topics in Radiation Dosimetry", Proc. I. A. E. A. Symposium, Vienna 1960, p. 315, 1961.

70. Möller, C., Z. Physik., 66: 513, 1930.

71. Möller, C., Ann. Phys., 14: 531, 1932.

72. Morehead, F. J. and Daniels, F., J. Chem. Phys., 27: 1318, 1957.

73. Mott, N. F., Proc. Roy. Soc., A126: 259, 1930.

74. Mott, N. F., Proc. Camb. Phil. Soc., 27: 553, 1931.

75. Mott, N. F., "Electronic Process in Ionic Crystals", Oxford University Press, 1940.

76. Nosenko, B. M. et al., Soviet. Phys. Tech. Phys., 1: 1983, 1956.

77. Nuclear Science Series, Report No. 39, NAS-NRC Publ. 1133, Washington, D. C., 1964.

78. Ovadia, J. and Uhlmann, E. M., Am. J. Roentgenol., 84: 754, 1960.

79. Pettersson, C. and Hettinger, G., Acta Radiol., 6: 160, 1967.

80. Pikaev, A. K. and Glazunov, P. Ya., Dokl. Akak. Nauk. SSSR, 130: 1051, 1960.

81. Pinkerton, A. P., USAEC Report AT(30-1): 3510, 1966.

82. Pinkerton, A. P. et al., Phys. Med. Biol., 11: 129, 1966.

83. Potterill, R. H. et al., Proc. Roy. Soc., A156: 561, 1936.

84. Randall, J. R. and Wilkins, M. H. F., Proc. Royl Soc., A184: 347, 1945.

85. Rotblat, J. and Sutton, H. C., Proc. Roy. Soc., A225: 490, 1960.

86. Scharf, K. and Lee, R. M., Rad. Res., 16: 115, 1962.

87. Schuler, R. H. and Allen, A. O., J. Chem. Phys., 24: 56, 1956.

88. Schulman, J. H. et al., Rev. Sci. Instr., 31: 1263, 1960.

89. Schulman, J. H. et al., In: "Luminescence Dosimetry", F. H. Attix (Ed.), USAEC, 8: 113, 1967.

90. Sinclair, W. K., Rad. Res., 20: 288, 1963.

91. Sinclair, W. K. and Schalek, R. J., Radiol., 70: 92, 1958.

92. Sternheimer, R. M., Phys. Rev., 88: 851, 1952; 103: 511, 1956; and 145: 247, 1966.

93. Svensson, H. and Pettersson, C., Arkiv For Fysik, 34: 377, 1967.

94. The Sub-Committee on Radiation Dosimetry (SCRAD), of the AAPM, Phys. Med. Biol., 11: 505, 1966.

95. Thomas, J.K. and Hart, E.J., Rad. Res., 17: 408, 1962.

96. Weiss, J. et al., Proc. Internat. Conf. Peaceful Uses of Atomic Energy, Geneva 1955, 14: 179, 1956.

97. Wheeler, J.A. and Lamb, W.E., Phys. Rev., 55: 858, 1939.

98. Wick, G.C., Nuovo Cimento (9), 1: 302, 1943.

99. Williams, E.J., Proc. Roy. Soc. (London), 130: 328, 1931.

100. Wittaker, B., Phys. Med. Biol., 10: 137, 1965.

101. Worton, R.G. and Holloway, A.F., Radiol., 87: 938, 1966.

102. Zsula, J. et al., Rad. Res., 6: 661, 1957.